EPA-600/2-76-204
July 1976

Environmental Protection Technology Series

EFFICIENT USE OF FIBROUS STRUCTURES IN FILTRATION

Industrial Environmental Research Laboratory
Office of Research and Development
U.S. Environmental Protection Agency
Research Triangle Park, North Carolina 27711

RESEARCH REPORTING SERIES

Research reports of the Office of Research and Development, U.S. Environmental Protection Agency, have been grouped into five series. These five broad categories were established to facilitate further development and application of environmental technology. Elimination of traditional grouping was consciously planned to foster technology transfer and a maximum interface in related fields. The five series are:

1. Environmental Health Effects Research
2. Environmental Protection Technology
3. Ecological Research
4. Environmental Monitoring
5. Socioeconomic Environmental Studies

This report has been assigned to the ENVIRONMENTAL PROTECTION TECHNOLOGY series. This series describes research performed to develop and demonstrate instrumentation, equipment, and methodology to repair or prevent environmental degradation from point and non-point sources of pollution. This work provides the new or improved technology required for the control and treatment of pollution sources to meet environmental quality standards.

EPA REVIEW NOTICE

This report has been reviewed by the U.S. Environmental Protection Agency, and approved for publication. Approval does not signify that the contents necessarily reflect the views and policy of the Agency, nor does mention of trade names or commercial products constitute endorsement or recommendation for use.

This document is available to the public through the National Technical Information Service, Springfield, Virginia 22161.

EPA-600/2-76-204
July 1976

EFFICIENT USE OF FIBROUS STRUCTURES IN FILTRATION

by

M. Mohamed and E. Afify

North Carolina State University
Schools of Engineering and Textiles
Raleigh, NC 27607

Grant No. R801441
Program Element No. EHE624

EPA Project Officer: J.H. Turner

Industrial Environmental Research Laboratory
Office of Energy, Minerals, and Industry
Research Triangle Park, NC 27711

Prepared for

U.S. ENVIRONMENTAL PROTECTION AGENCY
Office of Research and Development
Washington, DC 20460

CONTENTS

FIGURES

FIGURES (continued)

FIGURES (continued)

FIGURES (continued)

TABLES

TABLES (continued)

ACKNOWLEDGMENTS

The authors gratefully acknowledge the advice and cooperation of Dr. J. H. Turner and the Staff of the Industrial Environmental Research Laboratory, Environmental Research Center, EPA, Research Triangle Park, North Carolina, for conducting the bag testing experiments.

The assistance of Dr. R. W. Work, Professor Emeritus of Textile Chemistry, is highly appreciated. The following graduate students contributed greatly to the experimental work of the project in the course of their studies as research assistants:

J. W. Vogler	V. W. Herran
L. L. Saleh	M. A. Hassab
M. Venkatesan	Scott Penn
S. Sandukas	C. J. Thornton

The authors also wish to express their appreciation to E. I. duPont de Nemours and Company for providing the Reemay samples, Monsanto Textiles Company for providing the Cerex samples, Hercules, Inc. for manufacturing the bag fabrics at their Research Center, Research Triangle Park, North Carolina and The Torrington Company for providing the needles used in this project.

SECTION I

CONCLUSIONS AND RECOMMENDATIONS

Conclusions

The structure of needle punched fabrics offers in addition to the high efficiency characteristic of filter fabrics the advantage of low pressure drop. It also offers the advantage of using higher flow rates than are normally used in filtration using woven fabrics, which has economical implications in baghouse applications.

The results of the investigation of the various parameters and their influence on the fabric properties and filtration performance in batch testing led to the following conclusions:

1. Fiber length and orientation have no significant effect on most of the fabric properties. Random-laid webs give higher packing density and lower air permeability than cross-lapped webs.
2. Needle size and needle penetration are significant parameters. Large size needles produce undesirable fabrics for filtration. Increasing needle penetration improves the fabric. However, high level of needle penetration leads to fiber damage and deterioration in filtration performance.
3. Needle punched fabrics without reinforcement lack strength and dimensional stability. Spunbonded fabrics (Reemay and Cerex) when used as scrim improve the needle punched fabric properties without sacrificing its filtration performance.
4. Needling intensity is significant in affecting fabric properties. High levels of needling intensity achieved in one passage of the fabric through the needling process results in fiber and scrim damage. Needling with a small intensity and repeated over a number of passes and from both sides improves fabric characteristics.

5. Fabric weight per unit area and packing density are very important factors affecting the fabric characteristics. The air permeability-thickness product related more closely to the pressure drop for clean air than the air permeability alone.
6. Calendering needle punched fabrics damages the fabric structure and leads to a considerable increase in the pressure drop without a proportionate increase in efficiency.
7. Monodisperse particle testing indicates that the diffusion mechanism is not utilized effectively for the needle punched fabric samples tested in the submicron range without cake formation. In testing with hetrogeneous dust particles, the cake formed on needle punched fabrics differs distinctively from that formed on any other fibrous structure. The deposition of dust on the fabric shows three-dimensional mounds around the pores.
8. NCSU developed needle punched uncalendered fabrics with nonwoven scrim, were superior to commercial fabrics in some regimes of baghouse operation. With high levels of inlet loading and at high air-to-cloth ratios, more cleaning difficulties were encountered with NCSU fabrics than the commercial one.

Recommendations

The present investigation concentrated only on one type of fiber and round cross-section. It is felt that work is needed to study the use of different fibers (such as Teflon, Nomex, Nylon, etc.) with different fiber cross-sections and crimp in needle punched fabrics.

Modification of the structure of needle punched fabrics by various finishing treatments (such as shrinkage and resin applications) should improve the filtration performance, especially in the submicron range. This seems to be an important area for continuing the present work. It is also recommended to continue experiments to establish the durability of needle punched fabrics under different testing conditions. For the purpose of economy it is suggested that a special miniature baghouse apparatus be built for such experiments.

Optimizing filter specifications for best performance requires adequate information on the relationship between filter parameters and air-dust flow conditions. A single performance value (rather than pressure drop and efficiency) is needed to simplify the optimization problem required for the design of filter fabrics. This is particularly true for needle punched fabrics, since the specific cake resistance used by many researchers does not apply due to the nonhomogenity of the dust cake.

SECTION II

INTRODUCTION

The need for high-efficiency filtration of particulate matter from dusty atmospheres is ever increasing. Fibrous structures are widely used as filter media. Fabric filter technology has been growing steadily and plays an important role in air pollution control. It has been the general practice to use woven fabrics in the majority of baghouse applications. Woven fabrics are produced by interlacing two sets of parallel rows of yarns at right angles in a square array. In operation, dusty gas passes through the filter normal to the fabric surface. Filtration has been shown to take place over three phases [1]. At the start of the filtration, dust particles deposit on individual fibers and yarn surfaces. Additional particles then deposit and accumulate on already deposited particles forming aggregate structures which project into the gas stream. As deposition continues, openings between yarns become gradually filled with aggregates which eventually form the dust cake. Further accumulation of dust particles on the cake continues and the resistance to the gas flow increases until removal of the cake takes place during the cleaning cycle. The collection efficiency of woven fabrics has been found to be a function of the pore size distribution [2]. Bleeding or leakage of dust was found to be a function of the number of pores above a critical size which is related to size properties of the dust being filtered.

Structural properties of a fabric strongly affect its filtration performance and the fabric's interaction with a dust. Fabrics designed for capturing large particles, will leave the air contaminated with small particles. On the other hand, fabrics designed to collect fine particles must have small pore size which results in high resistance to the gas flow. economic considerations require minimum pressure drop through a filter, and normally a balance has to be made between the cost of cleaning and/or replacing a clogged filter and the power consumed in driving the flow.

Recently, nonwoven fabrics have been enjoying increasing interest and various structures have been looked at for many filteration applications. Nonwoven fabrics are normally less expensive than, and can be made as durable as, woven fabrics. With most nonwoven structures, high efficiency and low pressure drop in air filtration can be achieved. Spunbonded fabrics were found to be more efficient, longer lasting and cheaper than equivalent woven bags [3]. The performance of latex-bonded nonwoven fabrics was studied [4]. The results indicated that with suitable choices of fiber properties it is possible to improve efficiency and air drag characteristics to a significant extent. Another nonwoven structure which is becoming very widely used in filtration is needle punched fabrics. Needle punched fabrics have excellent features as a filter material. High collection efficiency at low pressure drop can be obtained.

This report deals mainly with the performance of needle punched fabrics in batch and baghouse testing.

SECTION III

THE NEEDLE PUNCHED STRUCTURE AND PARTICLE COLLECTION

The needle punched fabric is produced by penetrating barbed needles into a fibrous mat. The penetrating barbs transport surface fibers and embed them in the vertical direction, creating entanglements of fibers inside the pores (A Figure 1). The fibers pulled by the needles exert pressure on the fibers surrounding the pore (B Figure 1) thus causing an increase in packing density around the pores. The pore is not a free hole, simply because of the fiber entanglements as well as the disruption which takes place in the fiber order when the needles are withdrawn from the fabric. The number of punches per unit area is controlled by the distribution of needles on the needle board, the rate of fabric feed and the number of passages through the machine. The shape and size of the pores depend on the needle shape, size and penetration. Figure 2 is a micrograph showing the cross-section of a needled fabric.

Uncalendered needle punched fabric does not act as a sieve, because of the in-depth fiber entanglements in a venturi-like shape. This shape should offer a small resistance to the air flow resulting in better flow characteristics across the filter. Due to changes in the packing density over the area of the fabric, the air streamlines will be as shown in Figure 1, which leads to the deposition of large particles around the proes. Small particles will follow the streamlines through the pores and will be collected by the fibers in the pore. This gives needle punched fabrics an advantage over woven fabrics as far as dust-loading capacity is concerned. With needle punched fabrics, higher air-to-cloth ratio could also be used than with woven fabrics, which means that less fabric would be required to perform in a filtration unit.

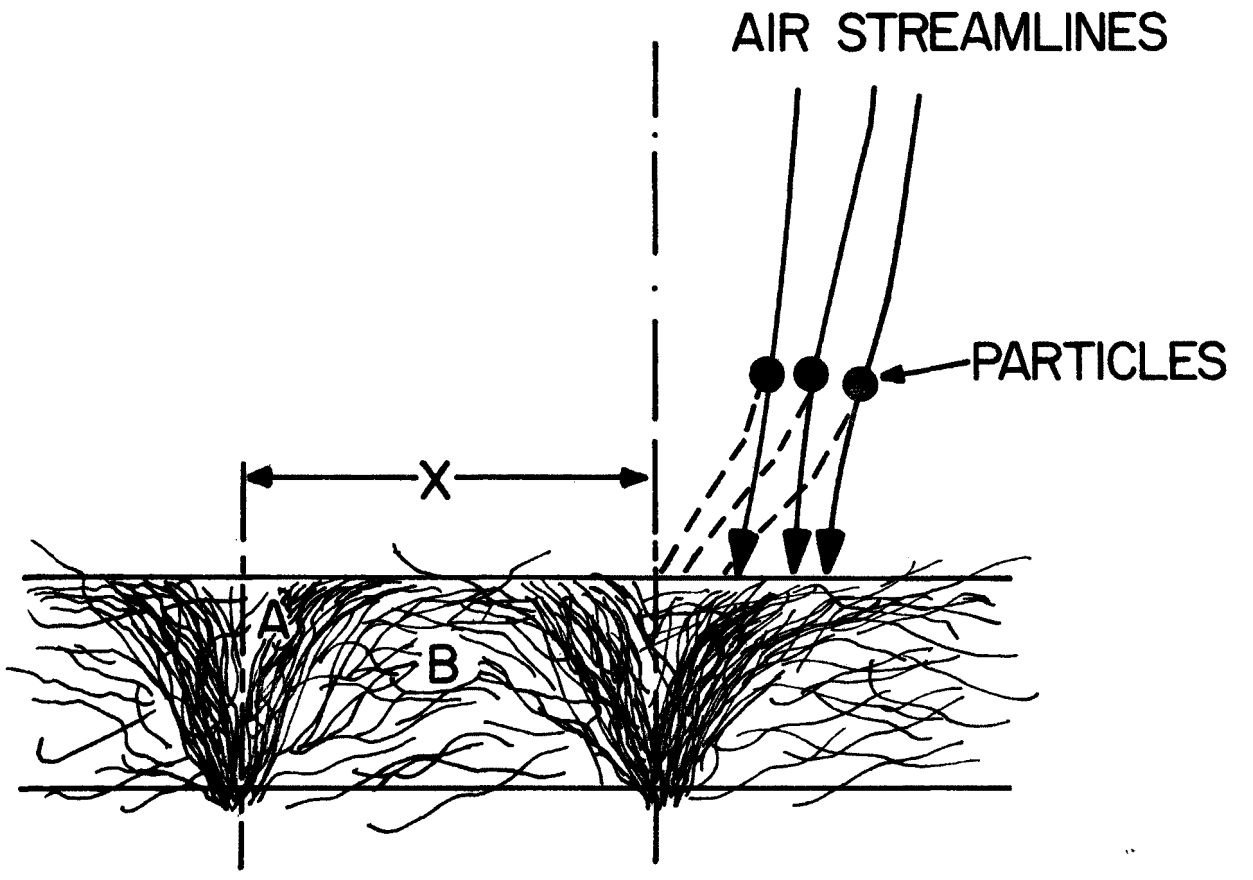

Figure 1. Needle - punched structure and particle collection

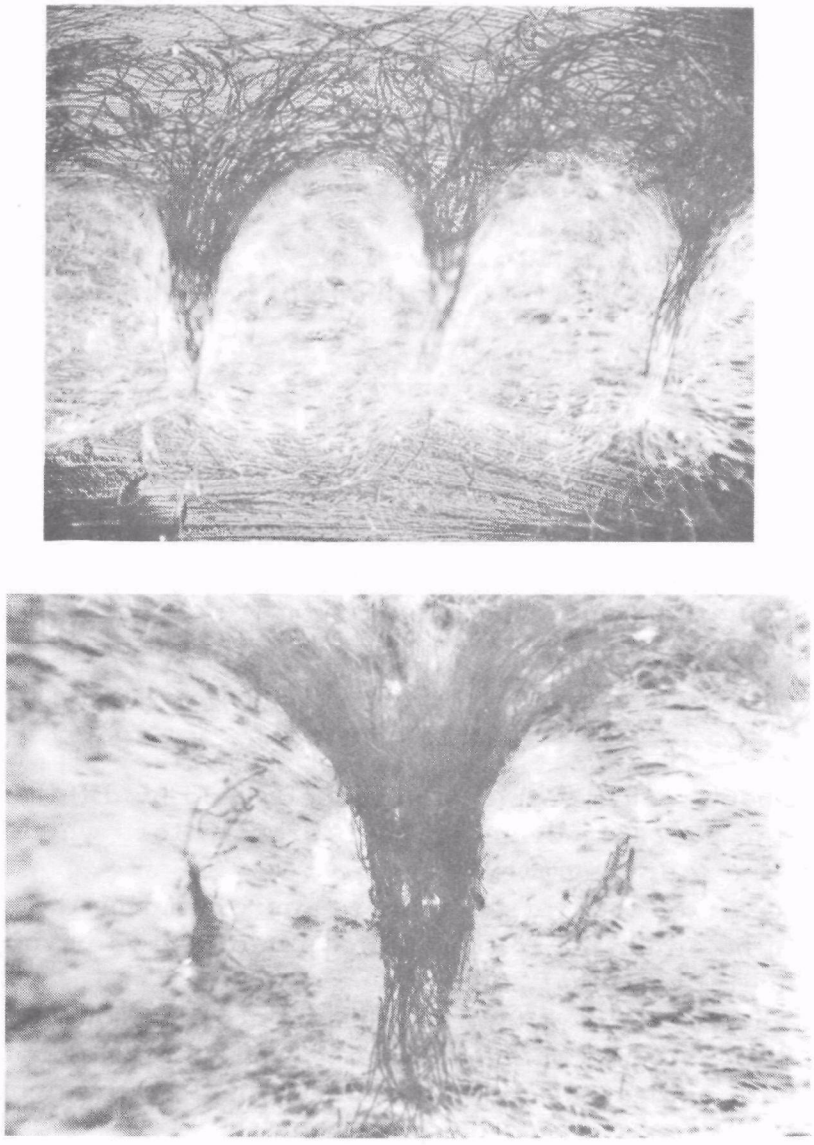

Figure 2 Cross Sections Showing Pore Formation in Needle Punched Fabric

SECTION IV

THEORY

4.1 Prediction of The Pressure Drop

The prediction and knowledge of the dependence of pressure drop on operating conditions and filter properties are essential for the development of needle punched fabrics for filteration.

4.1.1 Review of Literature

There have been many theories and models used by different investigators to predict the pressure drop through fibrous filters which can be grouped in the following two categories:

1. Idealized theoretical models approximating the actual situation to be amenable to the application of known physical and hydrodynamical concepts.
2. The variables affecting the system are grouped together from dimensional consideration to form empirical correlations with numerical constants determined experimentally through a simple curve fitting procedure.

The first of the two groups is preferred since the results can be applied to a wide range of actual untried conditions, providing the basic assumptions are valid. The second group is simpler but the results are limited in application, and their validity for other than the tried conditions is questionable.

Most of the theoretical models for sufficiently small flow through fibrous media are based on the well known Darcy's equation.

$$\Delta P = - k \mu U \Delta L \qquad (1)$$

Darcy's law implies that for sufficiently low flow through a porous medium the pressure drop is caused only by viscous energy losses. The validity of Darcy's equation for low Reynolds number Newtonian-flow has been established through many experimental studies, notably that of Chen [5] for continuum flow and that of Stern, Zeller [6] for slip flow.

Among the well known theoretical models are the channel theory, the drag theory, the theory of tortuosity, and the non-Darcy approach.

The "Channel Theory" or "Hydraulic Radius Theory"

The Channel theory has been reviewed by Chen [5] and Linkson [7]. This theory considers fibrous beds as a system of interconnected channels and the pressure drop through them is given by Darcy's law. The constant, k, in Darcy's relation is known as Darcy's drag coefficient. The reciprocal of k is commonly defined as the permeability of the medium. The dimension of the permeability is that of $(\text{length})^2$, this length was introduced by Kozeny [8] as the hydraulic radius. Darcy's equation was extended to partially include the porosity of the medium by defining an average pore velocity $\bar{v} = \frac{U}{\epsilon}$ and replacing U by $\bar{v}$ in Darcy's expression [9]

$$\Delta P = - k_a \mu \frac{U}{\epsilon} \Delta L \qquad (2)$$

and

$$k = \frac{k_a}{\epsilon} \qquad (3)$$

where k_a = constant

ϵ = porosity

Blake and Kozeny [10] used the concept of the mean hydraulic radius for correlating data on flow through granular beds and came out with the following relationship

$$\Delta P = - k_b \mu U \frac{S^2}{\epsilon^3} \Delta L \qquad (4)$$

Where S = surface area per unit volume of porous media. Carman [11] modified Kozeny relationship to relate Darcy's drag coefficient to the physical constants of the bed by the so-called Kozeny-Carman equation

$$k = \frac{k_c \, So^2 \, (1 - \epsilon)^2}{\epsilon^3} \qquad (5)$$

Where k_c is a constant found out to be 5.0 for granular beds of low porosity

So = Surface area per unit volume of solid material.

Sullivan [12] modified equation (5) to account for fiber orientations by the following relation.

$$k = \frac{k_d \, So^2 \, (1 - \epsilon)^2}{k_e \, \epsilon^3} \qquad (6)$$

Where k_d = shape factor having the same value for all geometrically similar channels.

k_e = an orientation factor, which has the value of 1 and 0.5 for fiber parallel to the flow and for fibers perpendicular to the flow respectively.

The "Drag Theory"

Brinkman [13] proved that equations based on the Channel theory are not applicable to highly porous media. Since the porosities of ordinary fibrous filters are higher than 75 percent, the application of the Channel theory is then in doubt. The Drag theory treats the walls of the fibers as obstacles to an otherwise straight flow of the viscous fluid. The pressure drop across a unit thickness of the filter is the total drag force on the fibers per unit volume of the filter. Iberall [14] used the Drag theory to obtain the pressure drop through a fibrous filter having an equipartition of the fibers in the three perpendicular direction. For fibers parallel to the direction of the superficial velocity, based on Emersleben [15] he estimated the drag froce to be

$$F = 4 \pi \mu \frac{U}{\epsilon} \qquad (7)$$

For fibers perpendicular to the direction of the superficial velocity he used Lamb's equation for the drag force of an isolated cylinder.

$$F = 8 \pi \mu \frac{U}{2(2 - \ln Re)} \qquad (8)$$

By adding the drag forces in the three perpendicular directions Iberall obtained the following equation for the pressure drop.

$$\frac{\Delta P}{\Delta LU} = \frac{16\mu}{3d_E^2} \frac{(1 - \epsilon)}{\epsilon} \frac{(4 - \text{InRe})}{2 - \text{InRe}} \tag{9}$$

Where d_E = effective fiber diameter.

Iberall found out that the experimental results were best fitted by the expression

$$\frac{\Delta P}{\Delta LU} = \frac{9.4\mu}{d_E^2} \frac{(1 - \epsilon)}{\epsilon} \frac{(2.4 - \text{InRe})}{2 - \text{InRe}} \tag{10}$$

The difference between Iberall equation and the hydraulic radius theory is that the permeability in Iberall equation is not only a function of the filter properties but also the Reynolds number. It also should be noted that equation (8) of Lamb does not take the effect of the neighboring fibers into consideration which results in underestimating the drag force especially at low Reynolds number.

Chen [5] accounted for the effect of the neighboring fibers by using Wong's [16] equation:

$$F_i = \frac{Cd_{\alpha i}}{2} \rho U^2 d_i$$

F_i = drag force per unit length of fiber with diameter d_i

$Cd_{\alpha i}$ = drag coefficient for fiber diameter d_i in filter with fiber volume fraction αi

By summing up all the drag forces on the fibers in a unit volume of filter as the pressure drop across unit thickness of filter he obtained

$$\Delta P = \frac{2}{\pi} \alpha \rho U^2 Cd_\alpha \frac{(df)_{av.}}{(df)_s^2} \Delta L$$

Where Cd_α = drag coefficient of a fiber of average size $(df)_{av}$ in a filter with fiber volume fraction α

Chen used the Wheat [17] equation rather than the Lamb equation to evaluate the coefficient Cd_α.

$$\frac{Cd_\alpha}{2} R_e = \frac{k_f}{\ln k_g \alpha^{-0.5}}$$

Accordingly the pressure drop is given by:

$$\Delta P = \frac{4}{\pi} \frac{k_f}{\ln (k_g \alpha^{-0.5})} \cdot \frac{\alpha}{1 - \alpha} \frac{\mu U \Delta L}{(df)_s^2} \qquad (11)$$

Where $(df)_s$ = surface average fiber diameter.

k_f, k_g = constants depend on the fiber orientations within the filter, and the manufacturing technique.

Chen used his experimental results to plot the group $\frac{Cd_\alpha}{2} Re$ against Re. He found that $\frac{Cd_\alpha}{2} Re$ calculated from data for one filter is independent of Re for Re < 1, which confirms Darcy's law. Wheat [17] noticed that filters containing fibers with diameters approaching the mean free path of the air molecules will show lower pressure drop at a given flow than would be expected by Darcy's law because of the slip flow phenomenon. He introduced the following relationship for Darcy's coefficient.

$$k = \frac{\bar{k}}{d_E^2} \frac{(1 - \epsilon)}{\epsilon} \qquad (12)$$

Where $\bar{k}$ is a function of Cunningham slip correction factor given by the following equation

$$\bar{k} = 0.034 + 0.601 (C - 1) \qquad (12a)$$

where C is the cunningham correction factor given by

$$C = 1 + \frac{\lambda}{d} \{2.46 + 0.82 \exp (-0.44\, d/\lambda)\} \qquad (13)$$

where λ = mean free path of the air molecules of value 6.45×10^{-6} Cm at 20°C and atmospheric pressure

d = fiber diameter

C can be approximated depending on the value of d.

For d <0.2 micron

$$C = 1 + \frac{\lambda}{d} \{2.46 + 0.82 (1 - 0.44\, d/\lambda)\} \qquad (14)$$

and for $d > 0.2$ micron

$$C = 1 + 2.46 \frac{\lambda}{d} \tag{15}$$

The scattered data used to derive equation (12) make its validity rather doubtful.

The preceeding discussion shows that the goal of the studies reviewed was to exclude as much as possible of the filter properties from Darcy's drag coefficient by introducing relations in form of $k = k^* f$ (filter properties ϵ, orientation, ---etc.) where k^* is a constant, to be evaluated experimentally, which depends only on the manufacturing technique and has the same value for all similarly constructed filters. There has also been some attempts by different investigators to evaluate theoretically Darcy's drag coefficient (k) using different mathematical models, such as the "Cell Model" and the "Brinkman Model".

The Cell Model

The Cell model or the free surface model has been developed and used to predict sedimentation by Kuwabara [18]. Kuwabara suggested for the case of parallel circular cylinders distributed at random and homogeneously in a viscous flow that there has to be an envelope or a free surface around each cylinder at which both the vorticity and the normal component of the velocity vanish. The imaginary free surface is assumed to be coaxial with the circular cylinder and of radius "b". The cross-sectional area πb^2 of the imaginary free surface is equal to the free area corresponding to each cylinder, namely

$$\pi b^2 = 1/n \tag{16}$$

where n = number of solid cylinders per unit area.

Happel [19] extended the application of Kuwabara cell model to fibrous filters. The only difference between Happel and Kuwabara's assumptions is that Happel assumed that the shear stresses, instead of the vorticity, vanish at the free surface. He applied Navier-Stokes equation in cylinderical coordinates in the complete form for the fibers parallel to the direction of superficial velocity and obtained the following expression for Darcy's drag coefficient

$$1/k_2 = \frac{1}{8b^2}\left(4a^2b^2 - a^4 - 3b^4 + 4b^4 \ln\frac{b}{a}\right) \qquad (17)$$

It should be noted that in this case the inertia terms vanish because there is no change of velocity along the fibers. For fibers normal to the flow, Happel neglected the inertia terms by applying Navier-Stokes equation in the creeping form. He obtained the following expression for Darcy's drag coefficient:

$$\frac{1}{k_1} = \frac{b^2}{4}\ln\frac{b}{a} - \frac{1}{2}\left(\frac{b^4 - a^4}{b^4 + a^4}\right) \qquad (18)$$

The value of "b" in equation (17) and (18) can be evaluated in terms of the fiber volume fraction (α) in the following way. From equation (16)

$$\pi b^2 = \frac{1}{n}$$

but
$$\alpha = \frac{n A \pi a^2 t}{A t} = n \pi a^2$$

$$\frac{1}{n} = \frac{\pi a^2}{\alpha}$$

substituting into equation (16) one gets

$$\pi b^2 = \frac{\pi a^2}{\alpha}$$

$$b = \frac{a}{\sqrt{\alpha}}$$

where A = cross section area of the filter
t = thickness of the filter
n = number of fibers per unit area.

It is clear that by decreasing the porosity, α will increase and "b" approaches "a" which means that the fibers are almost touching each other. For the above reason Happel solution fails at porosities smaller than 0.5.

Brinkman Model

Brinkman [20] stated that Darcy's drag coefficient for low velocities depends only on the filter properties and its geometrical construction

for continuum flow and also on the mean free path of air molecules for slip flow. This has been proved experimentally by Linkson et al. [7] on a wide range of glass filters by showing a linear relationship between the pressure drop per unit thickness and the superficial velocity up to 2.5 ft/sec. The relation deviates gradually from the linearity for Reynolds numbers higher than unity.

Since the pressure drop for small flow does not depend on the Reynolds number, Brinkman concluded that Stoke's law for creeping motion applies for the flow through the medium. In this case, the fiber boundaries in the vicinity of any given fiber must affect the fluid motion around that fiber in such a way that inertial effects remain negligible when compared with viscous effects through the entire region of flow. The essence of Brinkman hypothesis is that, on the average, the fluid in the proximity of an obstacle imbedded in a porous medium experiences a body damping force proportional to the velocity, in addition to viscous and pressure forces. The damping force accounts for the influence of the neighboring objects on the flow.

The essential difference between the Brinkman model and the Cell model is that Brinkman model implies that the neighboring fibers damp the ensemble average microscopic flow near the central fiber precisely the same way the fibers of the medium damp local flow through the medium when averaged over all conceivable fiber arrangement. While the "Cell Model" account for neighboring fibers influence by means of microscopic envelope around the central fiber. The characteristic envelope size depends on the microscopic voids.

The validity of Brinkman hypothesis is limited to conditions where the neighboring fibers are distributed about the central fiber in approximately the same way as they are generally distributed in the medium. The hypothesis, therefore, breaks down when applied to media of sufficiently low porosity because in this case the effect of many solid boundaries in the immediate proximity to the central object cannot be well described by a simple damping coefficient.

Brinkman [20] initially used his hypothesis to investigate flow through a swarm of spheres and hindered settling velocity. The model was also used by Debye and Bueche [21] to predict certain hydrodynamic properties of disolved polymer molecules.

Recently the Brinkman model was used by Spielman and Goren [22] to evaluate Darcy's drag coefficient mathematically for fibrous filters of different geometrical constructions and fiber orientations namely:

a. Filters with fiber axes all lying in planes perpendicular to the direction of the superficial velocity, but having completely random angles in those planes.
b. Fiber axes all parallel to the direction of the superficial velocity.
c. Fiber axes all lying in planes parallel to the direction of the superficial velocity, but having completely random angles in those planes.
d. Fiber axes completely randomly oriented in all directions.

The pressure drop results of Spielman and Goren showed better agreement with Davies [23] Empirical results than those of Kuwabara and Happel using the Cell model.

Theory of "Tortuosity"

Clarenburg and Pickaar [24] used a pure theoretical approach to predict the pressure drop through fibrous filters. The model used assumes the pores to be small capillary tubes with log-normal distribution. Starting with Poiseuilles law and using the pore distribution, they derived the following relationship.

$$\Delta P = 11.4\,\mu\,\Delta L\,\frac{U}{\epsilon}\cdot\frac{N_p}{\bar{l}^2}\left(\frac{L_E^2}{L}\right) \qquad (19)$$

where N_p = number of pores on surface area $\bar{l}^2$

$\bar{l}$ = mean fiber length

L_E = effective thickness

$\frac{L_E}{L}$ is known as Tortuosity Factor and given by

$$\left(\frac{L_E}{L}\right)^2 = 1 + (0.858\,\frac{\sqrt{1.865}}{\epsilon} - 1.024)^2\,0.389\,\frac{\bar{l}^2}{N_p\,\bar{d}^2} \qquad (20)$$

which is valid for $\epsilon < 0.94$

N_p is given by

$$N_p = \frac{N\,(N-1)}{\pi} - \frac{N}{2}$$

Where N = number of fibers in a slice of surface area $\bar{l}^2$ and thickness $2\bar{d}$

$$= \frac{8}{\pi}\,(1-\epsilon)\,\frac{\bar{d}\,\bar{l}}{d^{-2}}$$

The relationship was tested experimentally over a range of porosities 0.88 - 0.96, for which slight difference between theory and experiment were found in the high porosity range. It has been found that the theory of tortuosity leads to erroneous results for filter porosities exceeding 0.94.

Non-Darcy Approach

The one common assumption which underlines the theories and correlations so far, is the validity of Darcy's law which is only true if the flow through the medium is sufficiently low for the pressure drop to be caused only by viscous energy losses. As can be seen this assumption implies that for a given fluid flowing through a particular medium, the pressure drop is a linear function of the velocity, or simply

$$\frac{\Delta P}{\Delta L} = \gamma U$$

Where γ is a constant which is characteristic of the particular fluid and medium.

Linkson et al. [7] showed that the pressure drop is a linear function of the superficial velocity for Reynolds numbers up to unity after which a deviation from the linearity gradually appeared.

Beavers and Sparrow [25] used a more generalized equation for the pressure drop through fibrous media which is represented by

$$-\frac{\Delta P}{\Delta L} = k\,\mu\,U + \eta\,\rho\,U^2 \qquad (21)$$

where η = constant,
k = Darcy's drag coefficient.

Equation (21) differs from Darcy's equation by the term ($\eta \rho U^2$) which represents the inertial effects at high Reynolds numbers. The results of the experimental work of Beavers and Sparrow showed that the constant η is independent of the superficial velocity U.

Dimensional Analysis Approach

Davies [23] used the dimensional analysis approach to derive a relation between the pressure drop through fibrous filters and their solid fraction (α) for fibers with axes perpendicular to the direction of the superficial velocity U. From dimensional analysis, assuming Darcy's law of flow through porous media, Davies suggested that a unique relation must exist between α, the packing density, and the dimensionless group,

$$4 \frac{\Delta P}{\Delta L} \cdot \frac{A a_e^2}{Q}$$

where A = area of filter
a_e = mean fiber radius.

Davies had difficulty in defining the fiber radius as the dispersal of the fiber material is rarely so perfect that the fibers act individually. In fact, the effective fiber radius is usually greater than the actual radius measured under a microscope. Some tendency to clumping exists and the air prefers to flow through open interstices, avoiding the fine spaces within clumps. Errors due to these causes are diminished by introducing an effective radius (a_e) determined empirically. Measurements on actual pads made of wide variety of fibrous materials showed a small "scatter" about the curve.

$$4 \frac{\Delta P}{\Delta L} \frac{A a_e^2}{Q \mu} = 64 \alpha^{1.5} (1 + 56 \alpha^3) \qquad (22)$$

Davies stated that there is no appreciable dependence on the length of fiber. The left hand side of equation (22) is known as the permeability coefficient.

Davies claimed that his expression is valid for fiber diameter ranging from 1.6 - 80 microns and filter porosities ranging from 0.700 - 0.994. Davies equation does not show any dependence of the pressure drop on the structural arrangement of the fibers in the filter which has been shown by Chen [5] to be of importance.

Davies also neglected the effect of the slip flow for the low range of fiber diameter which has been pointed out by Wheat [17] to be of great importance.

Werner and Clarenburg [26] studied pressure drop through glass fiber filters for fiber diameters in the order of the mean free path of the air molecules for all fibers perpendicular to the direction of the superficial velocity. They found out a linear relation between Davies permeability coefficient and the porosity function defined by $(1 - \epsilon)^{3/2}$ for a given filter. The ratio between the permeability coefficient and the porosity function is known as the resistance coefficient. They plotted the experimental results between the resistance coefficient and Cunningham slip factor given by equations (13), (14), and (15), and came out with the following relationship.

$$\text{The resistance coefficient} = 180\ C^{-2.5} \tag{23}$$

and hence the pressure drop is given by

$$\Delta P = 180\ C^{-2.5}\ \frac{\mu\ \Delta L\ U}{d_e^2}\ (1 - \epsilon)^{3/2} \tag{24}$$

where C = Cunningham correction factor

4.1.2 Mathematical Development of The Pressure Drop For Needle Punched Fabrics

As needle punched fabrics are usually highly porous, it can be concluded from the review that the channel theory and the theory of tortuosity are not suitable to adopt. A geometrical model based on the drag theory is devised to describe the flow through the fabric. The Brinkman model, used by Spielman and Goren [22], has been adopted since their results were in better agreement with Davies empirical equation than those of Kuwabara and Happel using the cell model.

The model can be described, as shown in Figure 3, as:

a. The fibers around the pores are assumed to lie in planes perpendicular to the direction of flow, with the fibers randomly distributed in each plane.
b. The fibers in the pores are assumed parallel to the direction of flow.

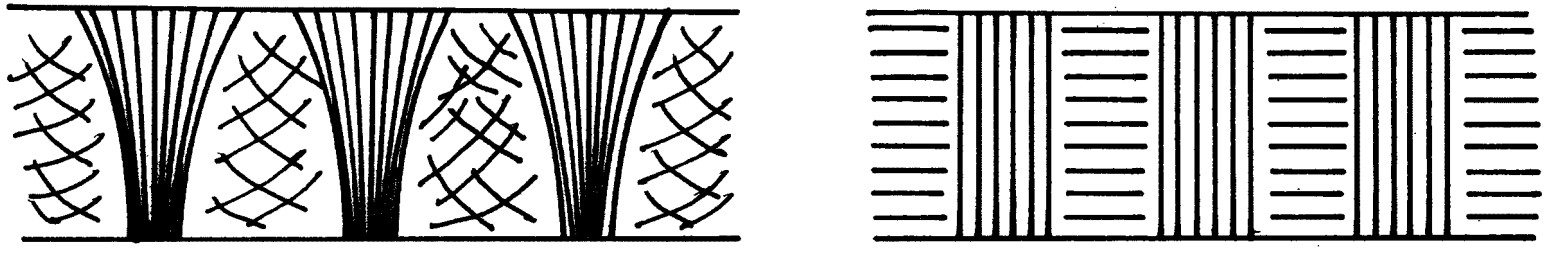

THE NEEDLE PUNCHED FABRIC THE MODEL

Figure 3.

Referring to the geometrical model, let α_1 be the volume of fibers per unit volume of fabric of the fibers in the areas around the needle pores; and α_2 be the volume of fibers in the pores per unit volume of fabric. The equivalent solid fraction of the fabric (α) may be expressed as:

$$\alpha = \alpha_1 + \alpha_2 \tag{25}$$

The total drag force per unit volume of the fabric may be predicted by calculating the drag force per unit length of the individual fibers in the fabric and then integrating over the length of all fibers per unit volume of the mat.

The Brinkman's equation gives:

$$\nabla P = \mu \nabla^2 \bar{u} - \mu k \bar{u} \tag{26}$$

∇P can be resolved into two components

$$\nabla P_1 = \mu \nabla^2 \bar{u}_1 - \mu k_1 \bar{u}_1 \tag{27}$$

normal to the fiber axis, and

$$\nabla P_2 = \mu \nabla^2 \bar{u}_2 - \mu k_2 \bar{u}_2 \tag{28}$$

parallel to the fiber. k_1 and k_2 are Darcy's coefficients normal and parallel to the fiber axis respectively.

For the first group of the mat fibers with all fiber axes normal to the direction of the superficial velocity equation (28) drops out and the governing equations are

$$\nabla P_1 = \mu \nabla^2 \bar{u}_1 - \mu k_1 \bar{u}_1$$

and

$$\nabla \cdot \bar{u}_1 = 0 \qquad \text{(continuity)}$$

The solution of the field (P_1, $\bar{u}_1$) is readily found by assuming the appropriate pressure and stream functions. According to Spielman and Goren [23] the drag force for slip flow is:

$$F_{D_1} / 4\pi \mu U = \tfrac{1}{2} (k_1 a^2) + G(k_n', k_1 a^2) \{1 + k_1^{\frac{1}{2}} a K_1 (k_1^{\frac{1}{2}} a) K_o K_1^{\frac{1}{2}} a)\} - 1$$

$$= \varphi_1 (k_n', k_1 a^2) \tag{29}$$

while for continuum flow is

$$F_{D_1} \Big/ 4\pi \mu U = \tfrac{1}{2} (k_1 a^2) + (k_1^{\frac{1}{2}} a) K_1 (k_1^{\frac{1}{2}} a) \quad K_o (k_1^{\frac{1}{2}} a) \equiv \varphi_1 (0, k_1 a^2) \tag{30}$$

where F_{D_1} is the drag force per unit length of the fibers of the first group K_0, K_1 are modified Bessel functions of zero and is first order.

The total drag froce of a unit volume of the mat due to the first group of fibers (normal) is given by

$$F_1 = F_{D_1} (\alpha_1 / \pi a^2) \tag{31}$$

For the second group of fibers (all axes parallel to the superficial velocity) there is only one component of velocity u_{2z} given by

$$u_{2z} = U \left[1 - \frac{K_o (k_2^{\frac{1}{2}} r)}{K_o (k_2^{\frac{1}{2}} a) + k_n' (1 + k_n')^{-1} k_2^{\frac{1}{2}} a K_1 (k_2^{\frac{1}{2}} a)} \right] \tag{32}$$

and the drag force per unit length for the second group of fibers (parallel) is given by

$$F_{D_2} \Big/ 4\pi \mu U = \tfrac{1}{2} \left| K_o (k_2^{\frac{1}{2}} a) \Big/ k_2^{\frac{1}{2}} a K_1 (k_2^{\frac{1}{2}} a) + k_n' \Big/ (1 + k_n') \right|^{-1}$$

$$\equiv \varphi_2 (k_n', k_2 a^2) \tag{33}$$

again for continuum flow

$$F_{D_2} \Big/ 4\pi \mu U = \tfrac{1}{2} \left[(k_2^{\frac{1}{2}} a) K_1 (k_2^{\frac{1}{2}} a) \Big/ K_o (k_2^{\frac{1}{2}} a) \right] = \varphi_2 (O, k_2 a^2) \tag{34}$$

The total drag force of a unit volume of the mat due to the second group of fibers (parallel) is given by

$$F_2 = F_{D_2} (\alpha_2 / \pi a^2) \tag{35}$$

The total drag force of a unit volume of the mat due to all fibers is given by

$$F = F_1 + F_2 = (F_{D_1}\alpha_1 + F_{D_2}\alpha_2) \Big/ \pi a^2 = (\varphi_1\alpha_1 + \varphi_2\alpha_2)\frac{4\mu U}{a^2} \quad (36)$$

Then

$$\frac{dp}{dL} = -\frac{4\mu U}{a^2}(\varphi_1\alpha_1 + \varphi_2\alpha_2) \quad (37)$$

Knowing the values of k_1 and k_2, the numerical values of the functions φ_1 and φ_2 can be evaluated and the pressure gradient can be calculated from equation (37) for the given medium and the fabric properties.

Determination of Darcy's Drag Coefficients k_1 and k_2

To determine the coefficient k_1 for the first group of fibers, consider a unit volume of a hypothetical fabric having geometrical construction similar to that of the fibers in the unpunched areas with solid fraction α_1^*. Using equation (31) along with Darcy's equation gives

$$F_1^* = F_{D1}\left(\frac{\alpha_1^*}{\pi a^2}\right) = \mu k_1 U \quad (38)$$

As the Knudsen number for the range of fiber diameters used in this investigation is very small the flow is considered continuum. Accordingly from equation (29)

$$F_1^* = 4\pi\mu U\left[\tfrac{1}{2}(k_1 a^2) + \frac{(k_1^{\frac{1}{2}} a) K_1 (k_1^{\frac{1}{2}} a)}{K_o (k_1^{\frac{1}{2}} a)}\right] \cdot \left(\frac{\alpha_1^*}{\pi a^2}\right) \quad (39)$$

and

$$k_1 = \frac{4\alpha_1^*}{a^2}\left[\tfrac{1}{2}(k_1 a^2) + \frac{(k_1^{\frac{1}{2}} a) K_1 (k_1^{\frac{1}{2}} a)}{K_o (k_1^{\frac{1}{2}} a)}\right] \quad (40)$$

This equation gives k_1 implicity with a_1^* as a parameter and can be solved by iteration. Newton's-Raphson method is adopted to insure covergence and to save computational time. The results are plotted in Figure 4 which gives values of k_1 for different values of α_1^*.

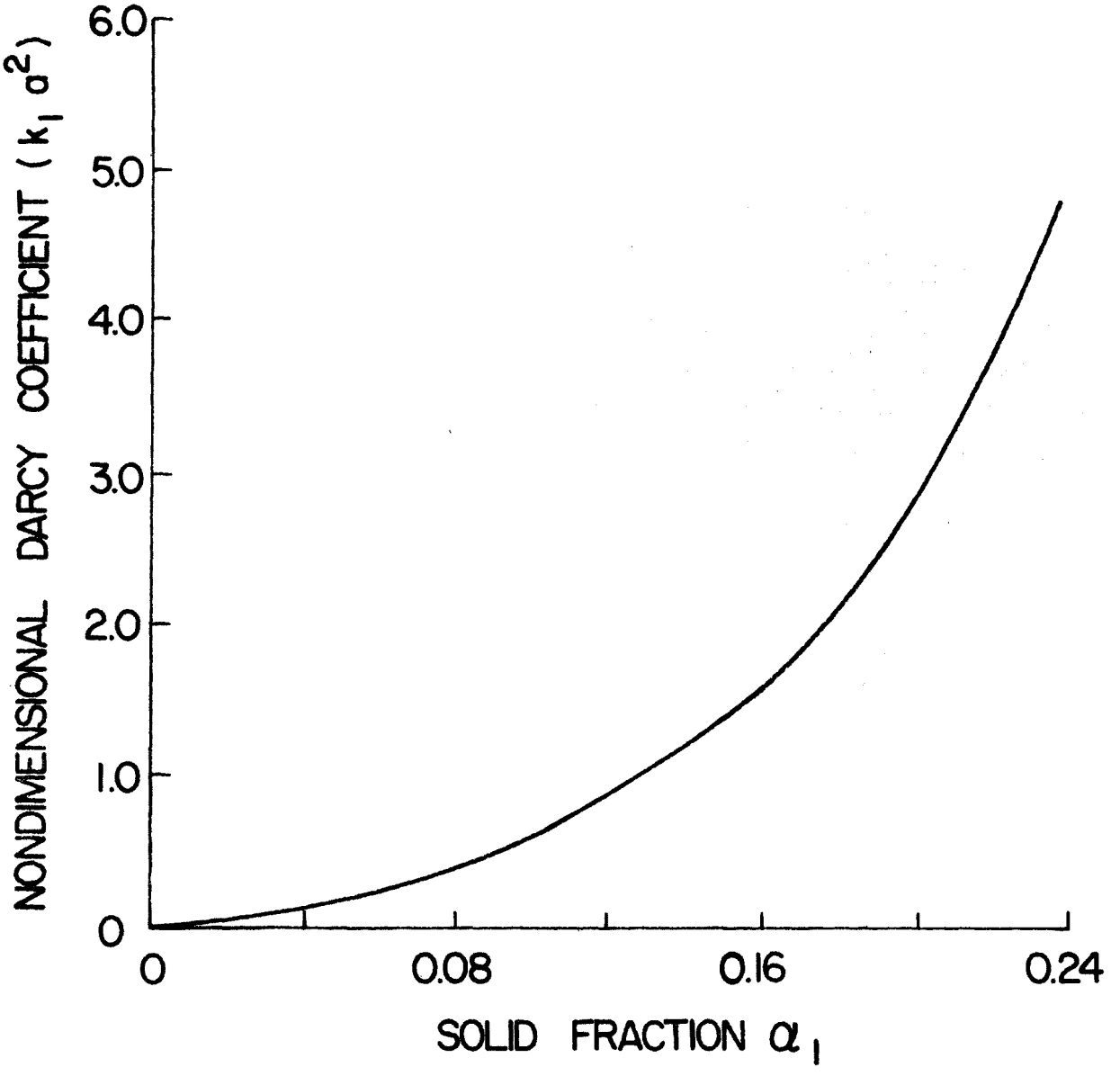

Figure 4. Nondimensional Darcy coefficient vs. solid fraction

To determine the coefficient k_2 for the second group of fibers, consider a unit volume of a fabric having geometrical construction similar to that of the fibers in the pores with solid fraction α_2^*. The total drag force of a unit volume of the mat is given by

$$F_2^* = F_{D_2} \left(\frac{\alpha_2^*}{\pi a^2}\right) = \mu k_2 U \tag{41}$$

From equation (34) and (41) k_2 can be expressed as

$$k_2 = \frac{2\alpha_2^*}{a^2}\left[\frac{(k_2^{\frac{1}{2}} a) K_1 (k_2^{\frac{1}{2}} a)}{K_o (k_2^{\frac{1}{2}} a)}\right] \tag{42}$$

To solve the above equation for k_2 with α_2^* as a parameter, an iteration technique similar to that used in the evaluation of k_1 is applied. Figure 5 gives the values of k_2 for different values of α_2^*.

Determination of α_1^* and α_2^* From The Physical Properties of The Filter

The most essential parameters which describe the needle punched filters are

the solid fraction α,
the needling intensity N^*(punches/inch^2),
the filter thickness ΔL (inch),
and the needle size D (inch).

If the actual number of punches per inch^2 is N^*, the number of fibers per pore is n, and the actual diameter of the pore is D^*. Then the volume of the punched pores per unit volume of the filter is equal to $\frac{\pi}{4} D^{*2} \cdot N^*$ and, the volume around the punches per unit volume of filter is equal to $1 - \frac{\pi}{4} D^{*2} \cdot N^*$.

By definition α_2^* is the volume of fibers per unit volume of fabric having geometrical construction similar to the pore construction of the actual fabric.

$$\therefore \quad \alpha_2^* = \frac{\pi a^2 n \cdot \Delta L}{\frac{\pi}{4} D^{*2} \cdot \Delta L}$$

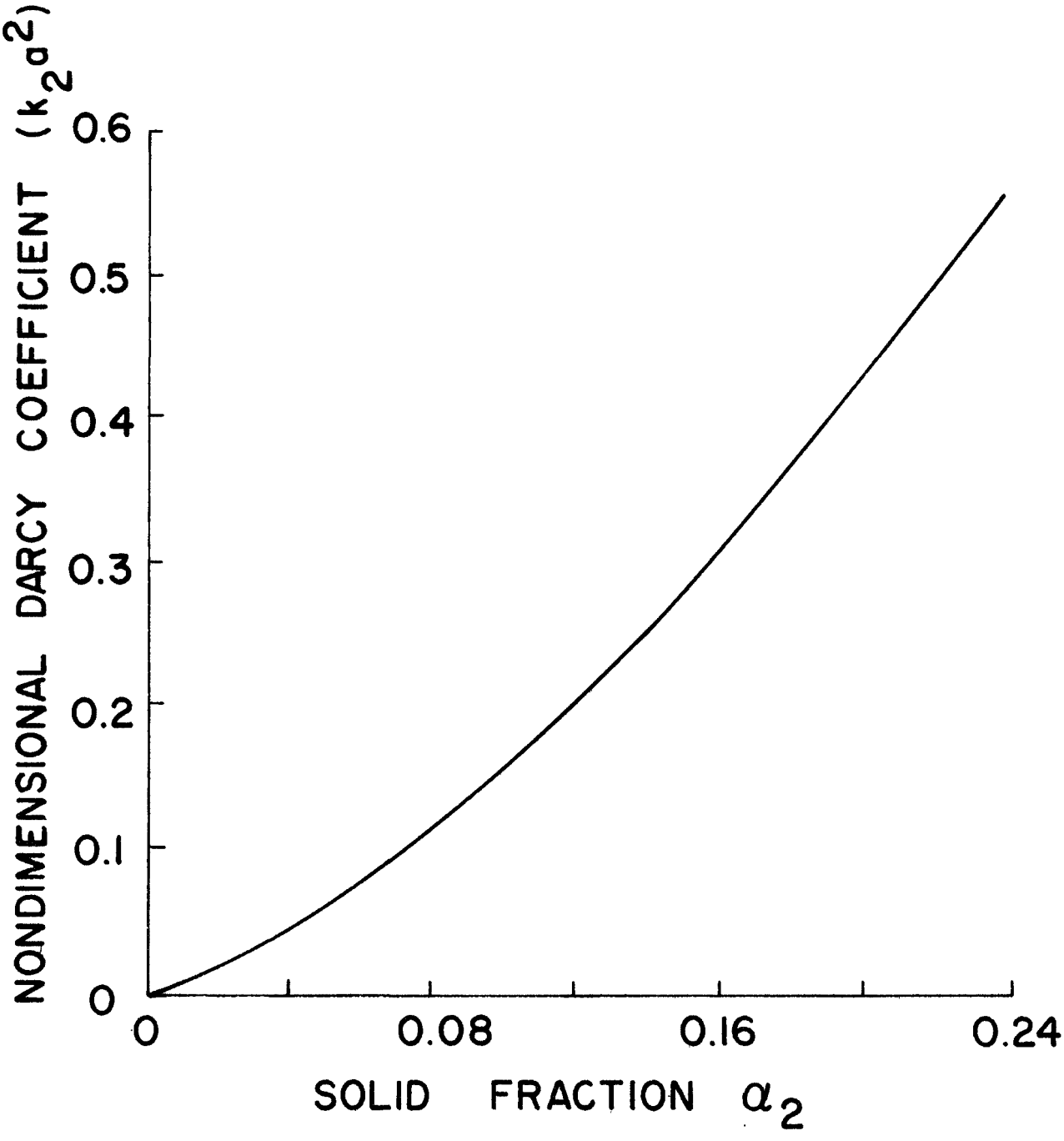

Figure 5. Nondimensional Darcy coefficient vs. solid fraction

$$\underline{i.e.} \quad \alpha_2^* = \frac{4\,a^2\,n}{D^{*2}} \tag{43}$$

Similarly for a filter having a surface area A and thickness ΔL

$$\alpha_1^* = \frac{\alpha\, A \cdot \Delta L - \pi a^2\, n \cdot A \cdot N^* \cdot \Delta L}{A \cdot \Delta L - \frac{\pi}{4} D^{*2} \cdot N^* \cdot A \cdot \Delta L}$$

$\underline{i.e.}$

$$\alpha_1^* = \frac{\alpha - \pi\, a^2\, n \cdot N^*}{1 - \frac{\pi}{4} D^{*2}\, N^*} \tag{44}$$

Equation (43) and (44) relates the solid fractions α_1^* and α_2^* to the actual parameters D^*, N^*, α and n of the filter.

It has been observed that the actual parameters of the filter such as D^* and N^* are different from the machine setting for the parameters D and N. This is mainly due to the overlapping of the pores and the relaxation of the fabric caused by the punching process.

Determination of α_1 and α_2 For The Actual Filter

For a needle punched filter α_1 is defined as the folume of fibers perpendicular to the flow per unit volume of the filter. If the solid fraction of the filter is α, A is the surface area and ΔL is the filter thickness.

$$\alpha_1 = \frac{\alpha\, A \cdot \Delta L - \pi a^2\, N^*\, n\, A \cdot \Delta L}{A \cdot \Delta L}$$

$\underline{i.e.}$

$$\alpha_1 = \alpha - \pi a^2\, n\, N^* \tag{45}$$

Similarly

$$\alpha_2 = \alpha - \alpha_1$$

$\underline{i.e.}$

$$\alpha_2 = \pi\, a^2\, n\, N^* \tag{46}$$

Prediction of The Pressure Drop

Based on the knowledge of the actual parameters (Appendix C) α, D^*, a, n, N^* and ΛL, the value of α_2^*, α_1^*, α_1 and α_2 can be calculated using equations (43), (44), (45), and (46) respectively. The Darcy's coefficients k_1 and k_2 can be evaluated using Figures 4 and 5 for the values of α_1^* and α_2^* determined previously. Using equations (30) and (34) which are presented graphically in Figures 6 and 7, the corresponding values of φ_1 and φ_2 can be obtained. The nondimensional pressure drop can then be determined using the values of φ_1, φ_2, α_1 and α_2 in equation (37).

4.2 Collection Efficiency

The mechanisms of collection that play an important role in filtration are the inertial, interception and diffusional. Although a wealth of information for the collection efficiency for each of the individual mechanisms is available, no satisfactory theoretical work exists that can generally quantify the share carried by these mechanisms when they act collectively. This is due to the fact that while most of the mechanisms are mainly affected by such variables as flow rate, size and density of dust, the filter characteristics and the properties of the medium, their effectiveness vary from one set of conditions to the other.

There are numerous theories for particulate collection developed for fibers or fibrous mats which could be applied to most nonwoven fabrics. In the case of needle punched fabrics, because of their unique structures, these theories do not apply. This is due to the in depth fiber orientation in the needle punched fabrics and the nonhomogenity of their packing density. Because of this it was felt necessary to examine the role of the various mechanisms of collection for needle punched fabrics. To this effect, the semi-empirical approach developed by Dorman [27] and used by Jonas et al. [28] and Hampl and Rimberg [29], to determine the collection efficiency was found to be best suited for this investigation.

Dorman developed the following formula, which allows for the relative contribution of inertial, diffusion and interception mechanisms of collection for particle size of 0.3 microns:

$$\log P\% = 2 - (k_R \Delta LV^2 + k_D \Lambda LV^{-2/3} + k_I \Lambda L) \qquad (47)$$

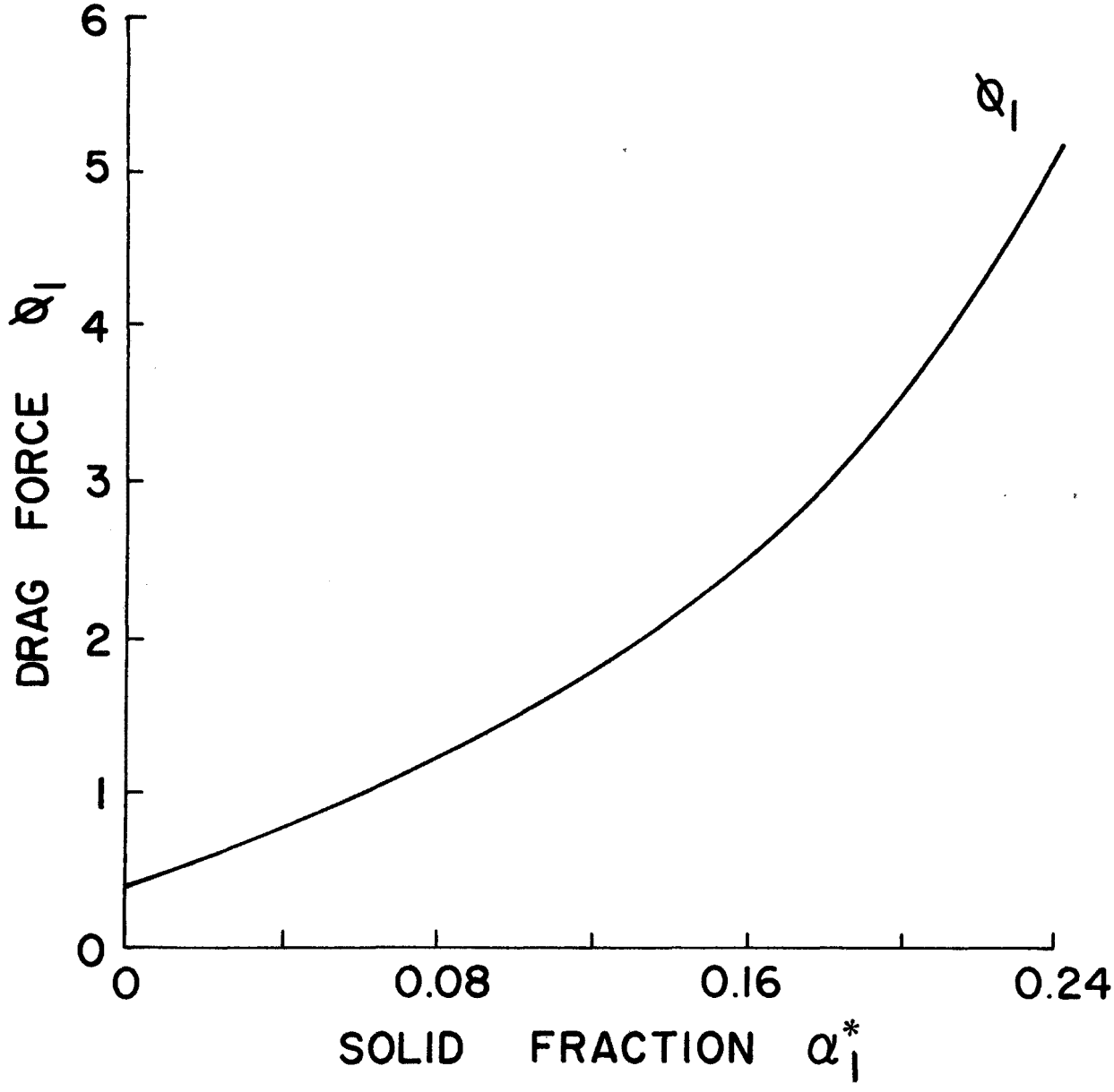

Figure 6. Drag force vs. solid fraction

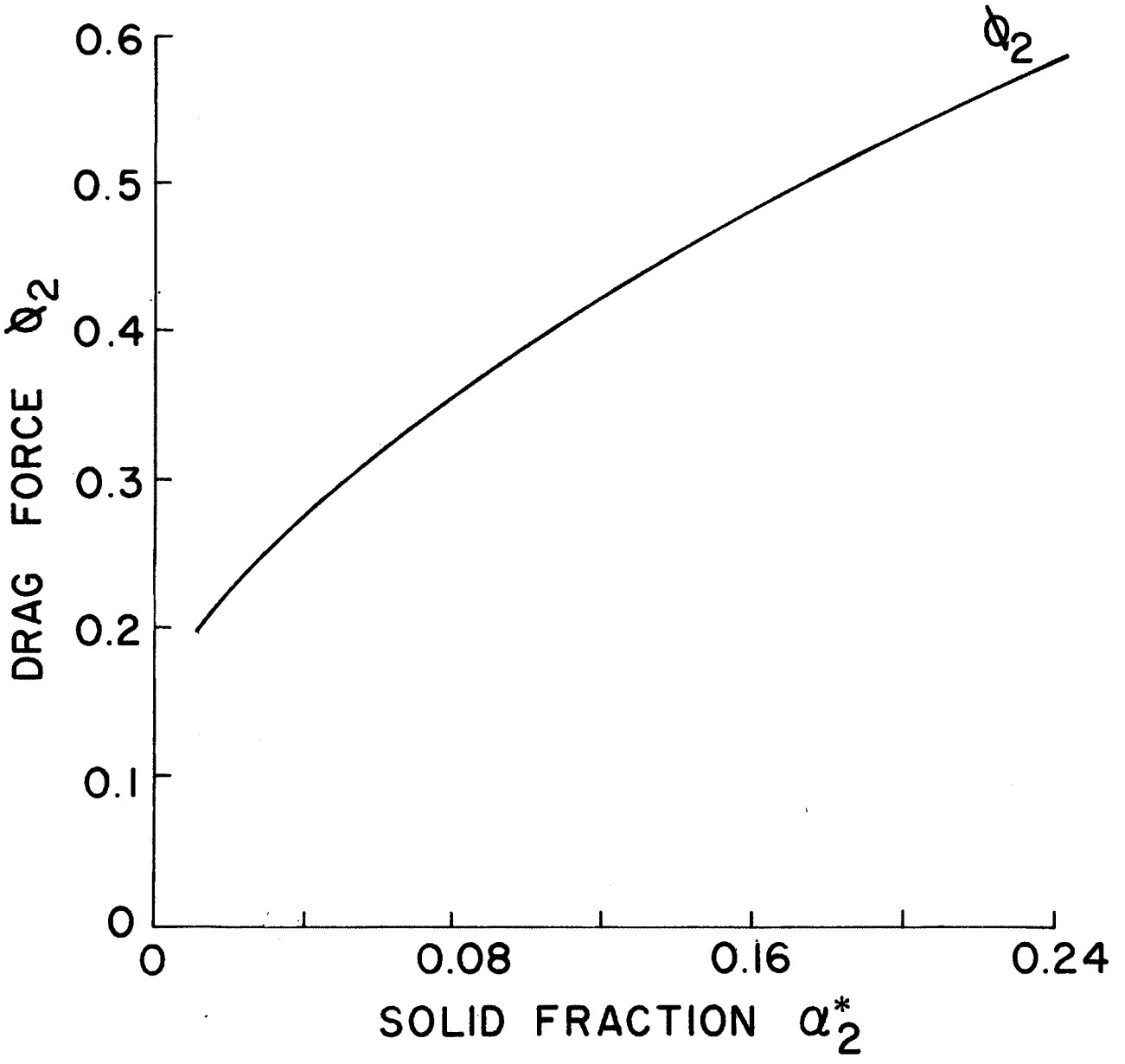

Figure 7. Drag force vs. solid fraction

where P% = percentage penetration
ΔL = filter thickness in cm
V = face velocity in cm/sec.
k_R = inertial impaction parameter in $cm.^{-3}$ sec^2
k_D = diffusion parameter in $cm.^{-1/3}$ $sec.^{-2/3}$
k_I = interception parameter in $cm.^{-1}$

Jonas et al. [38] modified Dorman's equation by using a discrete velocity for maximum aerosol penetration. When penetration is maximized, i.e., differentiating equation (47) w.r.t. V and equating to zero:

$$k_D = 3 k_R V_m^{8/3} \tag{48}$$

where V_m = the velocity at maximum penetration. Substituting for k_D in equation (47) by its value in equation (48) gives:

$$2 - \log P\% = k_R \Delta L (V^2 + 3V_m^{8/3} V^{-2/3}) - k_I \Delta L \tag{49}$$

Plotting 2 - log P% against $(V^2 + 3V_m^{8/3} V^{-2/3})$ yields a straight line whose intercept gives the value of k_I and its slope gives the value of k_R.

For the purpsoe of this investigation, not only the effect of variation in velocity on penetration was investigated, but also the effect of particle size. This sheds more light on the role of the mechanisms of collection involved and helps in the development of needle punched fabrics for filtration. This is of value in determining the contribution of the fabric structure in bag filtration, in spite of the fact that in bag filtration the dust cake plays a great role.

SECTION V

FABRIC PARAMETERS

The important parameters affecting needle punched fabric properties are: Fiber properties, fiber orientation, needling intensity, direction of needling, needle size, needle penetration, needle shape, number of barbs on the needle, the number of passages through the needling process and fabric finishing. For the purpose of this study, the needling intensity was taken as the independent variable and the effects of changing most of the other parameters is presented.

5.1 Fibers Used

The fibers used for this investigation are Dacron polyester. Polyester fibers gained general acceptance in filtration due to their excellent abrasion and dry heat resistance and low cost. In addition to these properties, it has good resistance to mineral acids and alkalies. Many types of polyester fibers are available but the major difference between these types that can be of significance in filtration, as far as nonwoven fabrics are concerned, is the specific gravity. Specific gravities of 1.22 and 1.38 are available. This means that fibers of the two types having the same denier do not have the same diameter. Most of the work was done using 1.5 inch staple x 3 denier fibers. Experiments to investigate fiber length were carried out and the results will be discussed. Since it is well known that the finer the fibers the better will be the filtration performance, attempts were made to produce fabrics from 1.5 denier fibers. Difficulties were encountered due to fiber damage and spreading which produced very weak fabrics. For this reason only the 3 denier results are presented. All fibers used had round cross-section.

5.2 Fiber Orientation

Since fiber orientation is known to be an important parameter in affecting the properties of nonwoven fabrics, two methods of producing fibrous batting have been used, these are: (a) Random-Laid; produced by air-laying of fibers on a Rando-feeder Rando-webber. To obtain the required weight a number of layers was used. (b) Cross-Lapped; produced by laying a number of layers of a cross-lapped web superimposed over each other in the same direction. Because of weight requirements, the angle of cross-lapping was 84 degrees to the direction of carding.

5.3 Needle Punching

Needle punching was carried out on a James Hunter experimental fiber locker. A wide range of needling intensity was obtained by using different fabric feeds varying between 1/16 and 3/8 inch per stroke. The fabrics were passed through the machines more than once, but in most cases the number of passages was kept down to two. The range of needling intensity used was from 122 to 735 punches/inch^2. Most fabrics were produced by needling the total number of layers without prepunching, later experiments were carried out in which prepunching the web layers was done. Three needle sizes were used, large (20 gauge), medium (25 gauge) and small (32 gauge). All needles were 3.5 inches long and had a triangular blade with 9 barbs spaced 0.083 inch apart. At the beginning, needle penetration was kept constant at one barb going through the fabric. The effect of needle penetration was later studied by increasing the penetration one barb for every experiment up to 4 barbs penetration. The number of needles used in the board was kept at 575 and the machine speed was 185 strokes/minute.

5.5 Fabrics Produced

Fabrics without scrim or support were first studied and then various types of scrim fabrics were used to provide strength and dimensional stability.

5.5 Fabric Finishing

Fabric finishing is a very important parameter in affecting the properties of a fabric. Shrinking, calendering, resin and heat treatments, etc., are possible finishing techniques which can improve the performance of needle punched fabric in filtration.

SECTION VI

FABRIC CHARACTERISTICS AND THEIR METHODS OF TESTING

Filter fabrics have to satisfy two basic requirements; to have high collection efficiency at low pressure drop and to endure the mechanical strains experienced in use. The physical properties investigated include fabric thickness, weight, density, air permeability, bursting and tensile strengths. Fabric resistance to the air flow for clean filters was measured for different rates of flow. Pressure drop and collection efficiency using flyash contaminated air were measured. Efficiency measurements using homogeneous size aerosol were also carried out. The following represents the relevant fabric characteristics and their methods of testing.

6.1 Fabric Thickness

The thickness measurements were made using a compressometer and according to ASTM Standard Method D 1777. The presser foot was 7 3/32 inches in diameter and the pressure applied was 0.005 psi (which is the lower limit recommended for nonwovens by the ASTM standard). The instrument precision was ±0.001 inch. Five measurements were made and the average was calculated.

6.2 Fabric Weight

The measurements were made for each fabric according to the ASTM Standard Method D 1910 and the average weight in oz./yd^2 was calculated.

6.3 Fabric Density

From the measurement of thickness and weight per unit area, the density of the fabrics in g/cm^3. was calculated. Since packing density, defined as the ratio between the volume of fibers to the volume of filter, is normally used to characterize filter fabrics, the values of the packing density were also calculated.

6.4 Air Permeability

The air permeability was measured according to the ASTM Standard Method D 737 using a Frazier Apparatus. The pressure drop was maintained constant at 0.5 inches of water. Five measurements were made and the average was calculated. For most textile applications the air permeability is measured in terms of the volume of air passing through the fabric per minute and per unit of area of fabric. In this case the fabric thickness is not considered important. In the case of nonwovens, such as used in this investigation, the fabric thickness varies considerably and had to be considered. Therefore the values of the modified permeability (air permeability-thickness product) were calculated.

6.5 Bursting Strength

Bursting strength is an important property for filter fabrics. The bursting strength was measured on the Scott Tester with a bursting attachment, according to ASTM Standard Method D 231. The diameter of the hole was 1.75 inch and the ball was 1 inch in diameter. Ten measurements were made and the average was calculated.

Since the fabric weight was a variable, the bursting strength was calculated by dividing the bursting load by the weight per unit area. Only bursting strength rather than tensile strength is considered since it closely relates to the deformations experienced in actual applications.

6.7 Pressure Drop and Efficiency

To test the filters for pressure drop and collection efficiency using flyash, an apparatus has been designed and constructed. It consists, as shown in Figures 8 and 9 of an air duct, a dust feeder, a testing section and a temperature and humidity control system. Efficiency

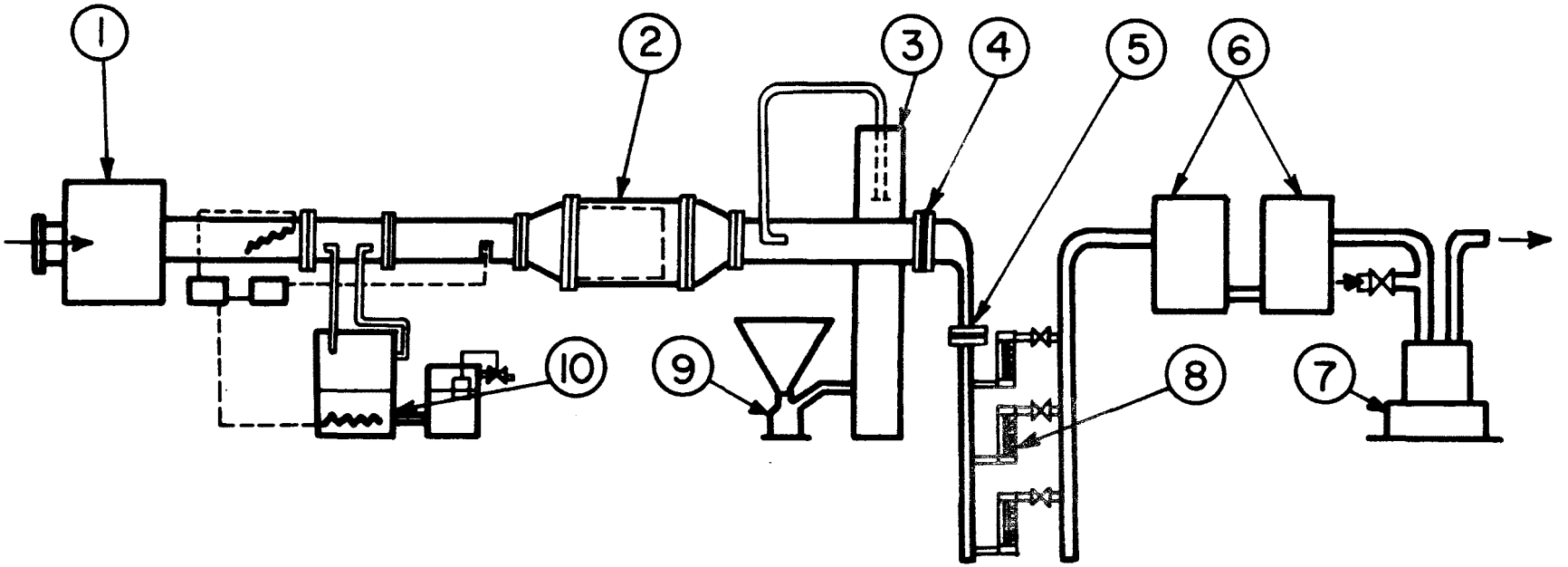

1. AIR COOLER
2. ABSOLUTE FILTER
3. SETTLING CHAMBER
4. TEST FILTER
5. HIGH EFFICIENCY FILTER
6. SURGE TANKS
7. BLOWER
8. ROTAMETER
9. DUST FEEDER
10. HUMIDIFIER

Figure 8. Apparatus

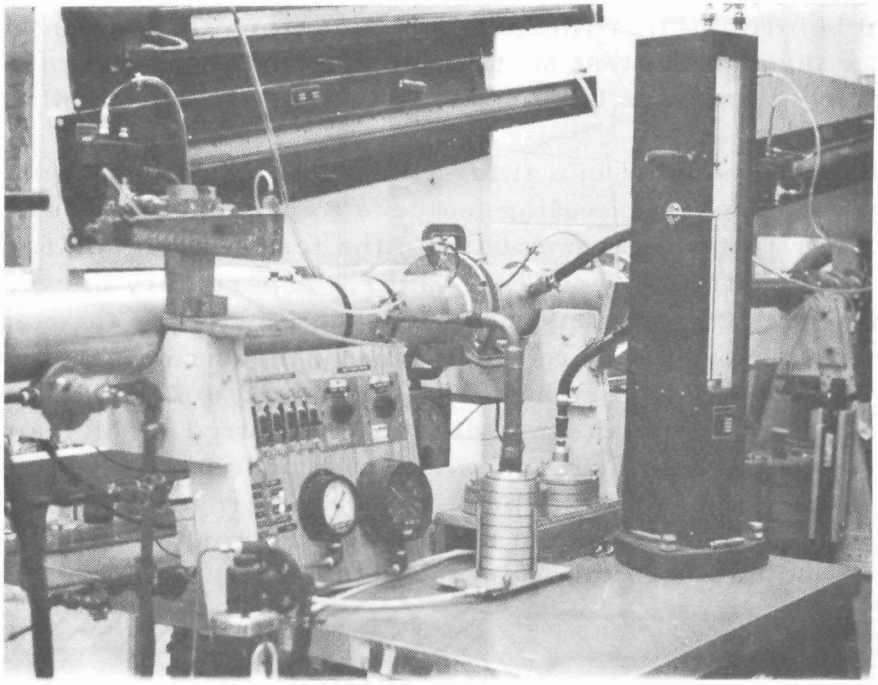

Figure 9. Centralized Controls
Flyash Apparatus

measurements using homogeneous size solid particulates were also carried out. For this purpose another apparatus consisting of an aerosol generator, test section and photometer was used.

6.7.1 Flyash Apparatus

6.7.1.1 Air Duct and Testing Section

The air duct is made of aluminum piping 4.5 inch inside diameter. An eight inch diameter section is provided at the upstream end of the duct to house an absolute prefilter to rid the incoming air from particulates larger than 0.3 micron. A 40 inch long calming section is provided before the test filter to insure uniform streamline flow. The air flow through the test section is governed by means of a gate valve and a by-pass valve located at the downstream end of the duct.

The test filter is mounted in a filter holder, as shown in Figure 10. It is designed with adequate sealing features to prevent any possible leakage either from the atmosphere to the test section or from upstream to downstream around the filter. A periphery blower having a capacity of 98.8 CFM is used to induce the flow of air through the duct. The air flow is measured by means of three rotameters manufactured by Brooks to cover the range from 0.22 to 22 CFM with precision of ±1%. A micromanometer manufactured by Meriam and having a range of 0 - 10 inches of water with precision ±.001 inch reading is used to measure the pressure drop across the filter. Two surge tanks in series are placed between the rotameter and the blower to eliminate fluctuation in the flow readings.

6.7.1.2 The Dust Feeder

The dust used for the collection efficiency tests was flyash having a classification as shown in Figure 11. A modified version of the dust feeder previously used by Lockheed-Georgia Company [30] has been adopted. A complete assembly of the feeder is shown in Figure 12 and 13. It consists of a conical dust hopper and a mixing chamber. The dust is fed from the hopper into the chamber by an auger placed centrally in a pipe extended from the bottom of the hopper. The rate of dust feeding is controlled by adjusting the speed of rotation of the auger.

A pressurized housing around the dust pipe at the exit of the dust hopper is designed with tangential air passages as shown in detail A of

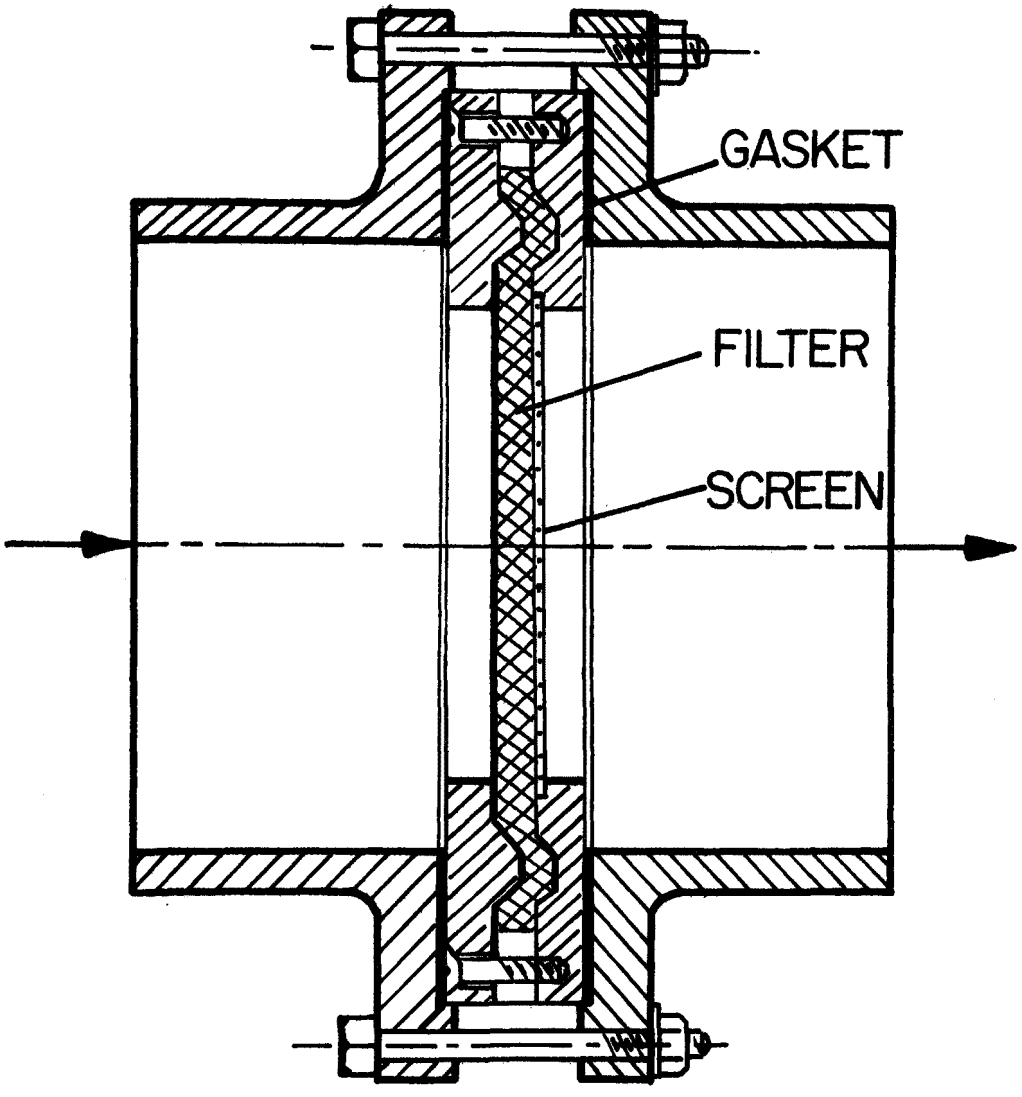

Figure 10. Filter holder

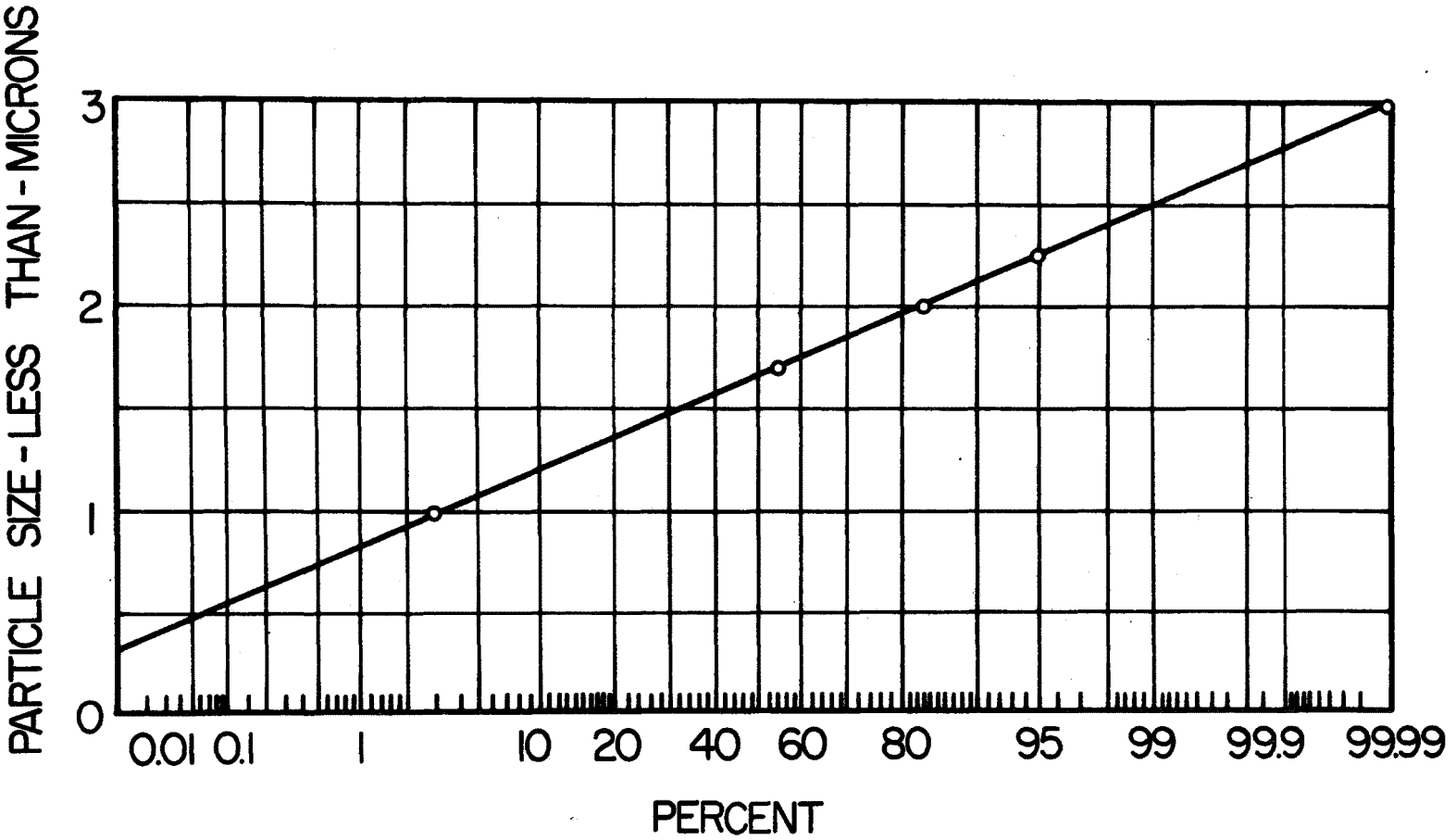

Figure 11. Cumulative particle size mass distribution

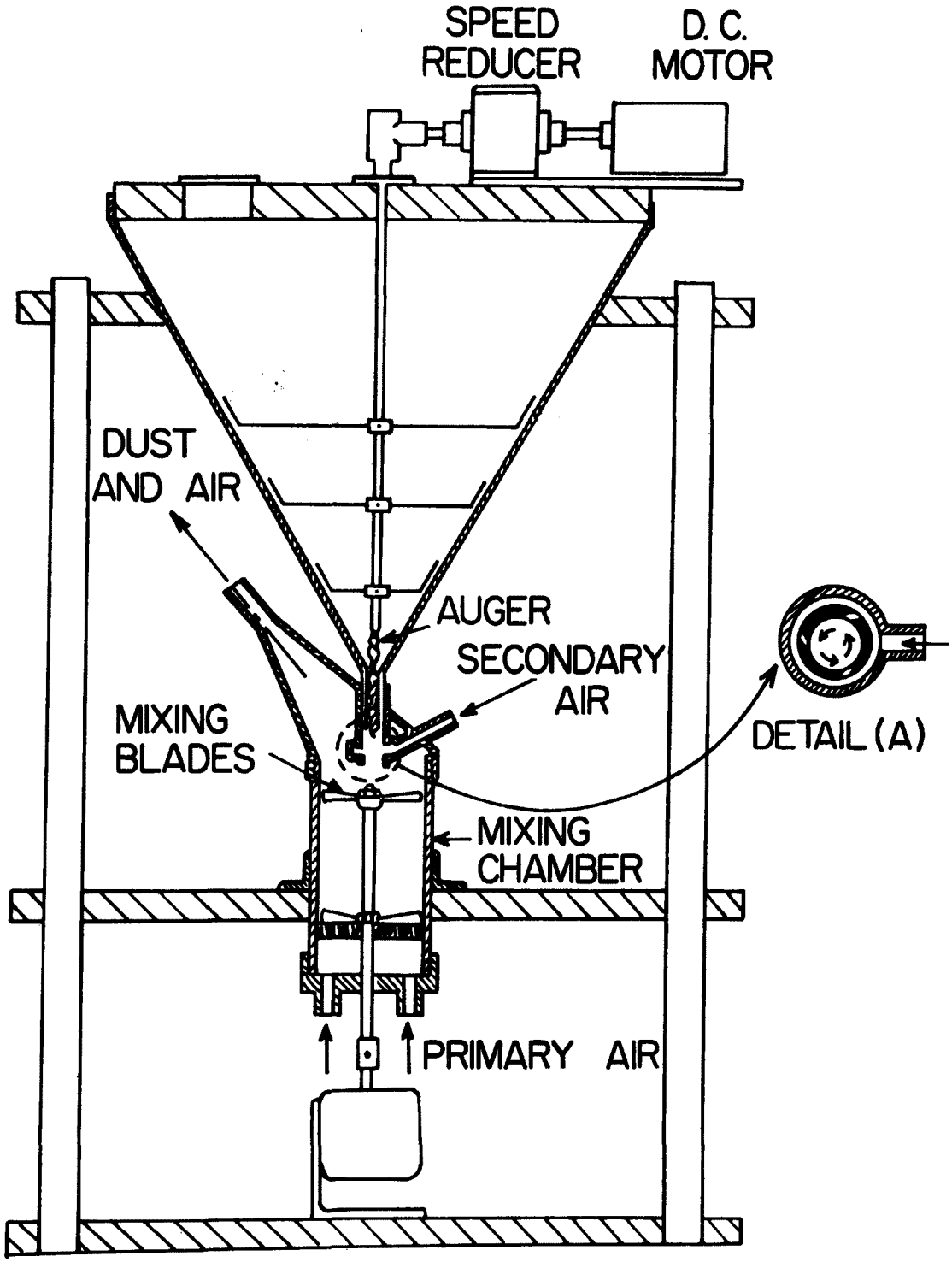

Figure 12. The dust feeder

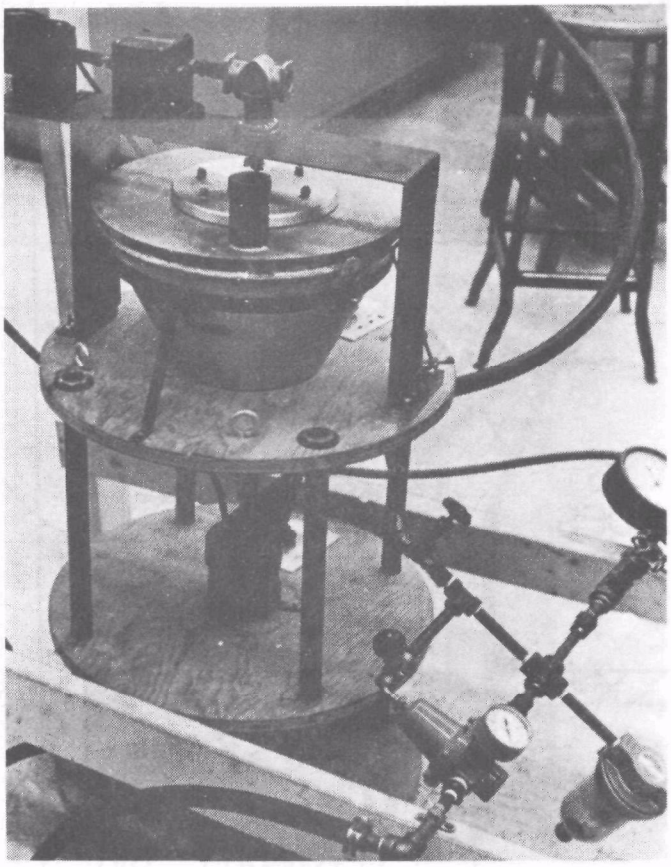

Figure 13. Dust feeder

Figure 12. This generates a swirl action which helps in breaking up any coagulated dust. Mixing blades are also used to this effect in the mixing chamber. Means to control the swirl is also instrumented in the design by controlling the air feed to the pressurized housing. The concentration and size of the particulates leaving the feeder is regulated by mixing it with controllable bled air in a vertical pipe (8 inch inside diameter and 6 feet long) before entering the main duct.

6.7.1.3 Temperature and Humidity Control System

In order to provide for specified temperature and relative humidity condition of the flowing stream, a temperature and relative humidity control system was designed and constructed as shown in Figure 14.

Air enters through an air cooling unit (1) where the temperature and humidity of the air stream are reduced from that of room conditions. An electric heater (2) is provided to raise the temperature of the air if required, while a humidifer (5) is provided to increase the relative humidity to the desired value. The humidifer is a steam generator working under atmospheric conditions. The level of the water is controlled by a float system (6). For safety purposes a low level alarm is also included whenever the float valve fails. The heating element is regulated by means of an electric control system which uses a humidity grid sensor, placed in the air stream, to sense its relative humidity.

The relative humidity of the system is controllable in the range of 30 - 99% at 75°F.

6.7.2 Latex Aerosol Apparatus

The apparatus consists of an aerosol generator, a test section, and a photometer as shown in Figure 15.

The aerosol generator is a Fluid Atomization Generator Model 7300*. It utilizes air-blast atomization and inertia impaction to produce a monodisperse aerosol. It produces aerosol at rates of up to 10^9 particles/second with size range of 0.03 to 3.0 micron.

The test section consists of a main duct 1 5/8 inch inside diameter pipe at the end of which a filter holder is attached.

*Manufactured by Environmental Research Corporation, St. Paul, Minn.

1. AIR CONDITIONER & AIR INTAKE
2. HEATING ELEMENT
3. VAPORIZOR INLET & OUTLET
4. HUMIDITY SENSING ELEMENT
5. STEAM GENERATOR
6. STEAM GENERATOR WATER LEVEL CONTROL & ALARM
7. HEATING ELEMENT CONTROLLER
8. HUMIDITY CONTROLLER

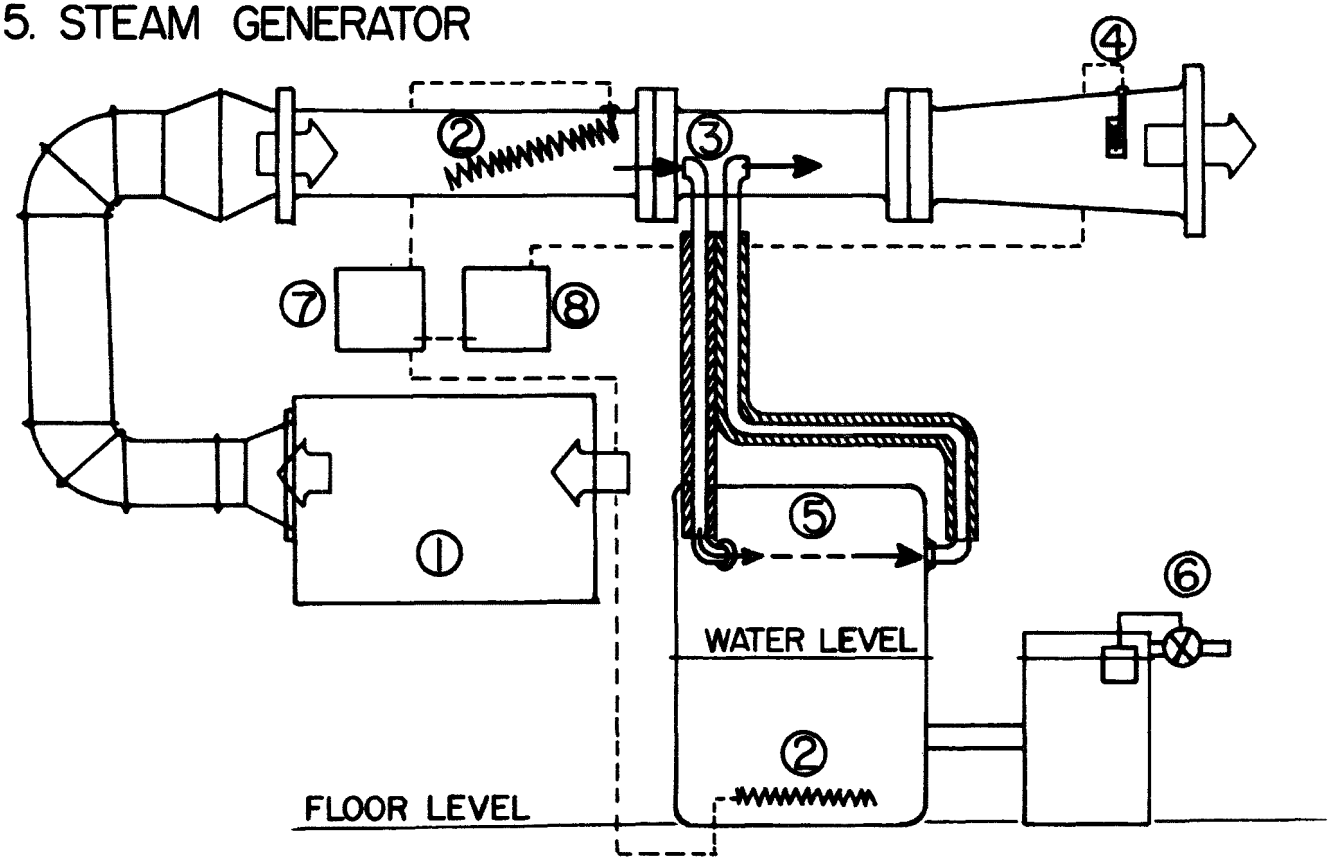

Figure 14. Temperature and humidity control system

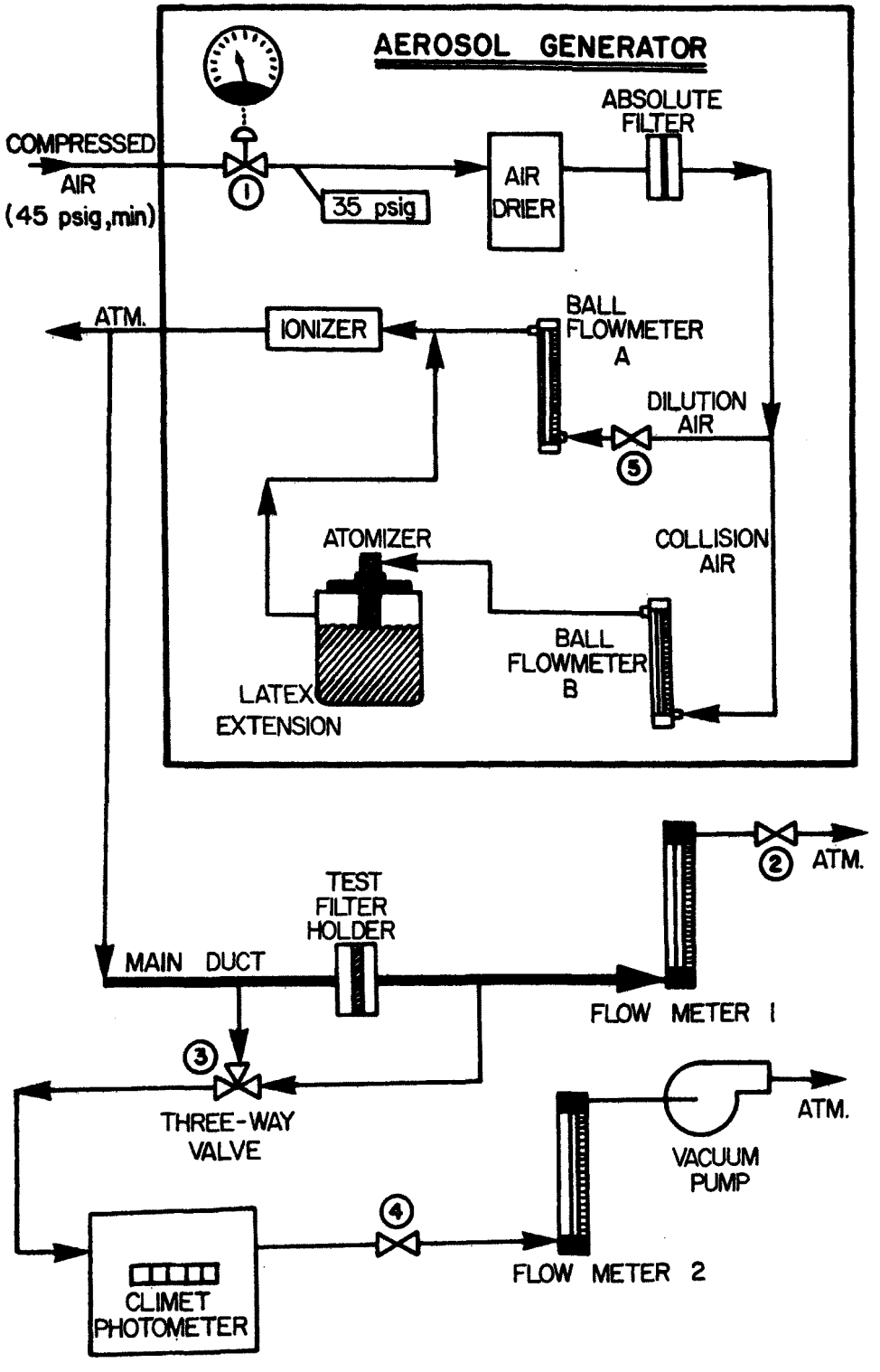

Figure 15. Aerosol penetration testing equipment

The photometer is a Climet CI-250 portable particle counter than can measure concentrations up to 10^6 particles/ft.^{3} and particle sizes larger than 0.5 micron.

6.7.3 Test Procedure

Experiments were made without dust to determine the effects of flow rate, needling intensity and the various fabric parameters on the pressure drop of the filters. The temperature and relative humidity of the air were kept at 75°F and 50% throughout these experiments and the flow rate was varied up to 200 feet/minute.

During the flyash experiments only one filtration cycle (starting with a clena filter) was used and the air velocity was maintained constant at 45 feet/minute. The efficiency of collection was determined by measuring the weight of flyash collected on the test filter and the weight of flyash penetrated during the test. Accordingly

$$\text{Collection efficiency} = \frac{\text{weight of flyash collected}}{\text{weight of flyash collected + weight of flyash penetrated}}$$

The weight of the flyash collected was obtained by weighing the test filter before and after the test. The weight of the flyash penetrated was determined by passing the air downstream through a high efficiency filter capable of capturing particulates down to 0.3 micron with 100 percent efficiency. The difference in weight of this filter before and after the test gave the weight of flyash penetrated through the test filter. The weighing was done on a sensitive balance with precision of $\pm 3 \times 10^5$g. The test duration was kept at 10 minutes and the pressure drop was recorded each minute.

In the aerosol experiments air is supplied to the aerosol generator (Figure 15) at 100 psig and is reduced to 35 psig by valve (1). After passing through a desicant air drier and an absolute filter, the air flow branches into collision air and dilution air. The collision air is always set at 9 liters/minute and the flow rate is indicated on flowmeter (B). The collision air passes through the atomizer and collides with the latex suspension which is introduced into its path. The dilution air is regulated by valve (5) to 67 liters/minute as indicated by flowmeter (A). This flow rate is sufficient to evaporate the moisture droplets in the aerosol mixture. The two branches then combine and form a mixture of air and latex particles. The aerosol then passes through the ionizer where charges on the particles are neutralized.

The aerosol is then passed through the main duct and the flow rate is varied by using valves (2) and (4). Any excess aerosol mixture is exhausted and thus the aerosol generator remains at a steady rate conditions while the system demand varies. The particles are counted by the Climet photometer before and after the test filter by means of a 3-way valve (3) for various velocities. For low velocities valve (2) is closed and the flow is controlled solely by valve (4) and the flow rate is measured by flowmeter (2). For high velocities (above 8.75 cm/sec) valve (2) is adjusted to allow a fixed flowrate to pass as indicated by flowmeter (1). Additional flow passes through the photometer and is controlled by valve (4) and measured with flow meter (2). The filter face velocity is found directly from the total flow from flowmeters (1) and (2).

SECTION VII

RESULTS AND DISCUSSIONS

In designing a filter fabric two major performance qualities have to be considered. First, the fabric performance as a filter in terms of collection efficiency and pressure drop. Second, the fabric has to possess certain mechanical properties to endure the stresses applied during filtration and cleaning cycles. The effects of the main fabric parameters on the properties of needle punched fabrics and their filtration performance are presented.

7.1 Effect of Fiber Orientation

Fabrics were produced using random-laid and cross-lapped webs having approximately the same weight per unit area. The various fabric properties were measured according to the previously mentioned procedure. Fabric thickness and weight per unit area values are given in Tables A-1 and A-2. In general, there is a considerable reduction in thickness and weight by increasing needling intensity. Random-laid fabrics had slightly lower thickness than cross-lapped fabrics. This is due to the low thickness of the original random-laid web caused by the air pressure on the fibers. Another important factor is the fiber spreading which normally takes place during needling.

Figures 16 to 18 show the effect of fiber orientation and needling intensity for the three needle sizes used. There were little differences between the density values for the two orientations, with the random-laid slightly higher than the cross-lapped. The density was increased at a diminishing rate with needling intensity, as expected. Table A-3 gives the corresponding values for the packing density.

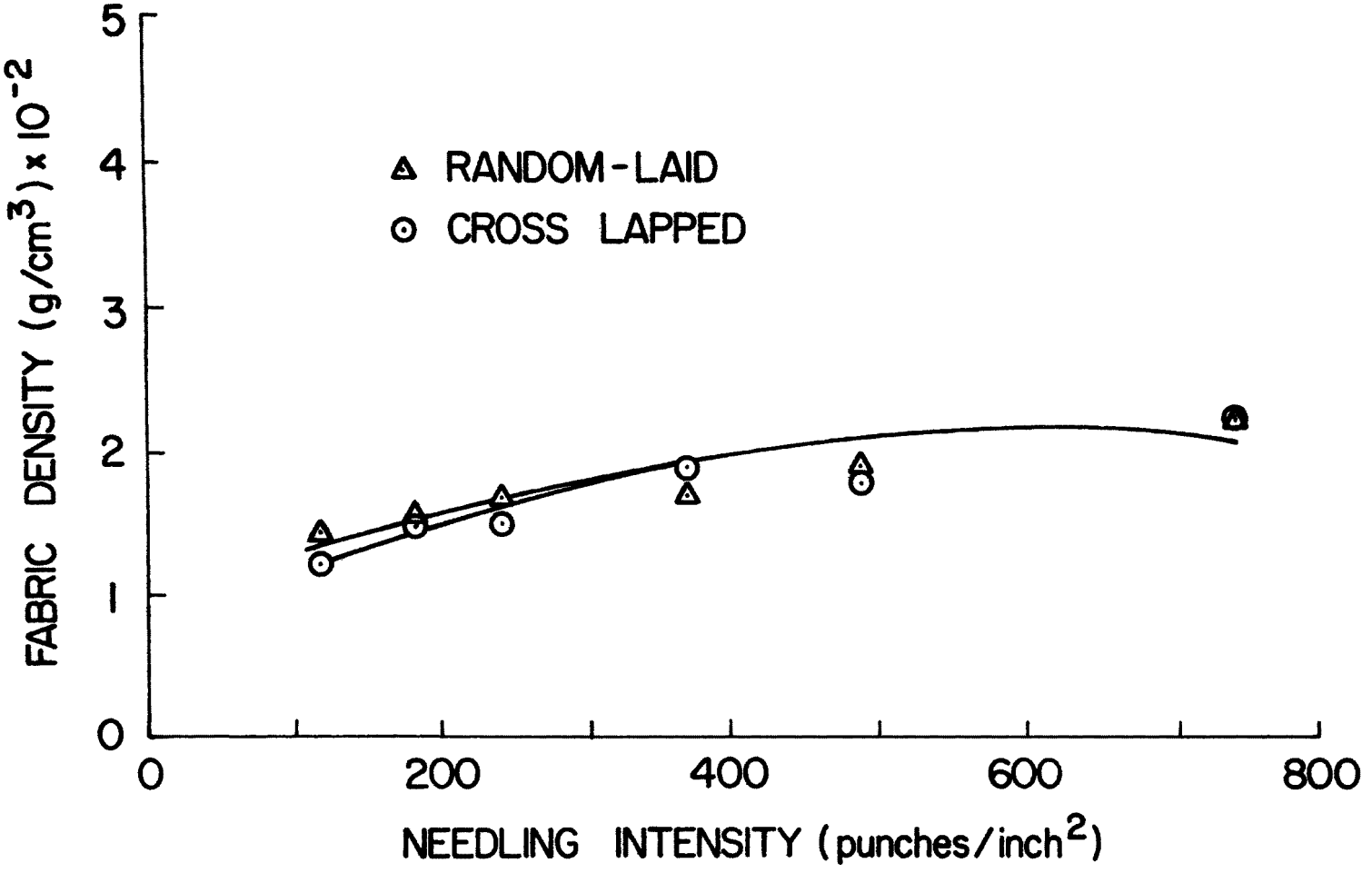

Figure 16. Fabric density vs. needling intensity (20 gauge)

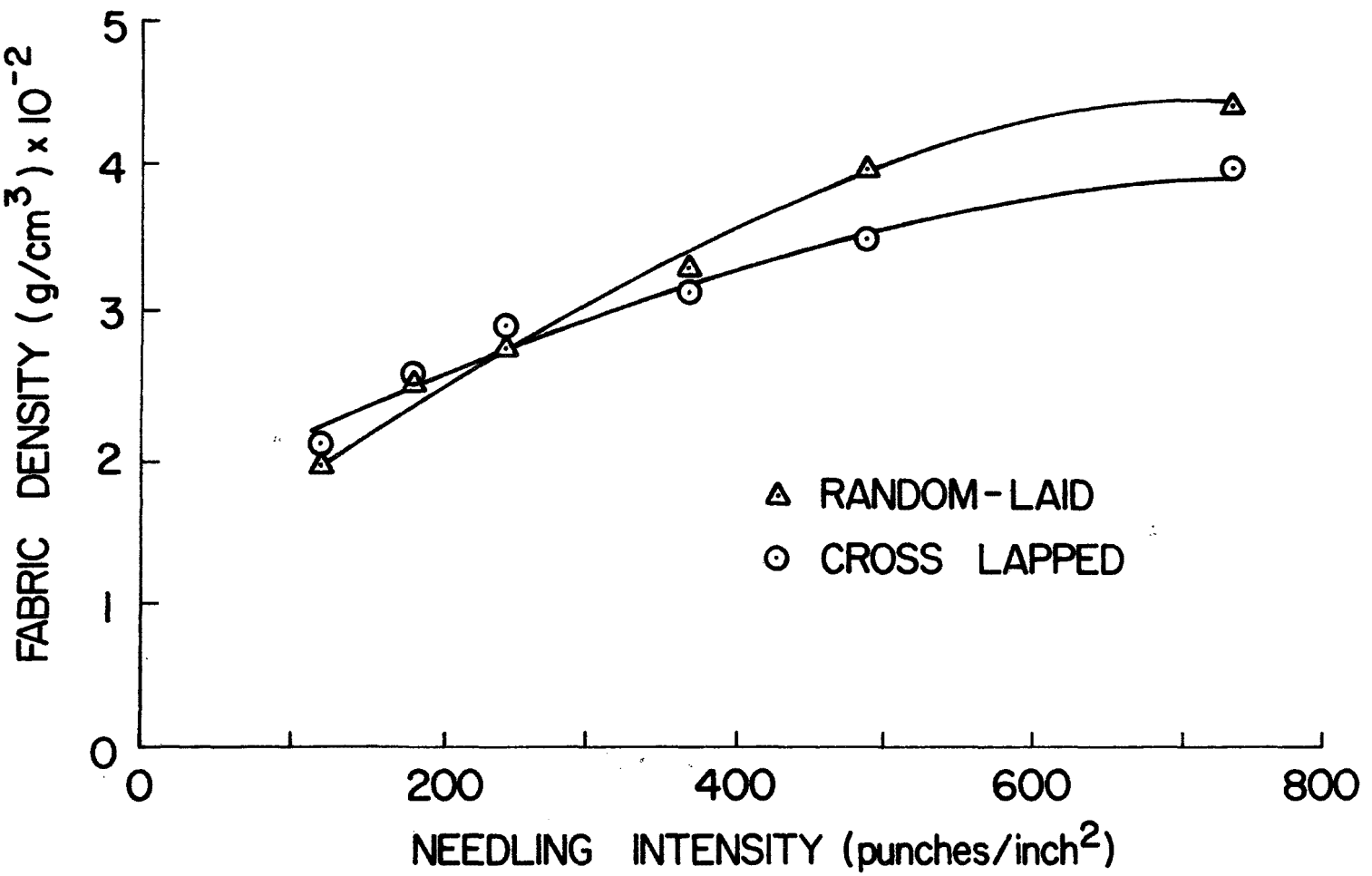

Figure 17. Fabric density vs. needling intensity (25 gauge)

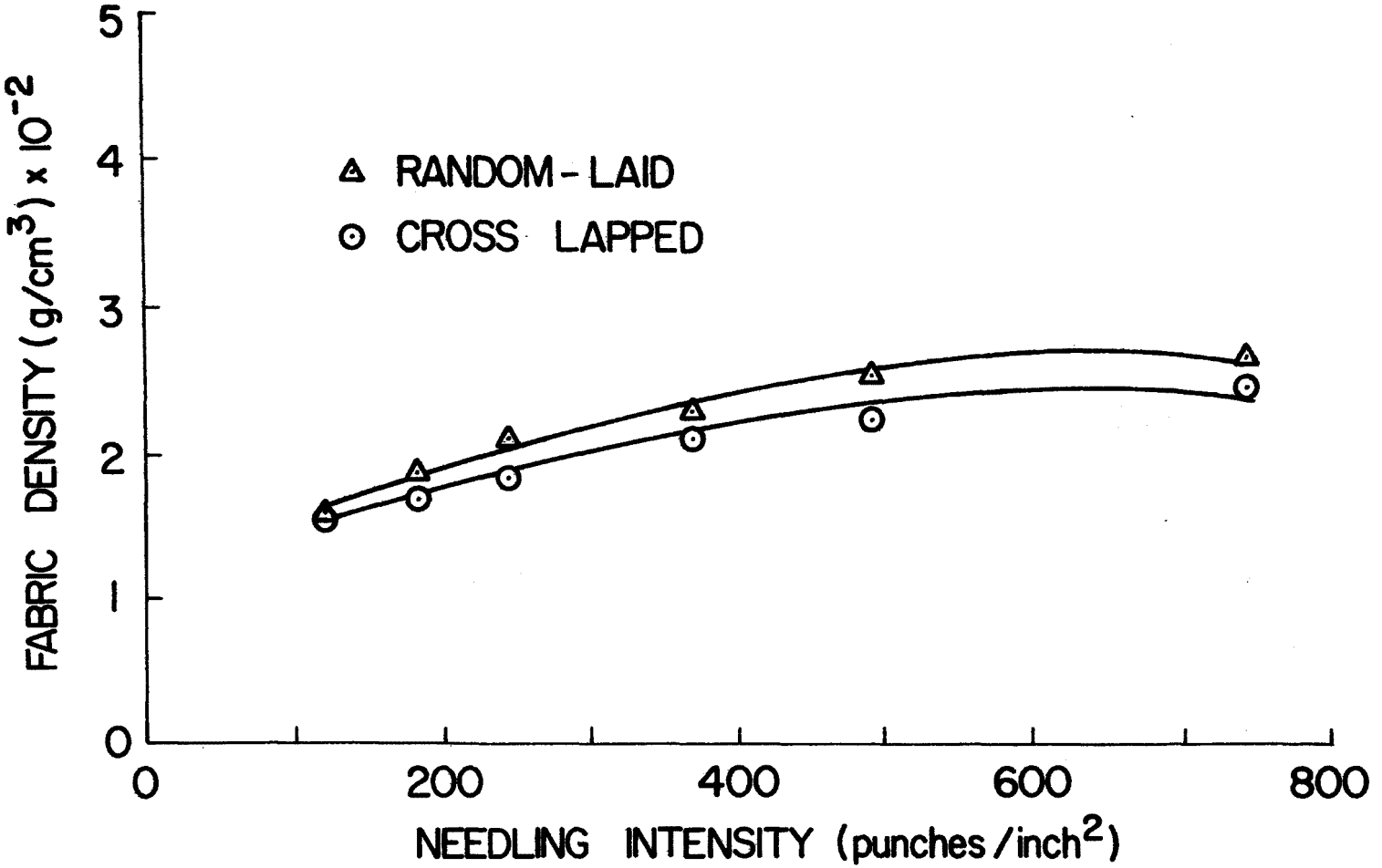

Figure 18. Fabric density vs. needling intensity (32 gauge)

Figures 19 to 21 give the air permeability results for the two fiber orientations. It can be seen that, the air permeability relationship with needling intensity shows a minimum. At low needling intensities, the effect of increasing the packing density dominates leading to the decrease in air permeability. At high needling intensities, however, the effect of punching is more pronounced and thus the increase in air permeability. It can also be seen that the effect of fiber orientation was not significant. Figures 22 to 24 show the relationship between the modified air permeability and needling intensity for the two fiber orientations. The effect of needling intensity is to reduce the air permeability-thickness product, even at high needling intensities, which is in agreement with the increase in fabric density. This shows that the air permeability-thickness product is a more accurate representation for the resistance of the needled fabric to the air flow than air permeability alone.

Bursting strength results are given in Figures 25 to 27. It is clear that bursting strength is increased with needling intensity in a similar manner to the fabric density.

The pressure drop was measured using clean air at different flow rates and the results are given in Appendix B. It was found that there were little differences in the values of the pressure drop per unit thickness at low levels of flow rate to make any conclusions related to changes in fabric structure. The results for flow rate of 90 feet/minute are presented for the two fiber orientations in Figures 28 to 30. The pressure drop per unit thickness increases with needling intensity with a diminishing rate. This is again similar to the change in fabric density with needling intensity. It can be seen that the effect of fiber orientation is very small.

Filtration results for the fabrics produced with the two orientations and the three needle sizes are given in Table 1. During the experiments, considerable variation in inlet concentration was found to occur. This was due to the extreme difficulty experienced in controlling the rate of dust feed from the hopper to the mixing chamber. For this reason the efficiency and pressure drop results are accompanied by the concentration values. It can be seen that the efficiency and pressure drop changed over a narrow range; however, on the average the random-laid fabrics gave higher efficiency than the cross-lapped fabrics.

From the foregoing discussion it was concluded that little differences existed between the fabrics produced with the two fiber orientations. In addition to the slight advantages mentioned for the random-laid

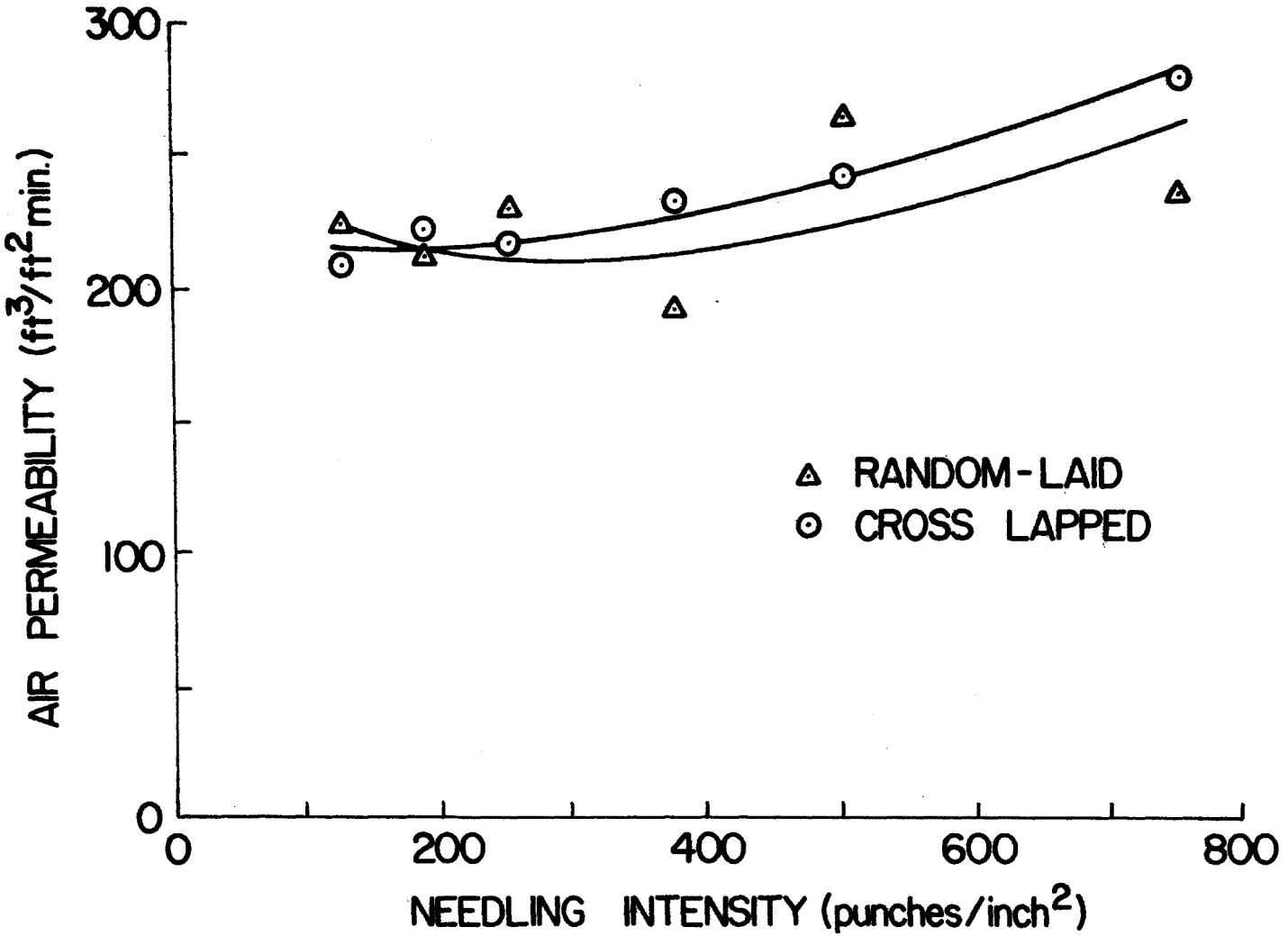

Figure 19. Air permeability vs. needling intensity (20 gauge)

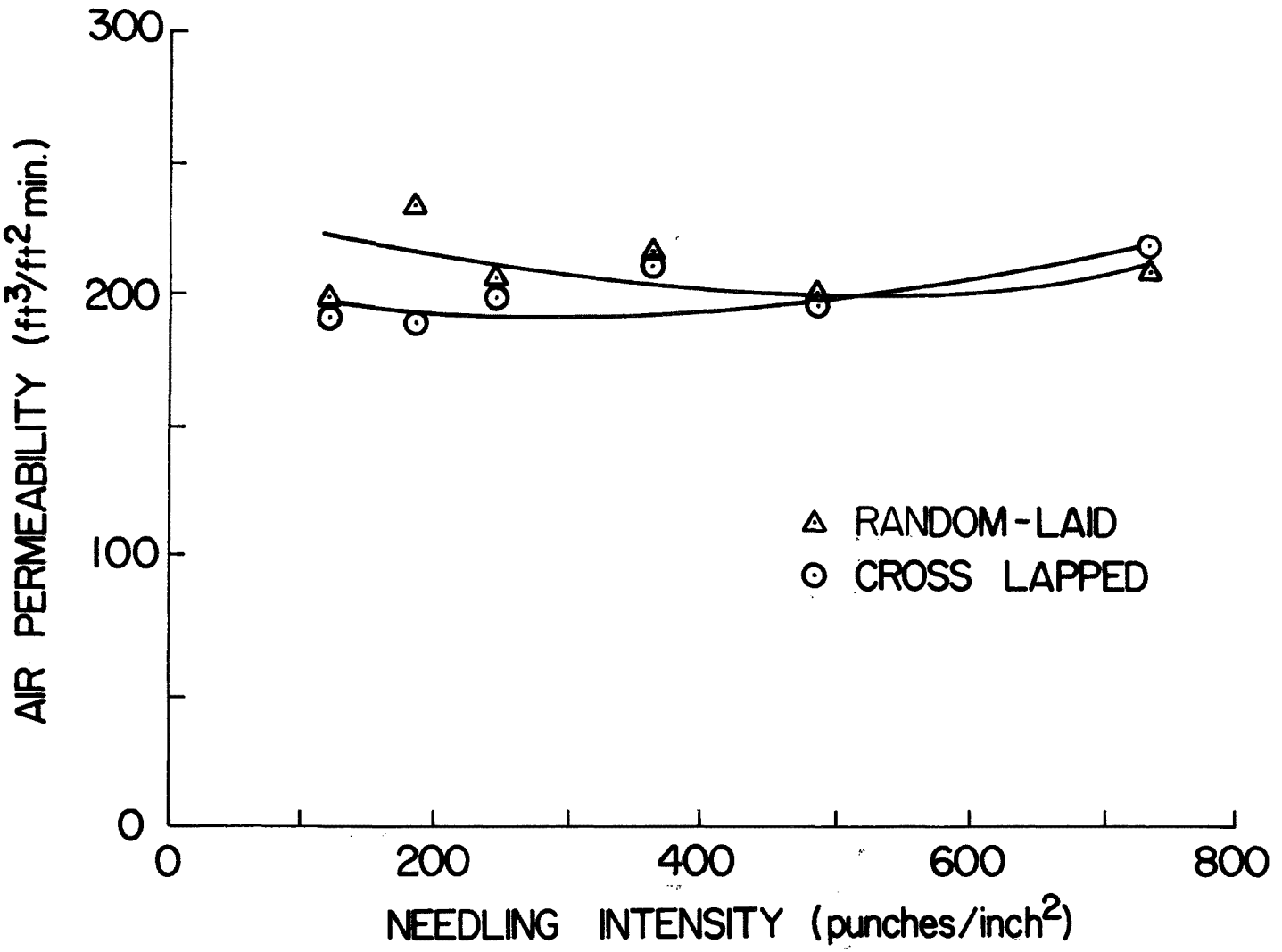

Figure 20. Air permeability vs. needling intensity (25 gauge)

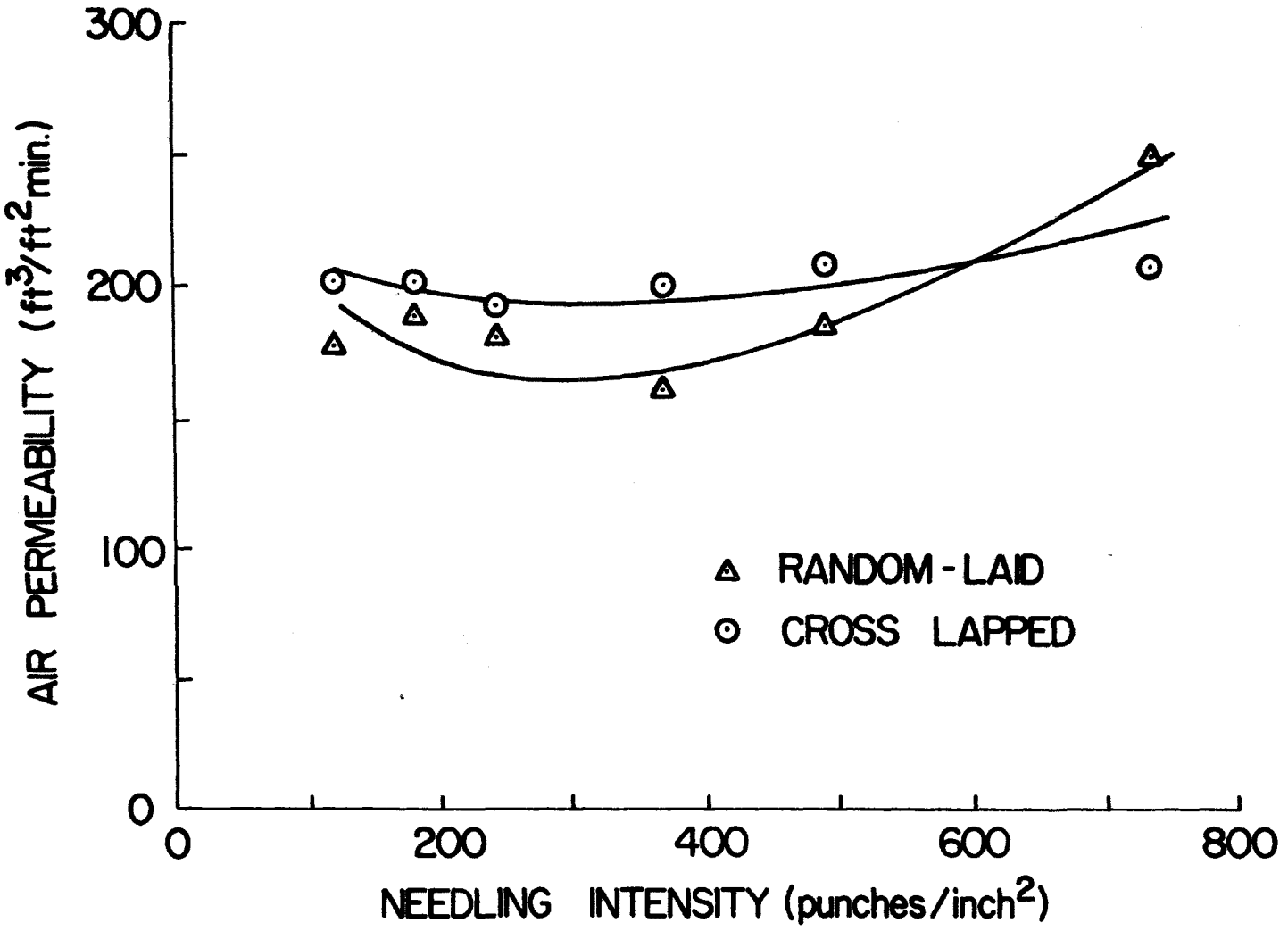

Figure 21. Air permeability vs. needling intensity (32 gauge)

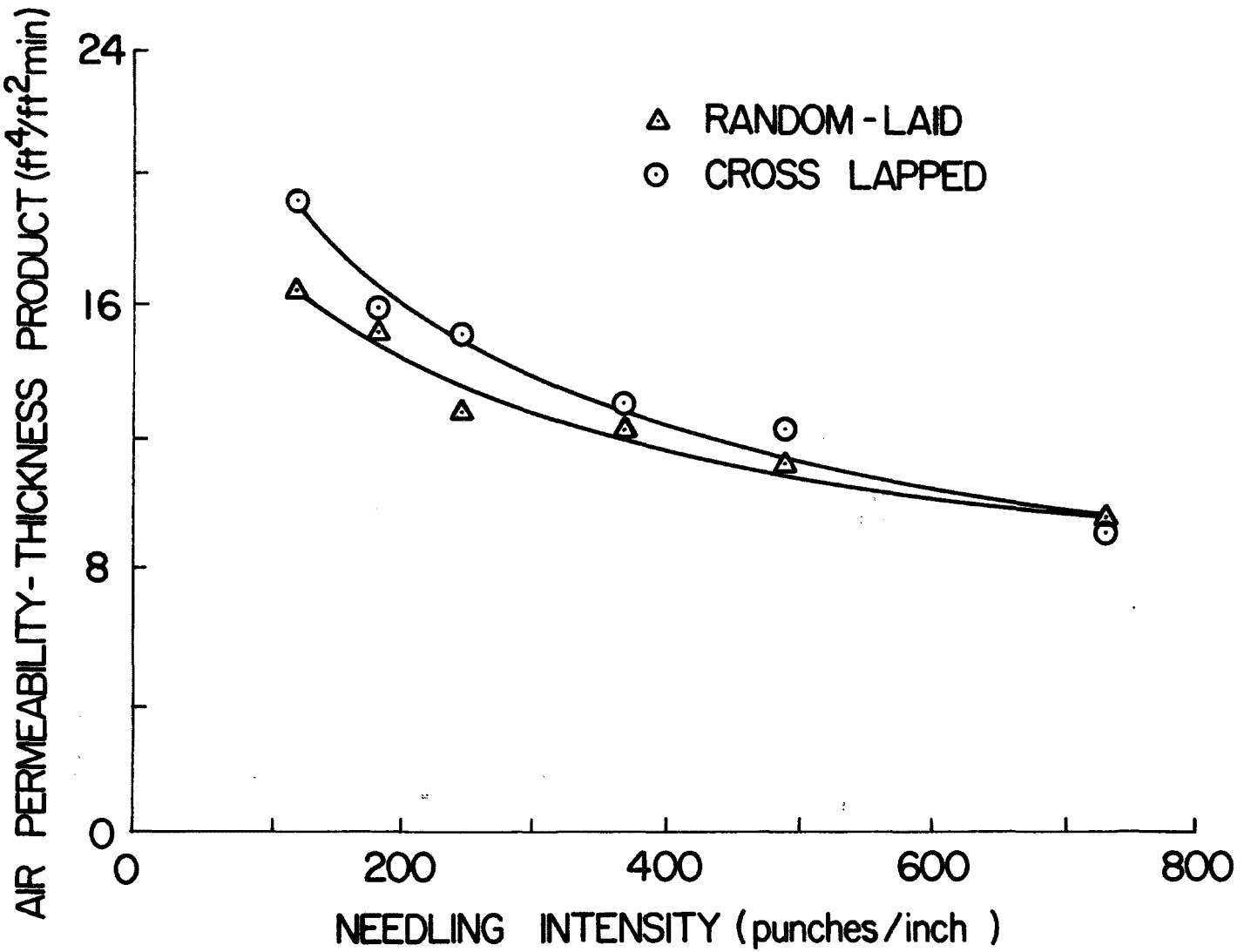

Figure 22. Air permeability - thickness product vs. needling intensity (20 gauge)

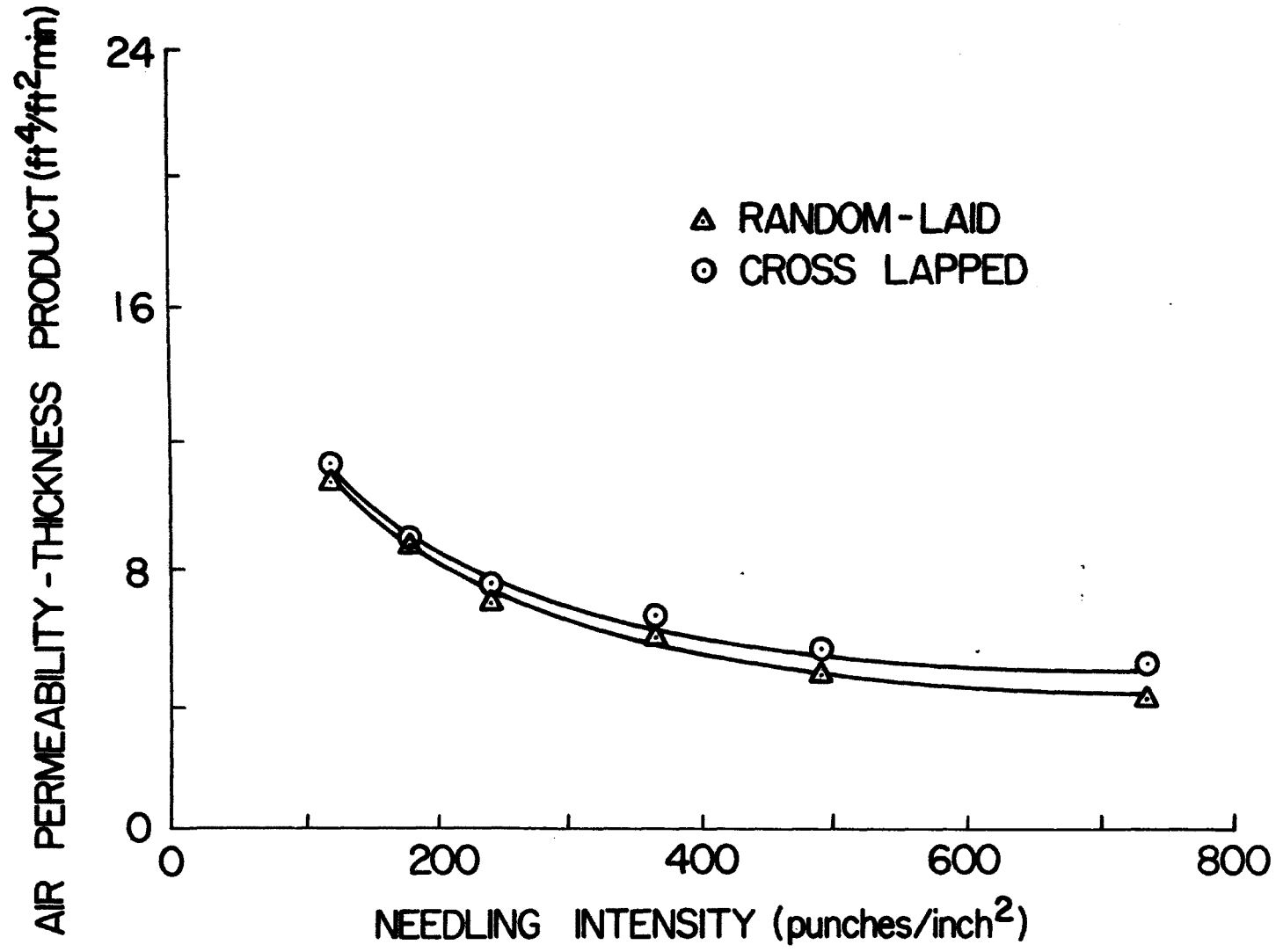

Figure 23. Air permeability-thickness product vs. needling intensity (25 gauge)

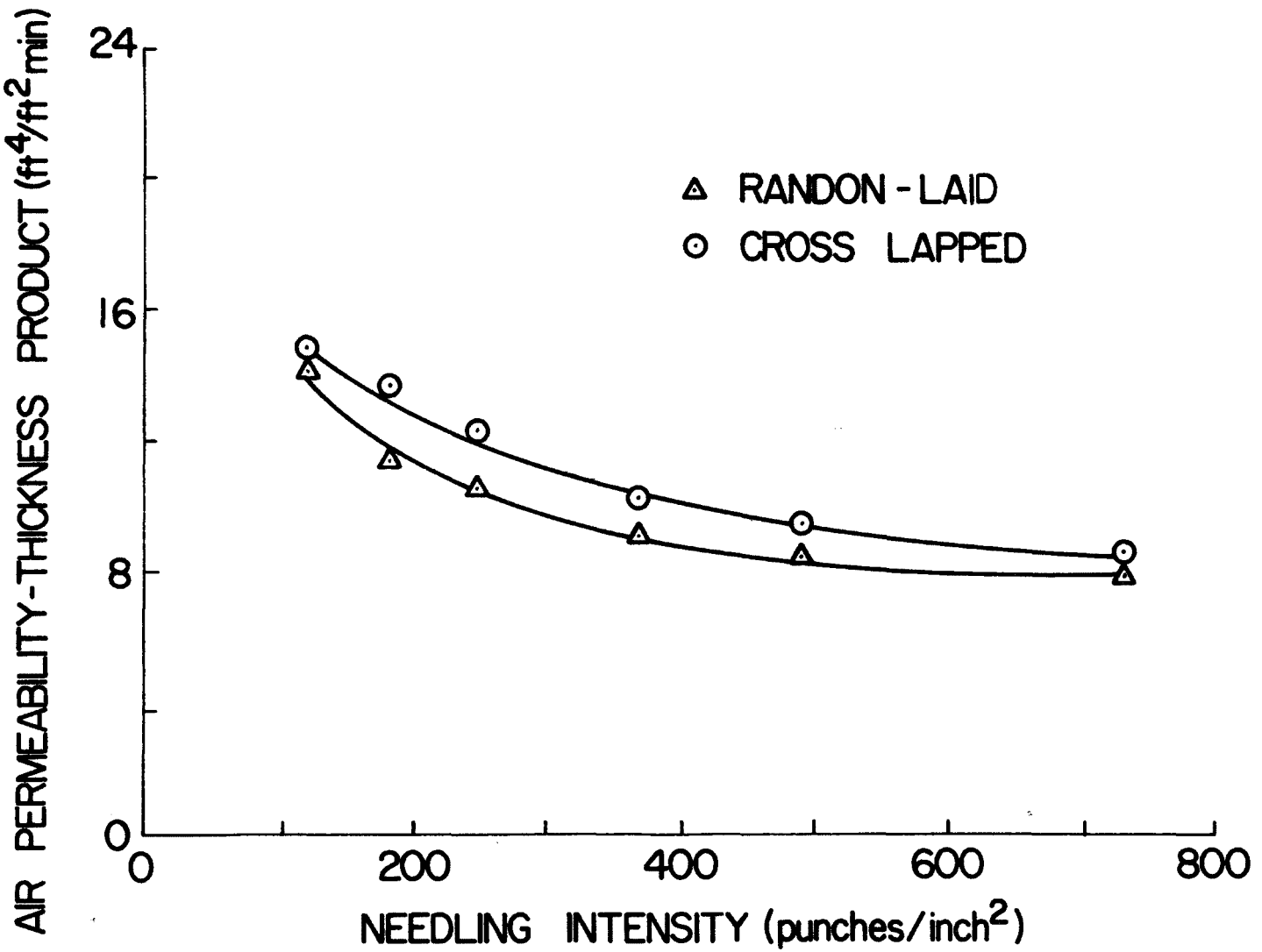

Figure 24. Air permeability-thickness product vs. needling intensity (32 gauge)

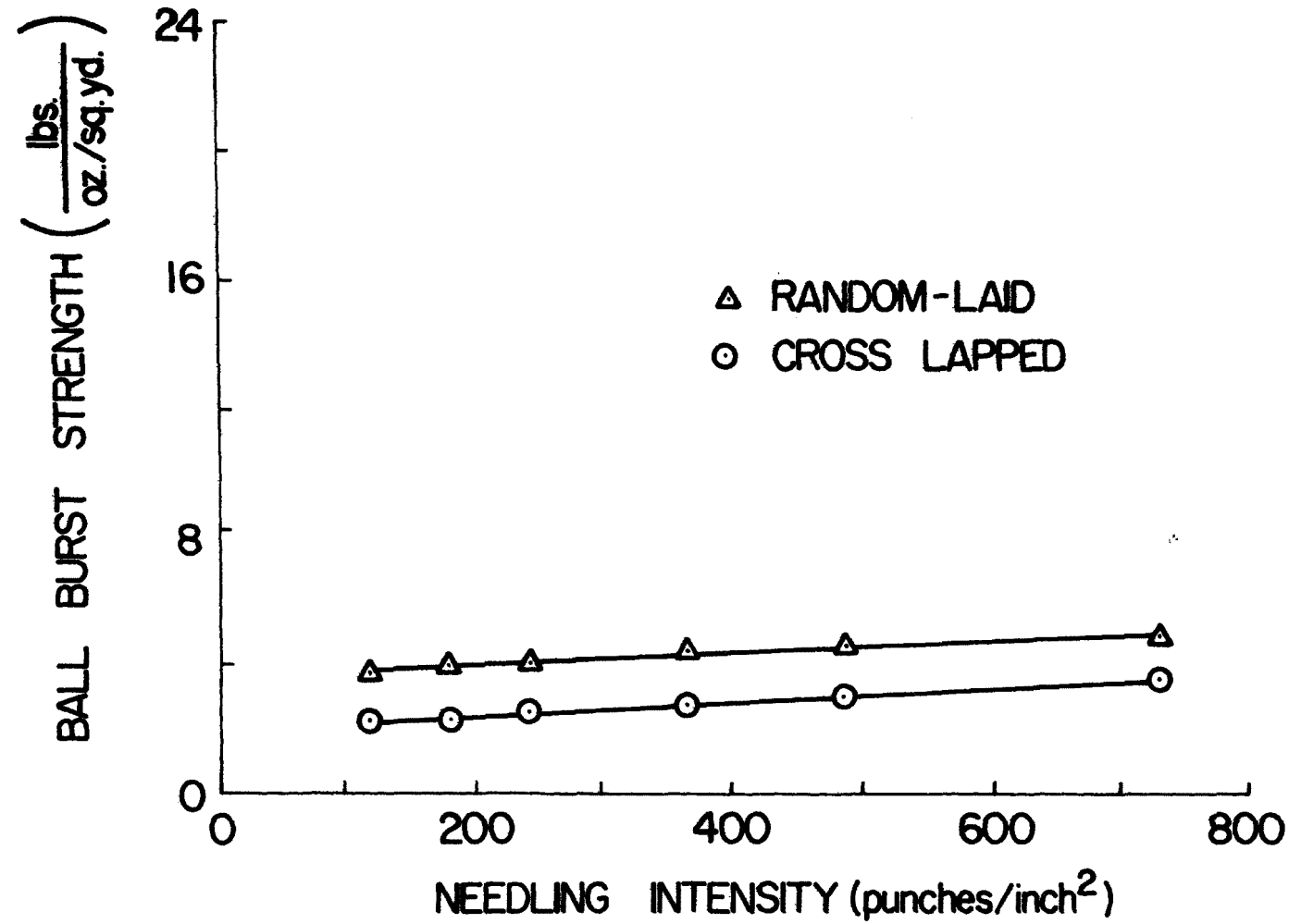

Figure 25. Bursting strength vs. needling intensity (20 gauge)

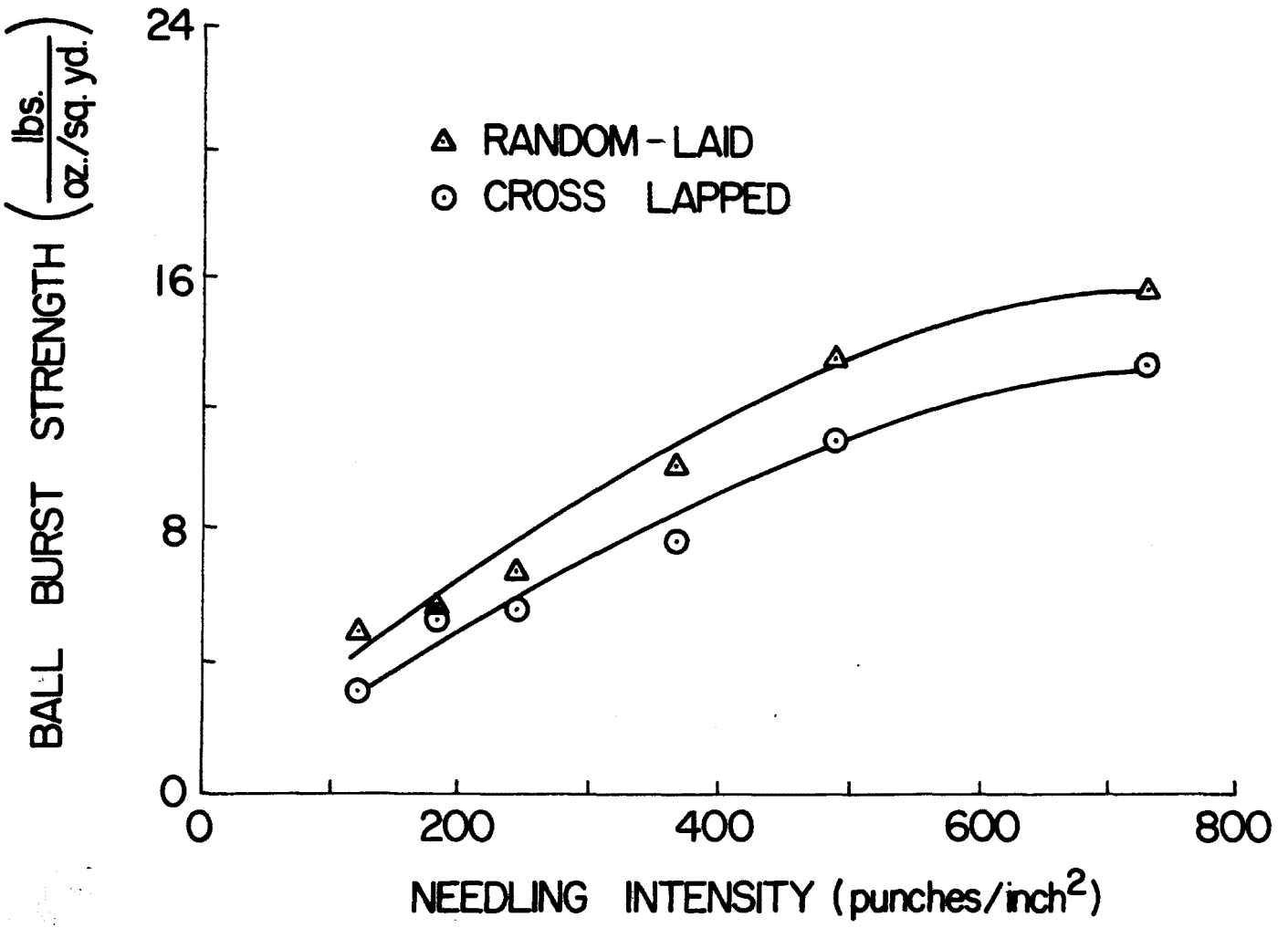

Figure 26. Bursting strength vs. needling intensity (25 gauge)

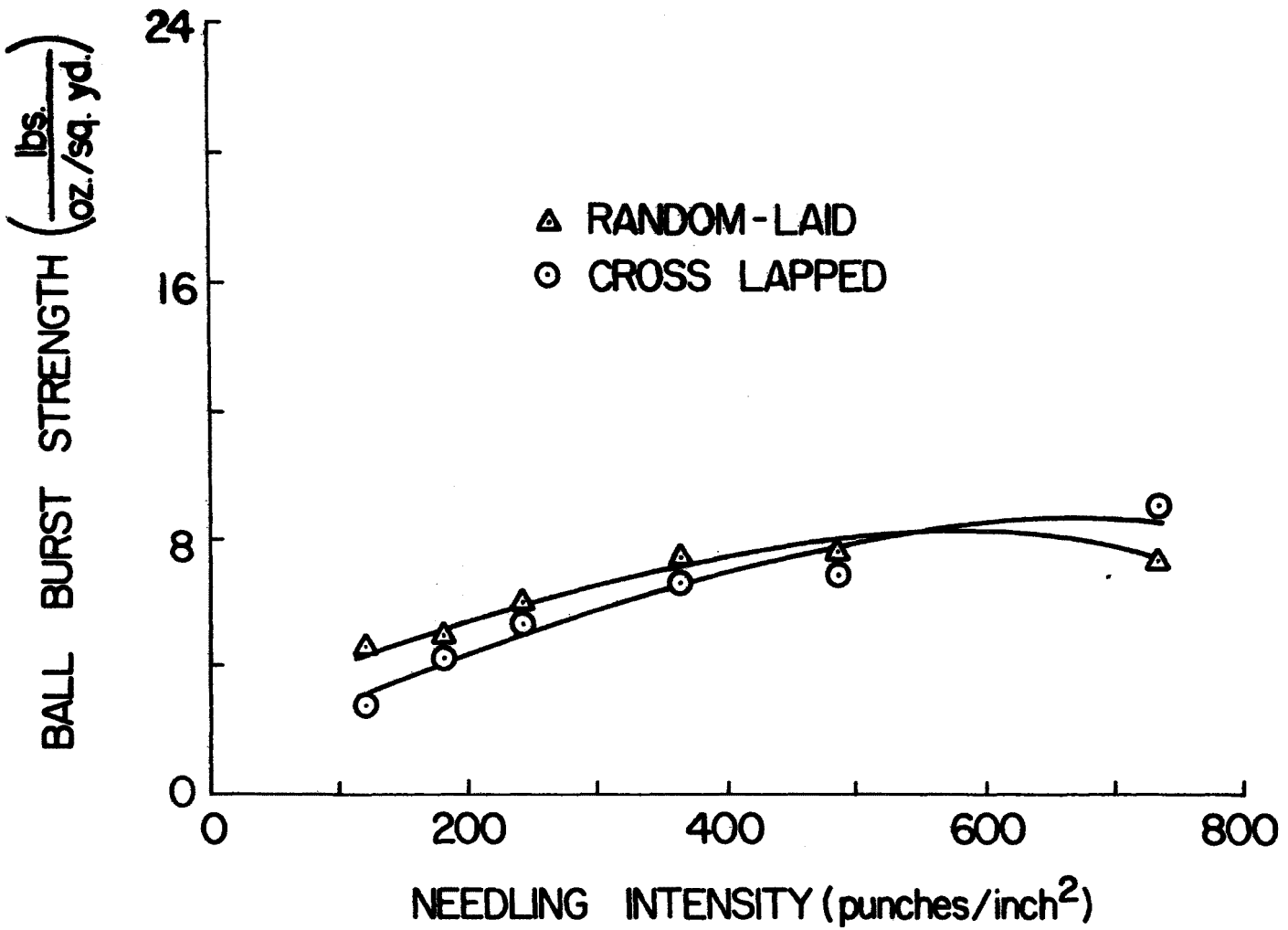

Figure 27. Bursting strength vs. needling intensity (32 gauge)

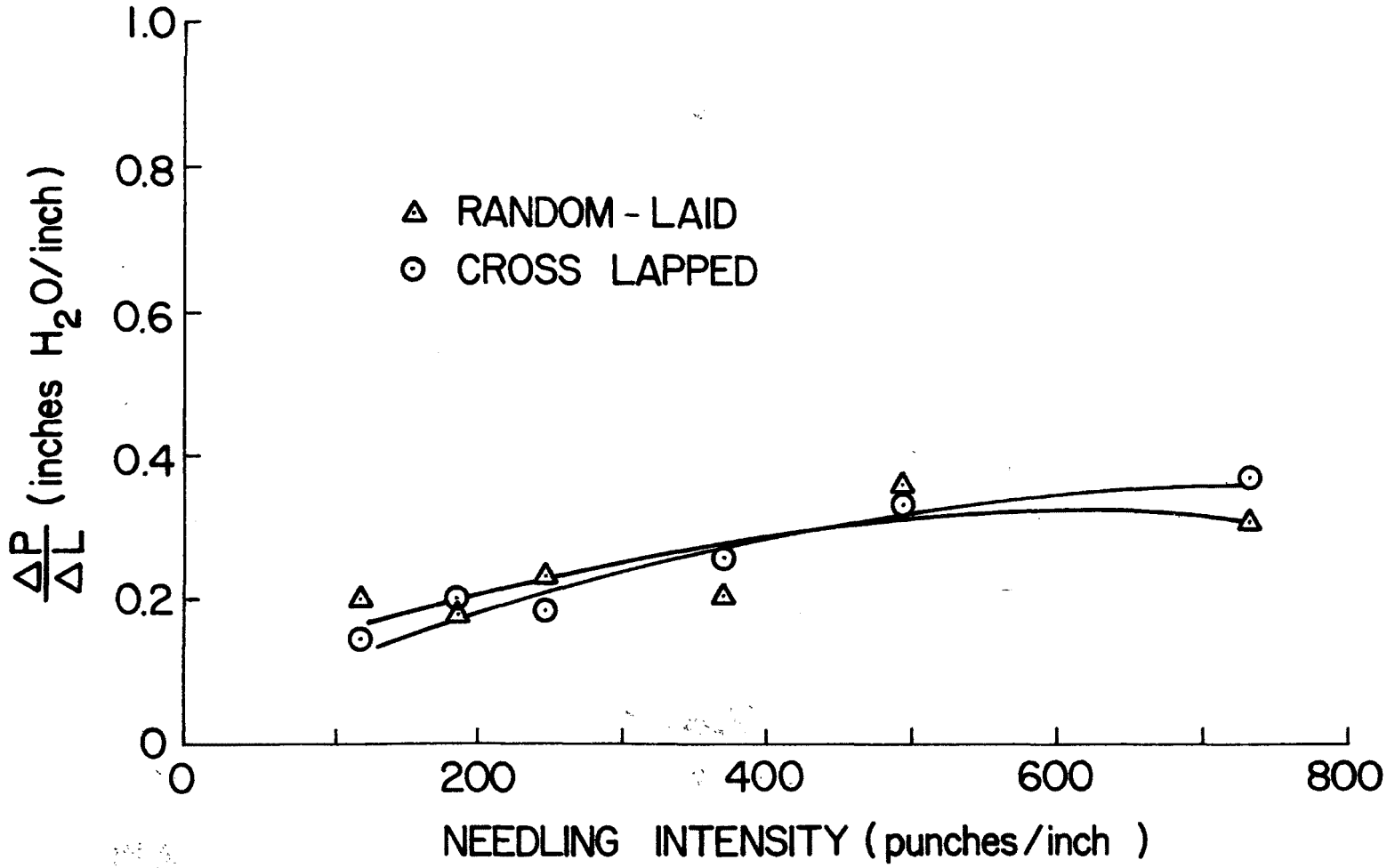

Figure 28. Pressure drop per unit thickness vs. needling intensity (air velocity 90 ft/min) (20 gauge)

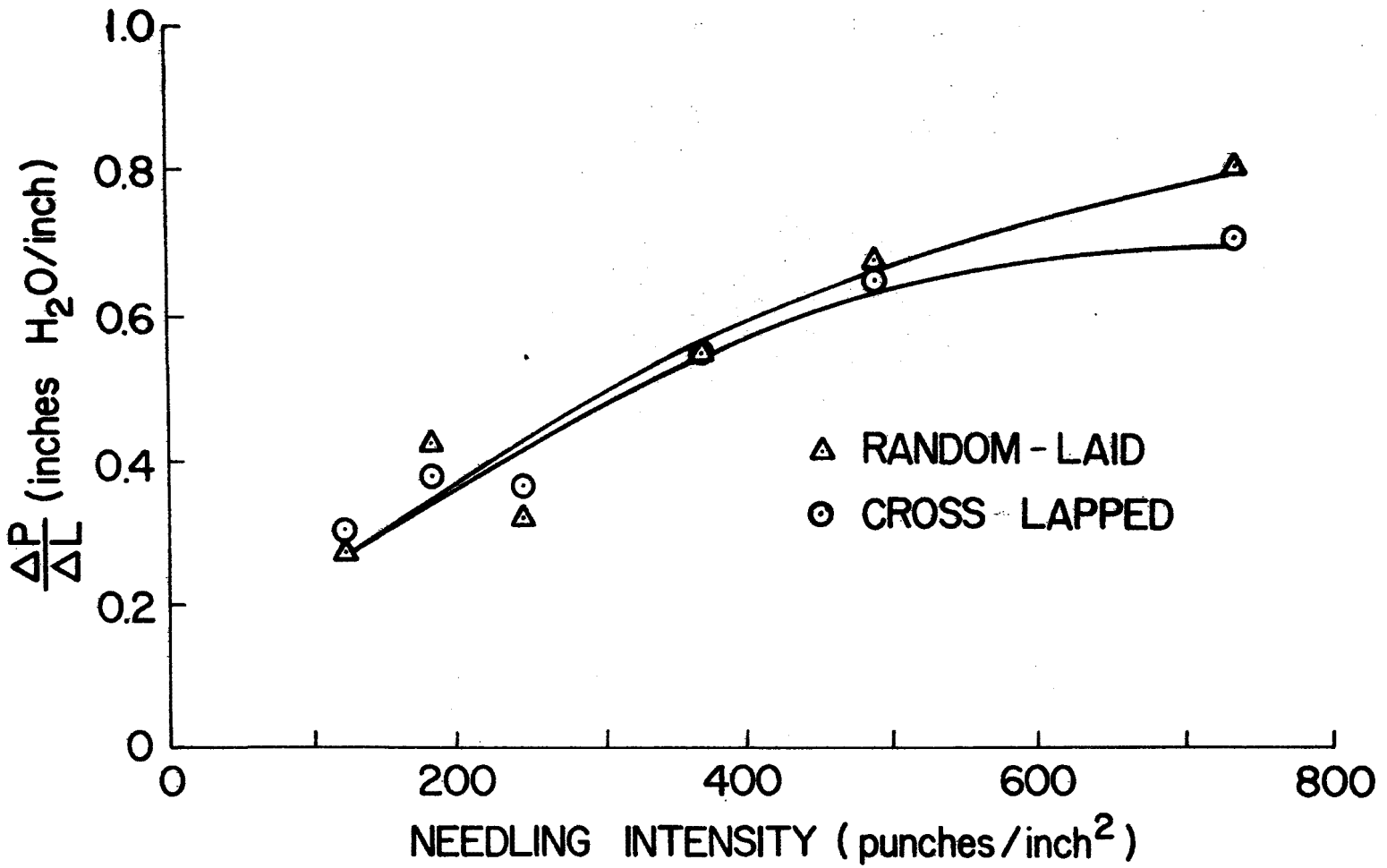

Figure 29. Pressure drop per unit thickness vs. needling intensity (air velocity 90 ft/min) (25 gauge)

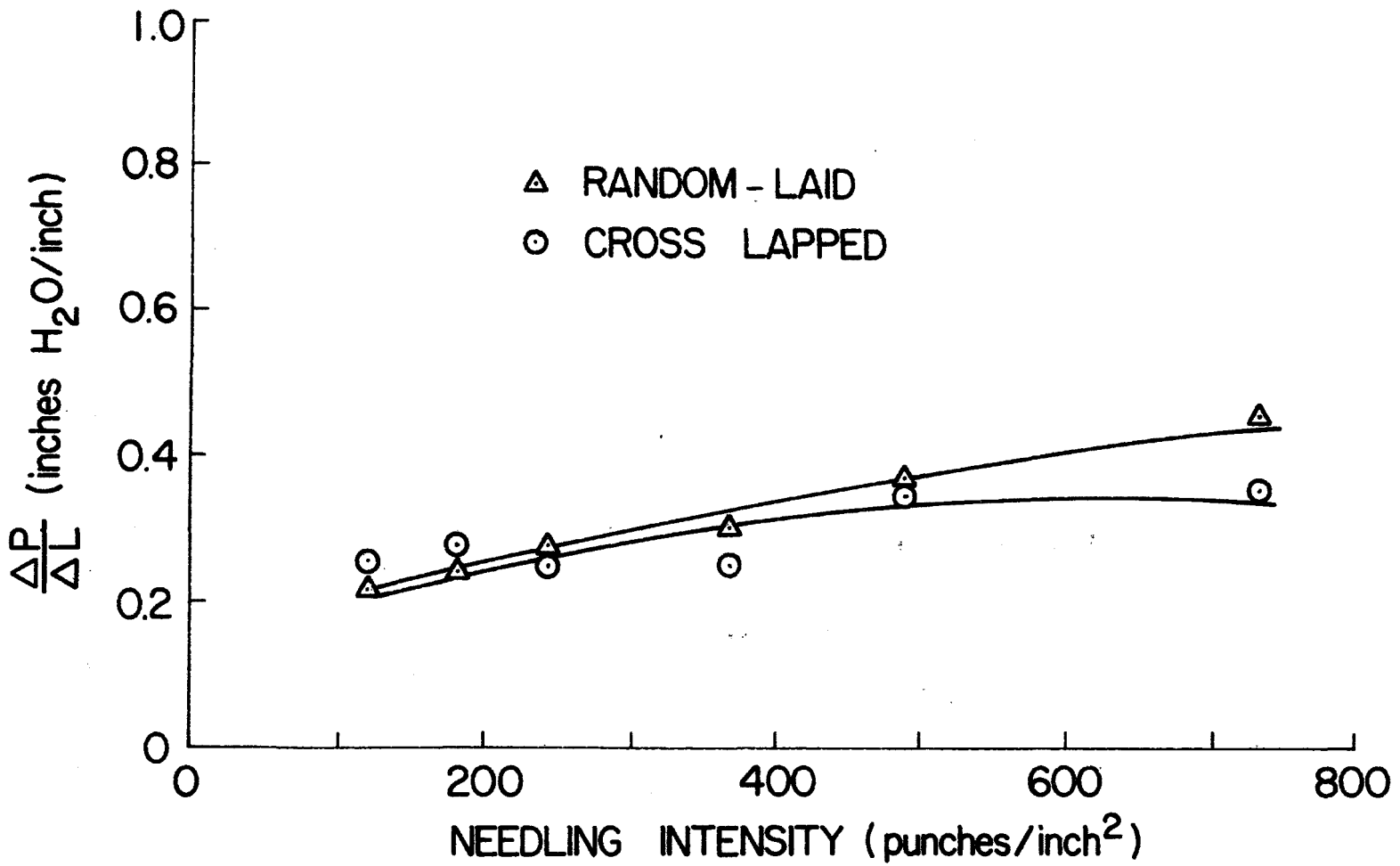

Figure 30. Pressure drop per unit thickness vs. needling intensity (air velocity 90 ft/min)(32 gauge)

Table 1. BATCH FILTRATION RESULTS
(Effects of fiber orientation and needle size)

Fiber Orientation	Needle Size	Needling Intensity Punches/in.^{2}	C_i gr./ft.^{3}	ΔP_c Inches H_2O	ΔP_f Inches H_2O	Efficiency %
Random-Laid	20 gauge	122	1.42	0.085	0.665	97.18
		245	2.39	0.080	0.890	97.66
		368	1.62	0.081	0.900	97.59
		490	2.46	0.080	0.940	97.68
		735	1.87	0.080	0.880	97.33
	25 gauge	122	2.07	0.120	0.755	98.60
		245	1.54	0.105	0.705	98.48
		368	1.69	0.090	0.800	97.28
		490	1.79	0.080	0.740	97.93
		735	2.00	0.070	0.795	98.00
	32 gauge	122	1.77	0.100	0.615	97.91
		245	2.06	0.100	0.880	98.25
		368	2.06	0.090	0.925	98.45
		490	1.28	0.110	0.645	97.42
		735	1.92	0.090	0.865	97.81
Cross-Lapped	20 gauge	122	2.39	0.080	0.835	97.91
		245	2.40	0.095	0.850	97.92
		368	1.69	0.060	0.590	96.69
		490	1.72	0.070	0.600	97.44
		735	1.89	0.068	0.610	97.30
	25 gauge	122	1.39	0.095	0.815	96.98
		245	1.82	0.075	0.785	97.80
		368	1.69	0.075	0.800	97.99
		490	1.80	0.090	0.830	98.17
		735	1.76	0.085	0.810	97.90
	32 gauge	122	1.72	0.105	0.850	98.14
		245	2.10	0.090	1.070	97.95
		368	1.77	0.070	0.890	97.74
		490	1.62	0.090	0.825	98.15
		735	1.85	0.080	0.790	97.95

Air Velocity = 45 ft./min.
ΔP_f = Pressure drop at the end of 10 minute duration tests.
ΔP_c = Pressure drop for clean filter
C_i = Inlet concentration
Needle penetration = 0.25 inches

fabrics, high production speeds in manufacturing the webs led to the decision in favor of using random-laid webs throughout the rest of this investigation.

7.2 Effect of Needle Size

In general, needle size is an important parameter affecting the properties of needled fabrics. Large needles normally reorient a large number of fibers into the pores, however, the larger the needle the more fiber disruption and fiber damage take place. In this investigation, it was necessary, to study the effect of needle size on the performance of needled fabrics in filtration.

Figure 31 shows the effect of needle size on fabric density. The 25 gauge needle gave the highest fabric density. It may be expected that the 20 gauge needle should give the highest density, but because of fiber disruption which occurs during needle withdrawal from the fabric the packing is reduced.

The effect of needle size on air permeability is presented in Figures 32 and 33. The air permeability-thickness product shows clearly the effect of needle size. The fabrics made by the 25 gauge needles gave the lowest values which is in good agreement with the density results.

Figure 34 shows the effect of needle size on the fabric bursting strength and again the results agree with the explanation mentioned earlier for the fiber damage caused by the 20 gauge needle. It is clear that the 25 gauge needle gave the highest fabric strength.

The pressure drop per unit thickness results shown in Figure 35 also show that the 25 gauge needle gave the highest pressure drop per unit thickness as a result of the high packing density. However, the flyash test results given in Table 1 indicate that the pressure drop (ΔP_c) for the fabrics made by the 25 gauge needles did not differ appreciably from those of the other fabrics. The efficiency values show a slight advantage for the 25 gauge fabrics. Based on these results the decision was made to eliminate the 20 gauge needle and to limit the range of needling intensity to 122-490 punches/inch^2. During the study of the other parameters the 25 gauge needle was mostly used.

7.3 Effect of Fiber Length

To study the effects of fiber length on the performance of needle punched fabrics, Dacron® type 54, 3 denier fiber of length $1\frac{1}{2}$, 2, $2\frac{1}{2}$,

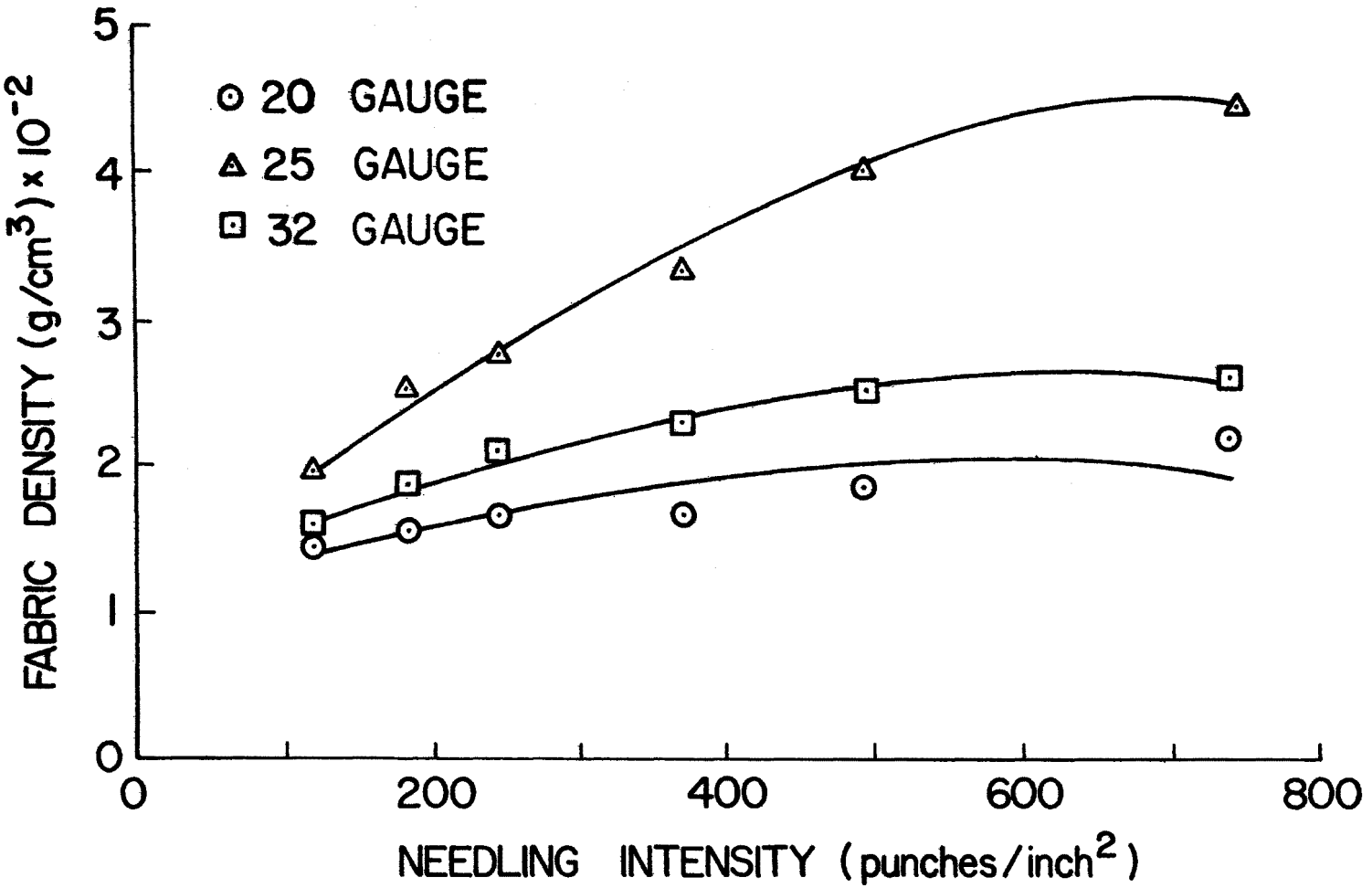

Figure 31. Fabric density vs. needling intensity (random-laid)

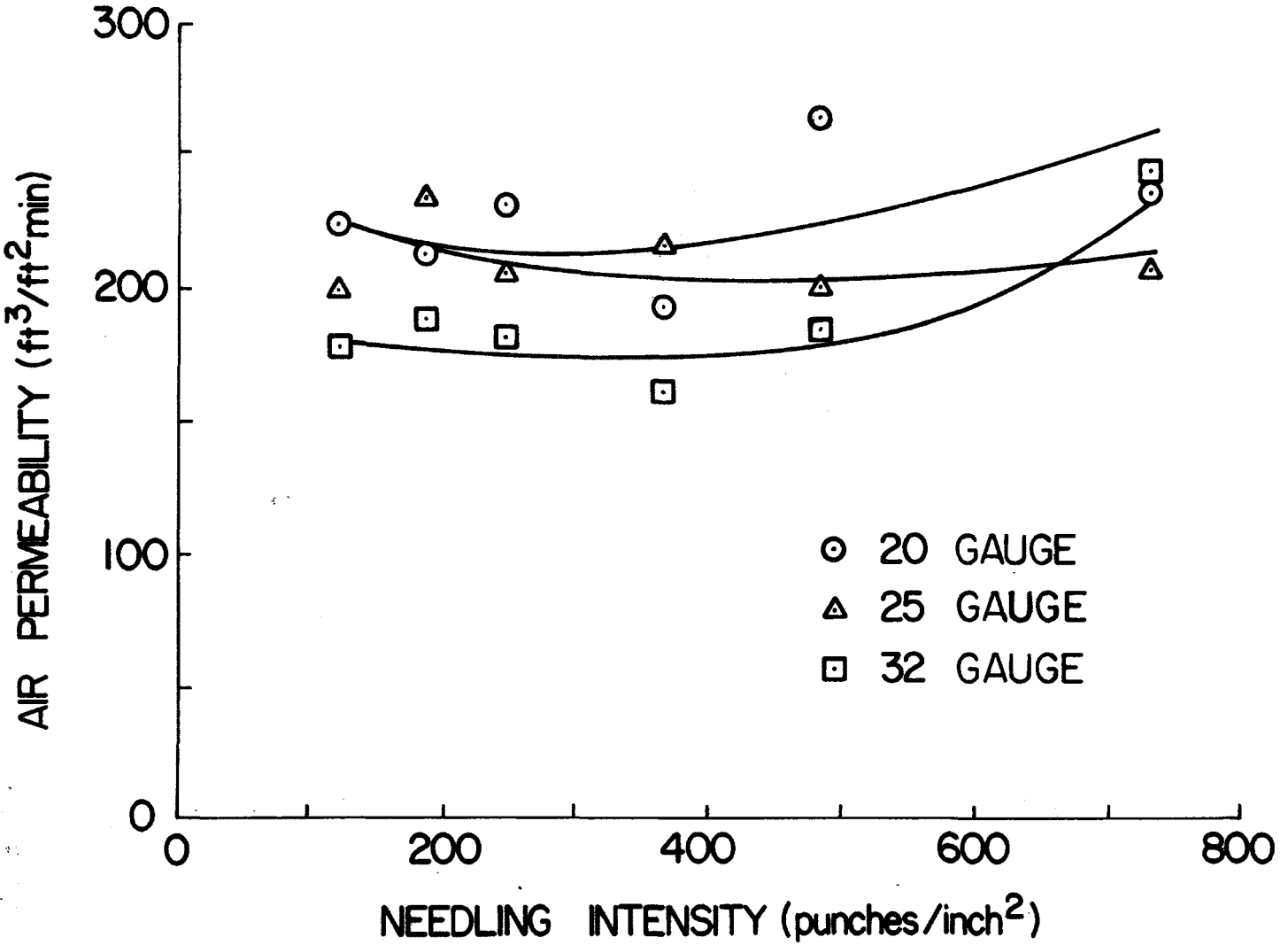

Figure 32. Air permeability vs. needling intensity (random-laid)

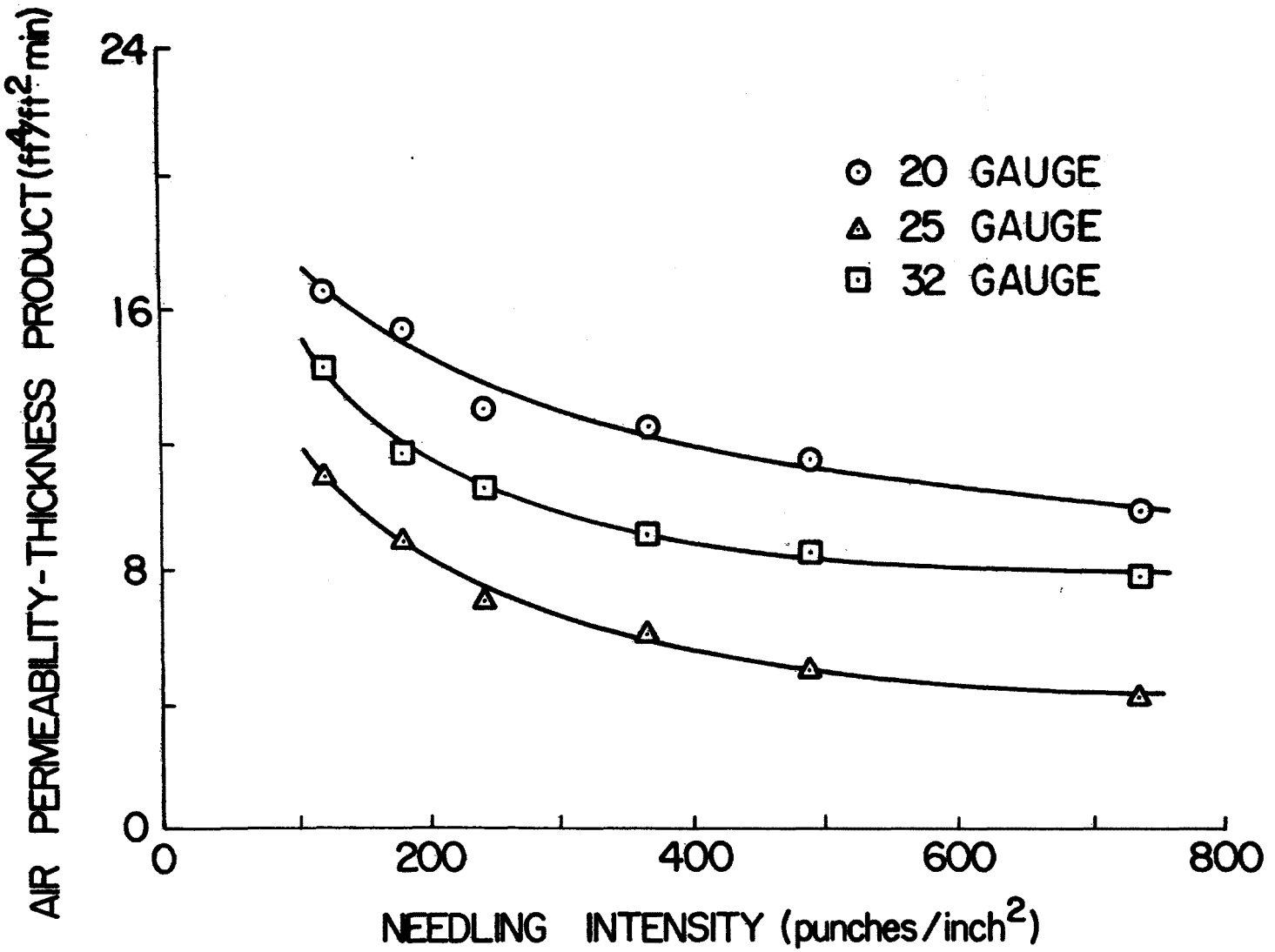

Figure 33. Air permeability-thickness product vs. needling intensity (random-laid)

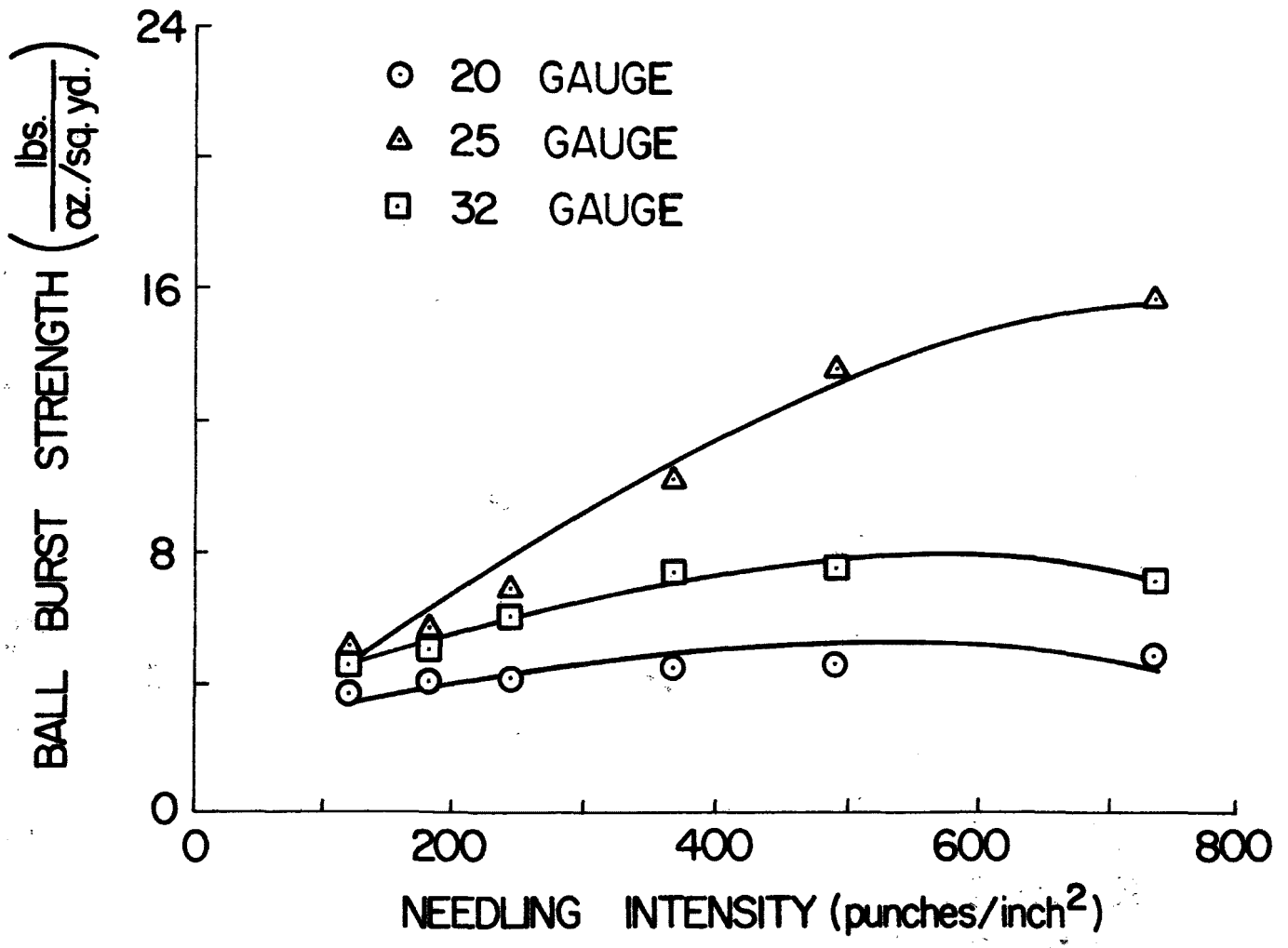

Figure 34. Bursting strength vs. needling intensity (random-laid)

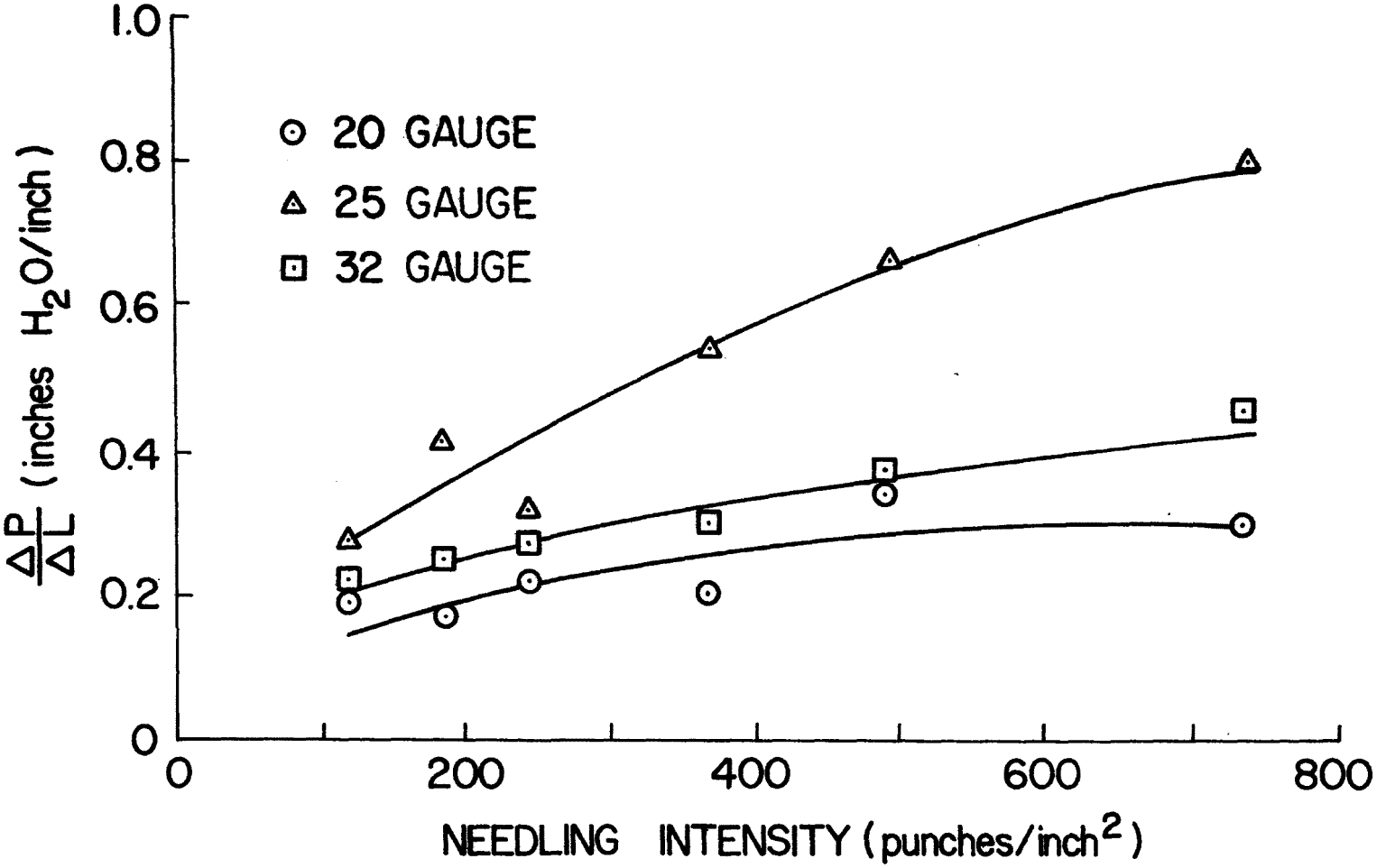

Figure 35. Pressure drop per unit thickness vs. needling intensity (air velocity 90 ft/min) (random-laid)

and 3 inches, were used. The results are presented in Figures 36 to 40. Generally there was no significant change in all the fabric properties due to fiber length. The reason for the high bursting strength shown in Figure 40 for the 3-inch fabric is the fact that the sample size is $2\frac{1}{2}$-inch in diameter. This means that the structure does not play any role and the strength is derived from the long fibers in the sample.

The results of the batch filtration experiments also showed no appreciable effect for fiber length on the pressure drop or efficiency of collection as shown in Table 2. Accordingly, the $1\frac{1}{2}$-inch fiber was chosen for its easy handling on the Rando-Feeder Rando-Webber Machine.

7.4 Effect of Needle Penetration

To study the effect of needle penetration it is useful to present the definition of penetration [31]. Figure 41 shows a schematic drawing for the arrangement of needles and the guide plates. The penetration is given by the length of the needle protruding below the top surface of the bottom guide plate. During this investigation four levels of needle penetration were used ranging from 0.25 to 0.5 inches with a step of one barb penetration of 0.083 inch, in batch testing.

Table 3 gives the results of fabric packing density for different needle penetrations. The packing density was increased with the increase in needle penetration as expected. The air permeability-thickness product values are given in Table 4. This shows that the air permeability-thickness product is reduced with increasing the needle penetration due to the increase in packing density. Table 5 gives the results of the fabric ball bursting strength which increases with penetration up to a certain level. At high needle penetration the bursting strength decreased indicating an increased level of fiber damage. Table 6 gives the filtration results for the various needle penetrations and on average a 0.333 inch penetration (p_2) gives the best results for efficiency and ΔP_f. In making the comparison, it is clear that penetrations p_1 and p_4 had disadvantages; fabrics with p_1 had low packing density and bursting strength, whereas, those with p_4 had high packing density and low bursting strength. The decision was to use penetration p_2 since this setting resulted in a low level of needle damage during punching. Therefore all the fabrics presented in the remainder of this report were produced with needle penetration setting p_2 (0.333 inch).

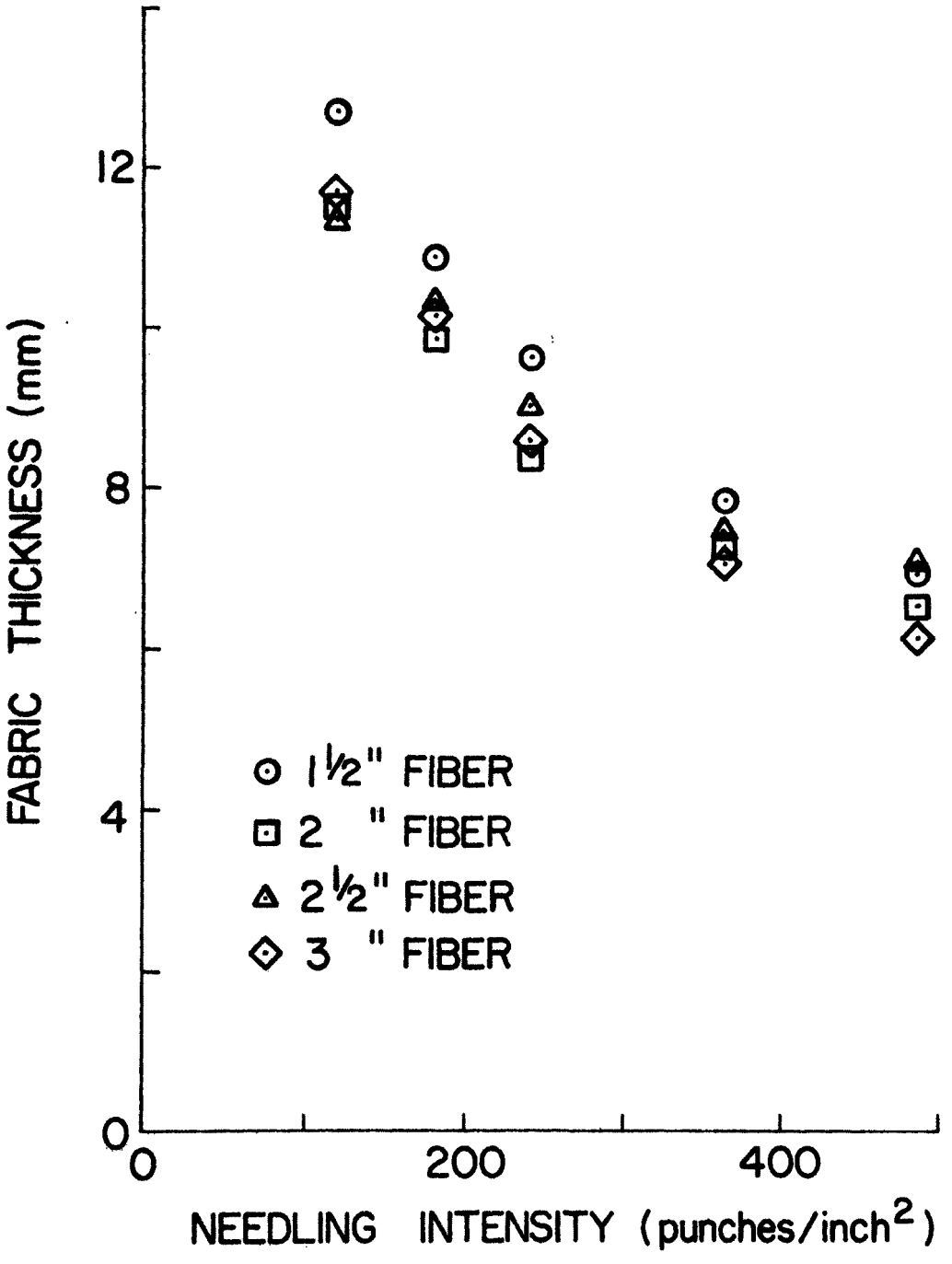

Figure 36. Fabric thickness vs. needling intensity effect of fiber length

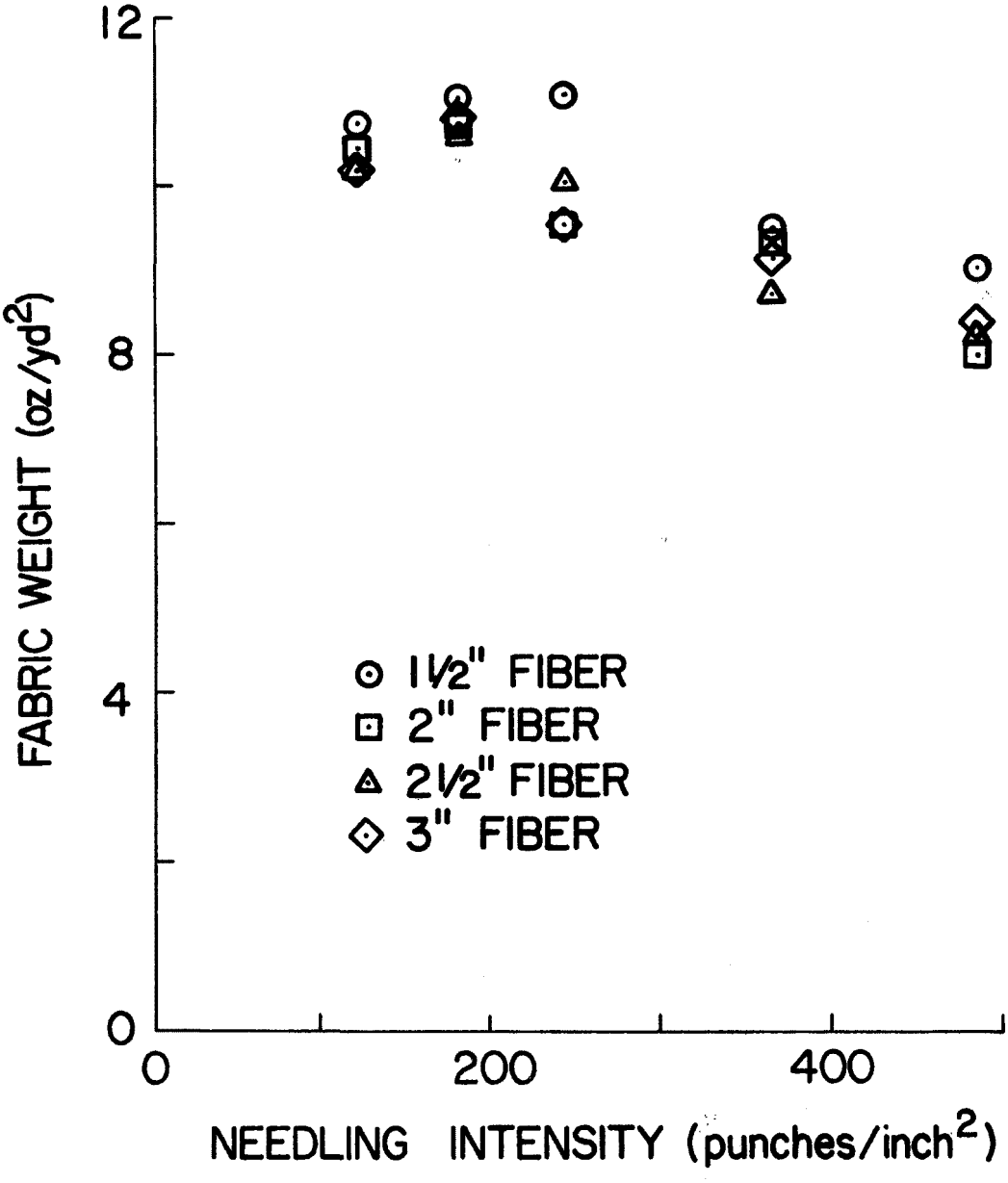

Figure 37. Fabric weight vs. needling intensity effect of fiber length

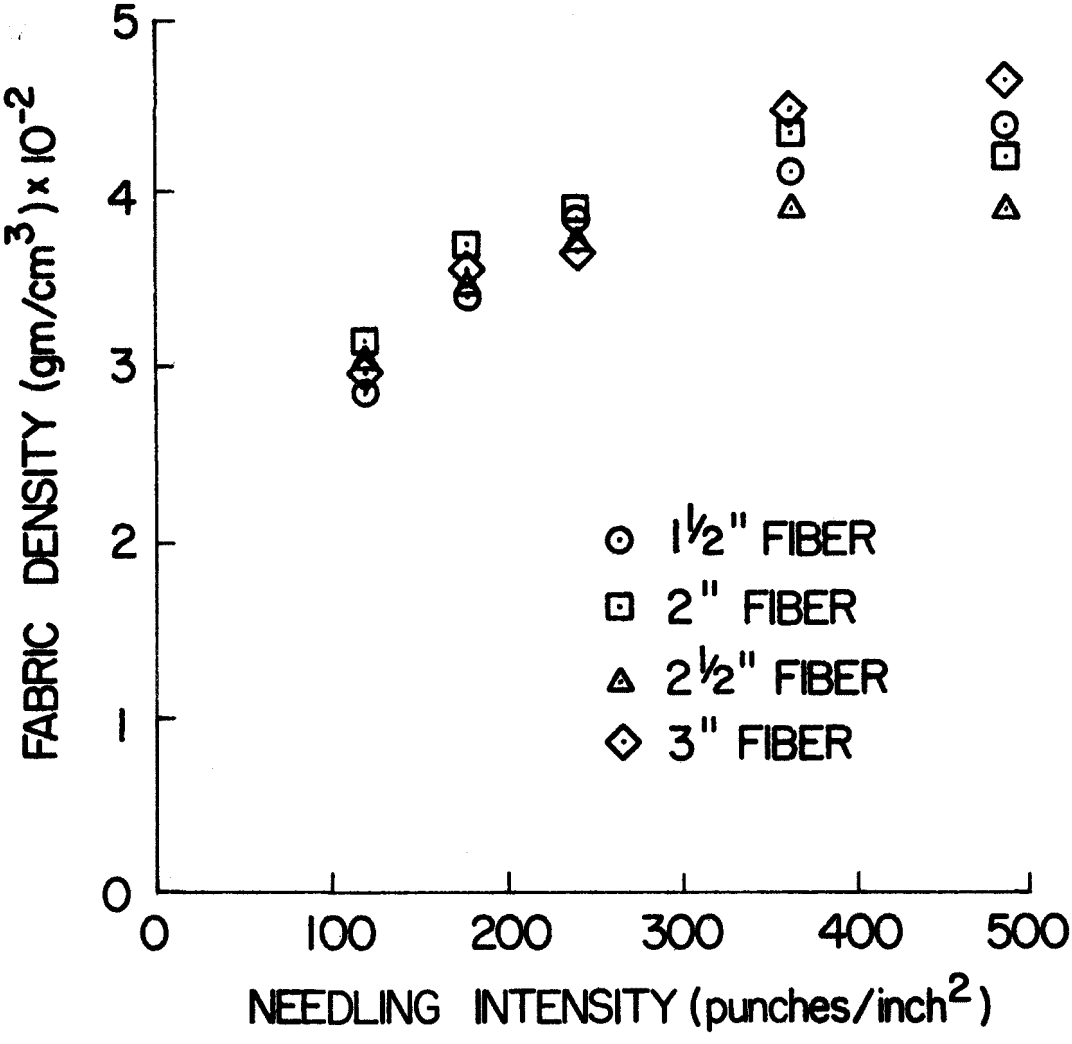

Figure 38. Fabric density vs. needling intensity effect of fiber length

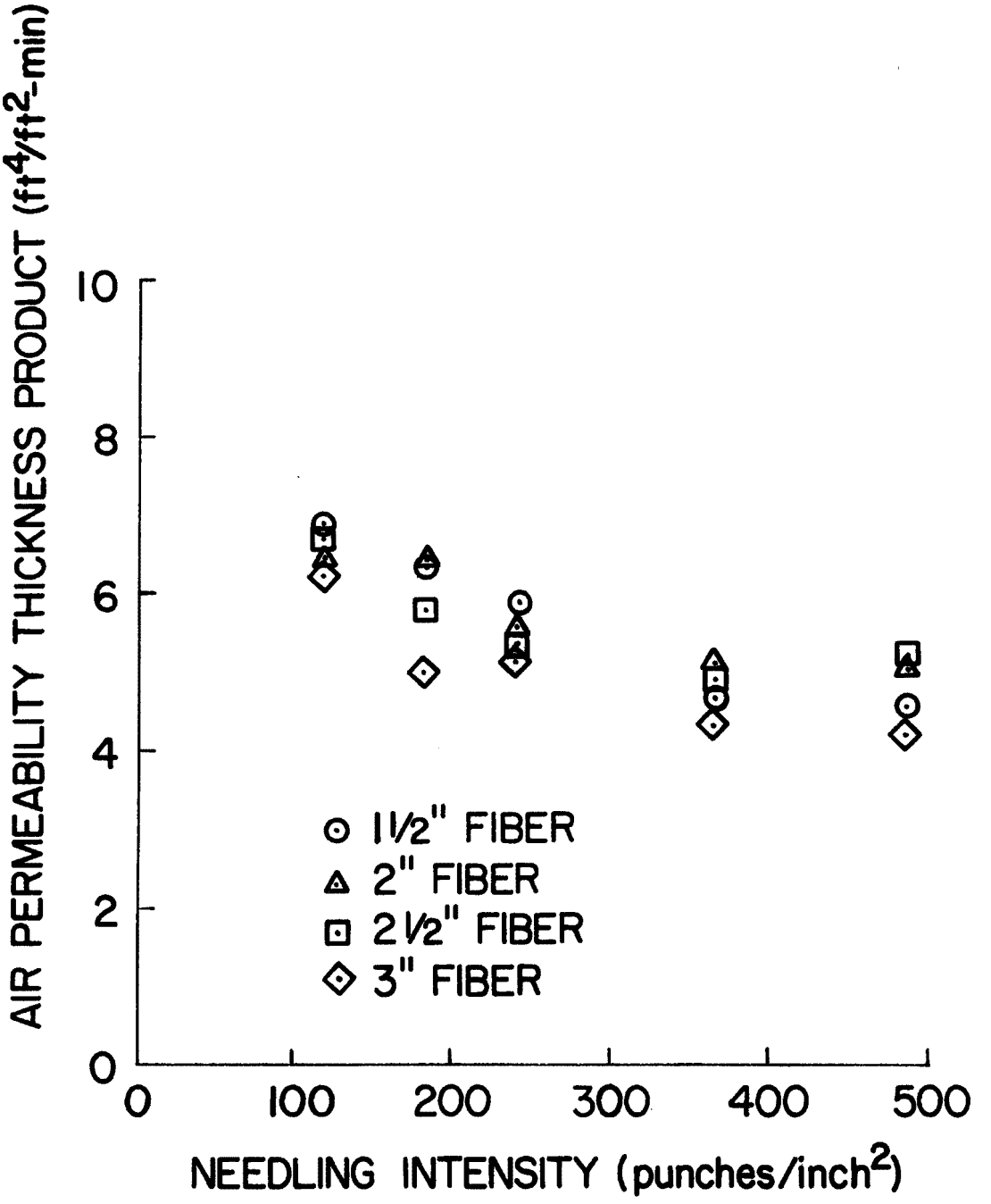

Figure 39. Air permeability-thickness product vs. needling intensity (effect of fiber length)

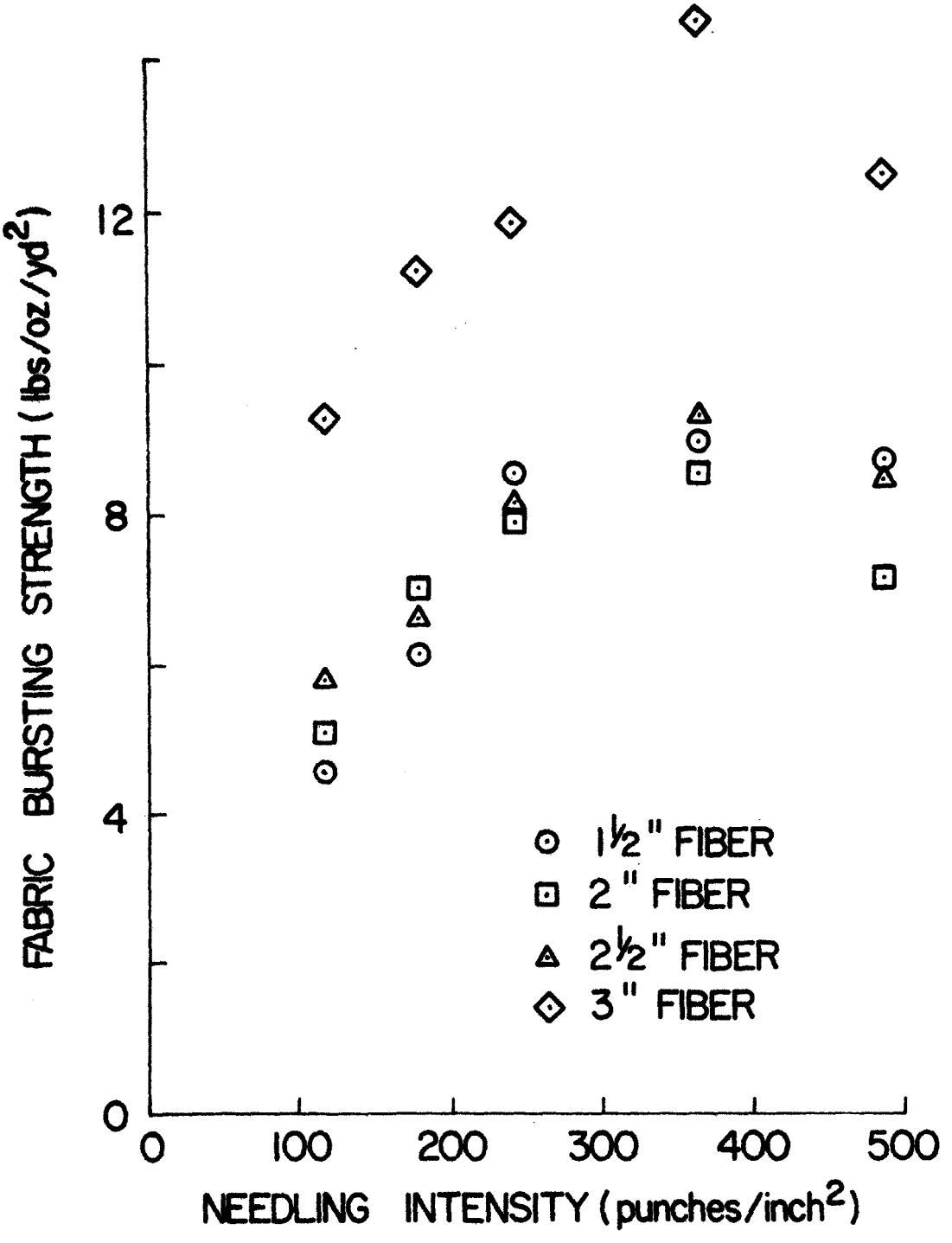

Figure 40. Fabric bursting strength vs. needling intensity
(effect of fiber length)

Table 2. BATCH FILTRATION PERFORMANCE
(Effect of Fiber Length)*

Fiber Length	Needling Intensity Punches/in.^{2}	C_i gr./ft.^{3}	ΔP_c Inches H_2O	ΔP_f Inches H_2O	Efficiency %
$1\frac{1}{2}$"	122	2.45	0.100	0.96	97.88
	245	2.25	0.055	1.18	97.96
	368	2.00	0.085	0.73	98.14
	490	2.38	0.090	0.85	98.27
2"	122	2.03	0.120	1.05	98.02
	245	1.89	0.115	0.94	98.54
	368	2.27	0.090	1.01	98.17
	490	1.81	0.088	1.05	98.83
$2\frac{1}{2}$"	122	2.02	0.110	.98	98.33
	245	1.80	0.100	1.06	98.2
	368	2.16	0.090	0.92	98.10
	490	1.83	0.100	0.93	98.03
3"	122	1.76	0.105	0.84	98.04
	245	1.74	.095	0.74	98.3
	368	2.04	.110	1.04	98.44
	490	1.66	.090	1.79	97.62

Air velocity = 45 ft/min.
Needle penetration = 0.333 inch

*Random laid webs

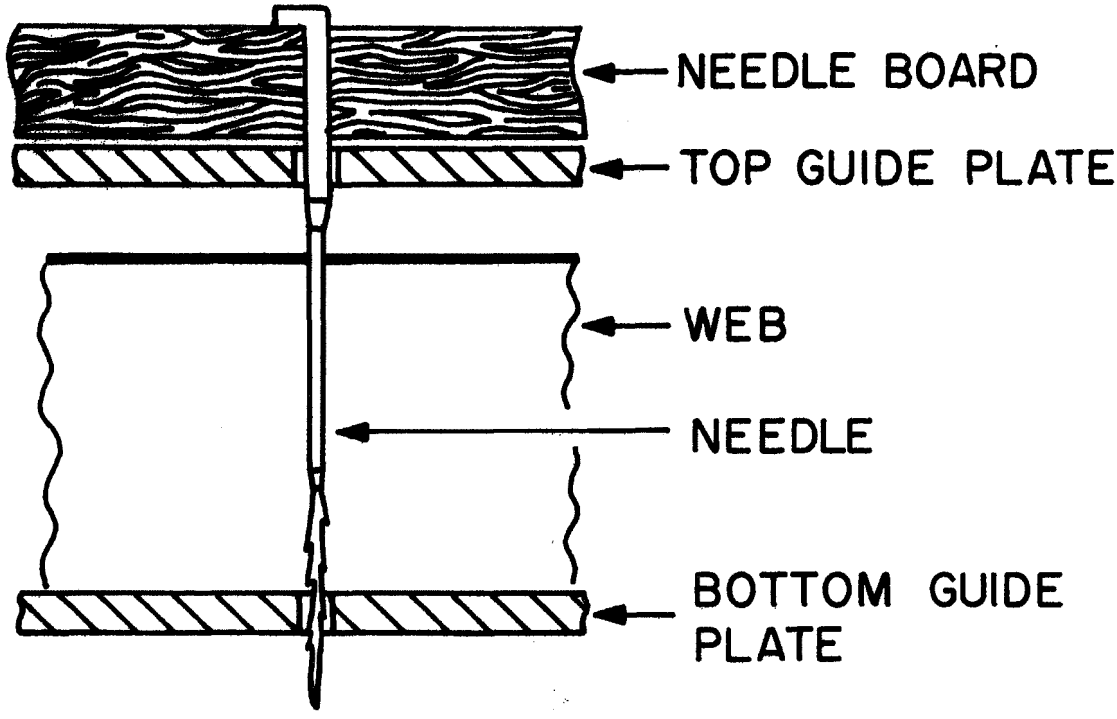

Figure 41. Arrangement of needle and plates

Table 3. EFFECT OF NEEDLE PENETRATION ON PACKING DENSITY

Needling Intensity	Packing Density %			
Punches/in.^{2}	p_1	p_2	p_3	p_4
122	1.4	1.9	2.0	3.0
245	2.0	2.4	2.6	2.9
368	2.4	2.8	2.9	3.4
490	2.9	3.2	3.3	3.5

Table 4. EFFECT OF NEEDLE PENETRATION ON AIR PERMEABILITY-THICKNESS PRODUCT

Needling Intensity	Air Permeability-Thickness Product (ft.^{4}/ft.^{2} min.)			
Punches/in.^{2}	p_1	p_2	p_3	p_4
122	16.5	8.8	7.1	4.6
246	13.0	6.1	5.2	4.0
368	12.4	4.9	5.2	3.9
490	11.4	4.2	4.5	3.9

Random-laid, 25-gauge, Dacron® $1\frac{1}{2}$" x 3.0 denier
p_1 = 0.250", p_2 = 0.333", p_3 = 0.416", p_4 = 0.500"

Table 5. EFFECT OF NEEDLE PENETRATION ON BALL BURSTING STRENGTH

Needling Intensity	Ball Bursting Strength lbs./oz./sq. yd.			
Punches/in.^{2}	p_1	p_2	p_3	p_4
122	5.0	5.5	8.7	7.9
245	6.8	9.0	11.4	10.4
368	10.0	12.0	11.9	10.6
490	13.4	14.2	14.4	11.3

Random-laid, 25-gauge, Dacron $1\frac{1}{2}$" x 3.0 denier
p_1 = 0.250", p_2 = 0.333", p_3 = 0.416", p_4 = 0.500"

Table 6. BATCH FILTRATION RESULTS
(Effect of Needle Penetration)

Needle Penetration	Needling Intensity Punches/in.^{2}	C_i gr./ft.^{3}	ΔP_c Inches H_2O	ΔP_f Inches H_2O	Efficiency %
p_1	122	2.07	0.120	0.755	98.60
	245	1.54	0.105	0.705	98.48
	368	1.69	0.090	0.800	97.28
	490	1.79	0.080	0.740	97.93
p_2	122	1.85	0.140	0.820	98.42
	245	1.63	0.110	0.735	98.26
	368	1.64	0.125	0.730	98.42
	490	1.50	0.130	0.700	98.32
p_3	122	1.62	0.140	0.825	97.61
	245	1.61	0.130	0.770	98.32
	368	1.68	0.120	0.875	98.30
	490	1.77	0.080	0.870	97.67
p_4	122	1.66	0.080	0.730	98.23
	245	1.84	0.090	0.835	98.34
	368	1.71	0.120	0.785	98.49
	490	1.77	0.080	0.870	97.67

Air velocity = 45 ft/min.
Random-laid, 25-gauge, Dacron $1\frac{1}{2}$" x 3.0 denier
p_1 = 0.250", p_2 = 0.333", p_3 = 0.416", p_4 = 0.500"

7.5 Effect of Scrim Material

Needle punched fabrics without scrims were used in the earlier part of this investigation to study the effects of the fabric parameters without the complications of the effect of the scrim material. Tensile strength and elongation data for a series of these fabrics are given in Tables A-4 and A-5 respectively. The data indicated that these fabrics had low strength and high elongation making them dimensionally unstable. This is not suitable for bag filtration, since changes in the dimensions of the bag affect the filtration performance. It is also doubtful that such fabric will stand the strain of filtration and cleaning cycles for a reasonable lifetime, although some commercial fabrics are made without scrims.

Woven scrim fabrics are normally used to reinforce needle punched fabrics in applications other than filtration. In these applications the major goal is strength and dimensional stability. In filtration, however, the use of closely woven fabrics as scrim material leads to an increase in the pressure drop. If open woven scrims are used there is very little gain in dimensional stability. This was supported by preliminary experiments.

Examination of the various nonwoven structures indicated that spunbonded fabric have considerable strength and dimensional stability to be used as a scrim material. Two spunbonded fabrics were selected, one in which the filaments are nylon (Cerex) and the other made from polyester (Reemay). Fabric weight is very important in the scrim application. Light weight fabrics do not give the desired effect while heavy fabrics lead to considerable needle damage and to problems during manufacturing. Experiments carried out to determine the best fabric weight indicated that 1.0 and 1.5 oz./yd^2 were the most suitable.

To study the effect of needling on the scrim itself, experiments were carried out on the Reemay and Cerex fabrics using 25 gauge needles and the results are presented in Figures 42 to 44. It can be seen from Figure 42 that needling, in general, had very little effect on the fabric weight but the Cerex 1.5 oz./yd^2 fabric showed more change than the corresponding weight of the Reemay. This may be attributed to the movement of the filaments in Reemay which also reduces the level of needle damage. Figure 43 showed the changes in air permeability for the two cases; and it is clear that the increase in needling results in an appreciable increase in the air permeability of the Cerex fabrics. This can also be related to the high packing of the Cerex which leads to

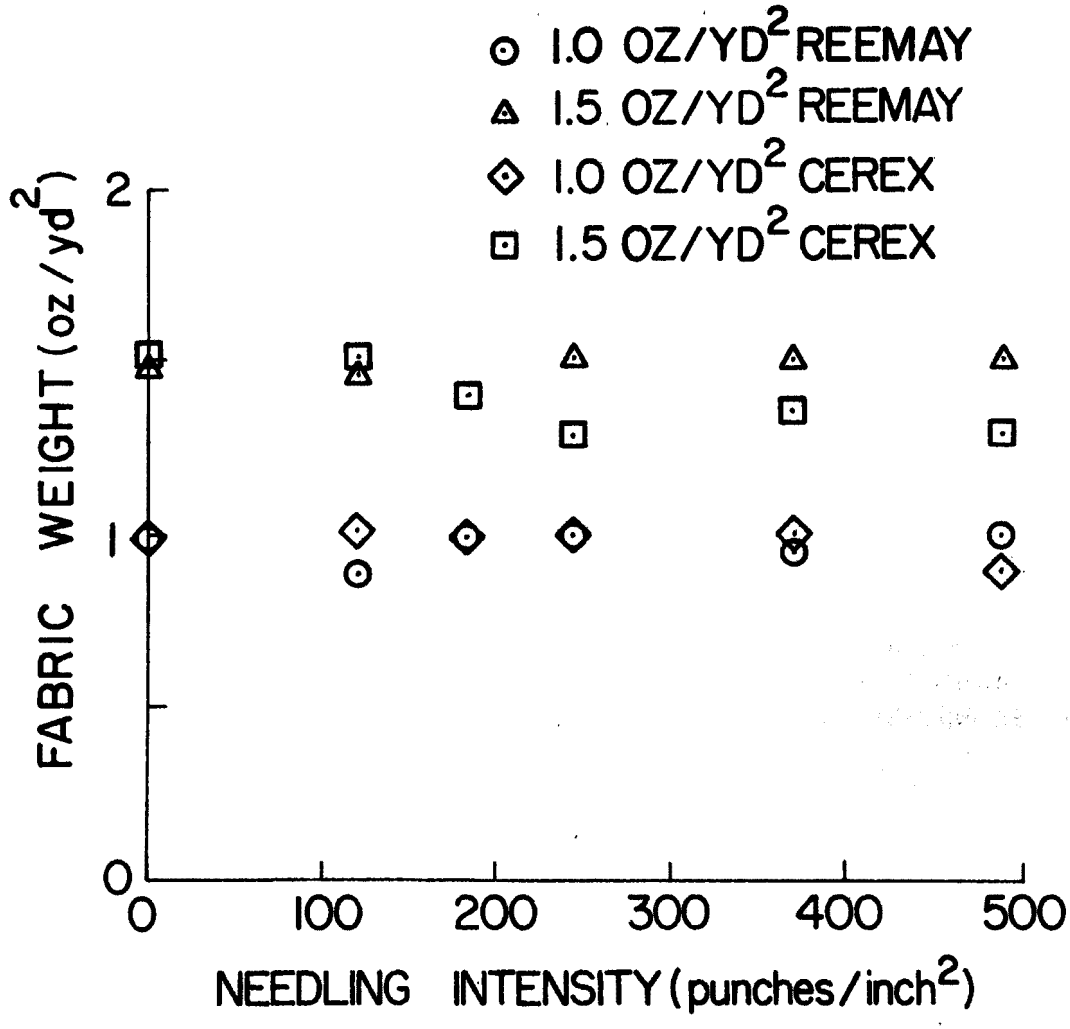

Figure 42. Fabric weight vs. needling intensity (Cerex and Reemay spunbonded fabric only)

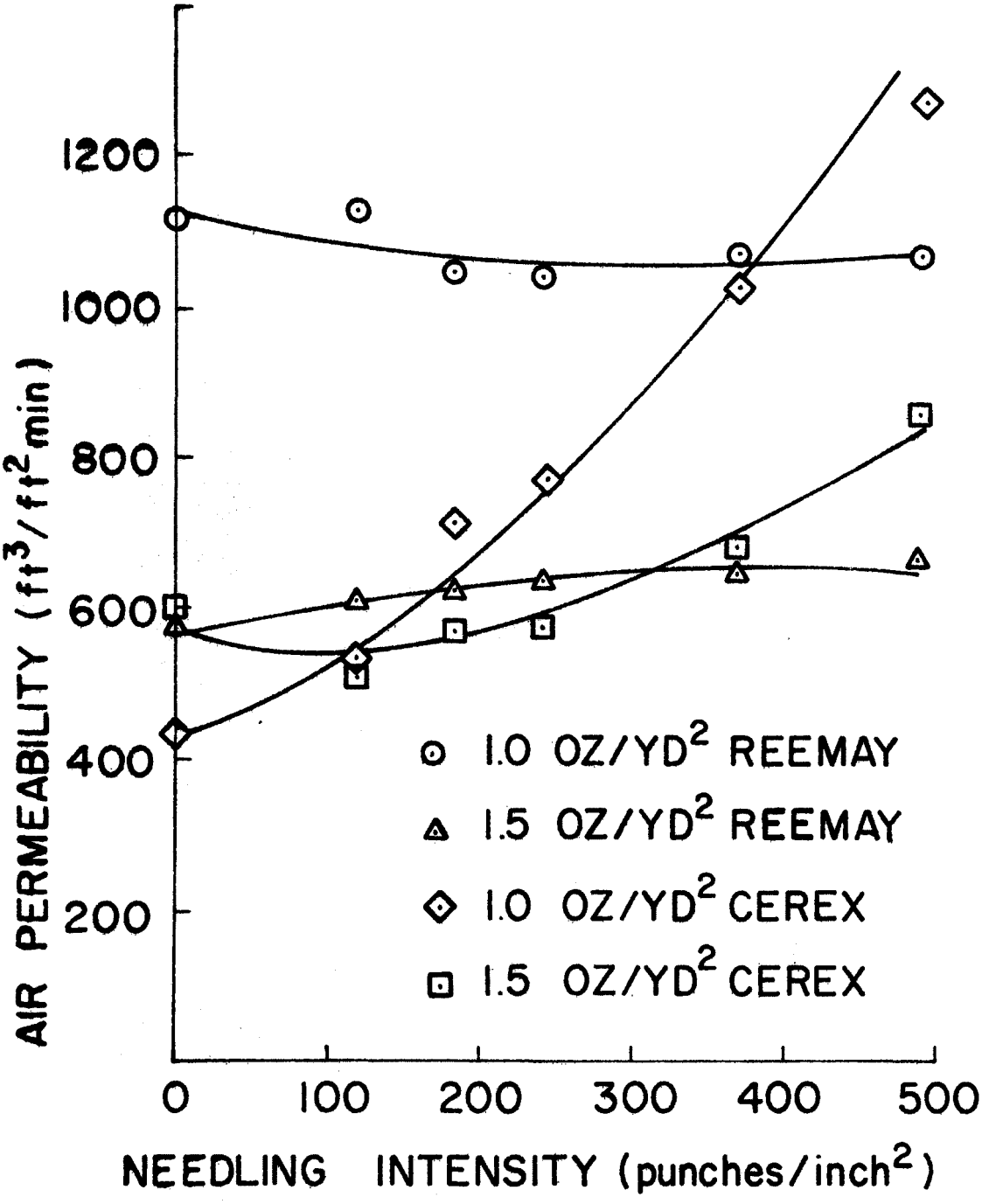

Figure 43. Air permeability vs. needling intensity (Cerex and Reemay spunbonded fabric only)

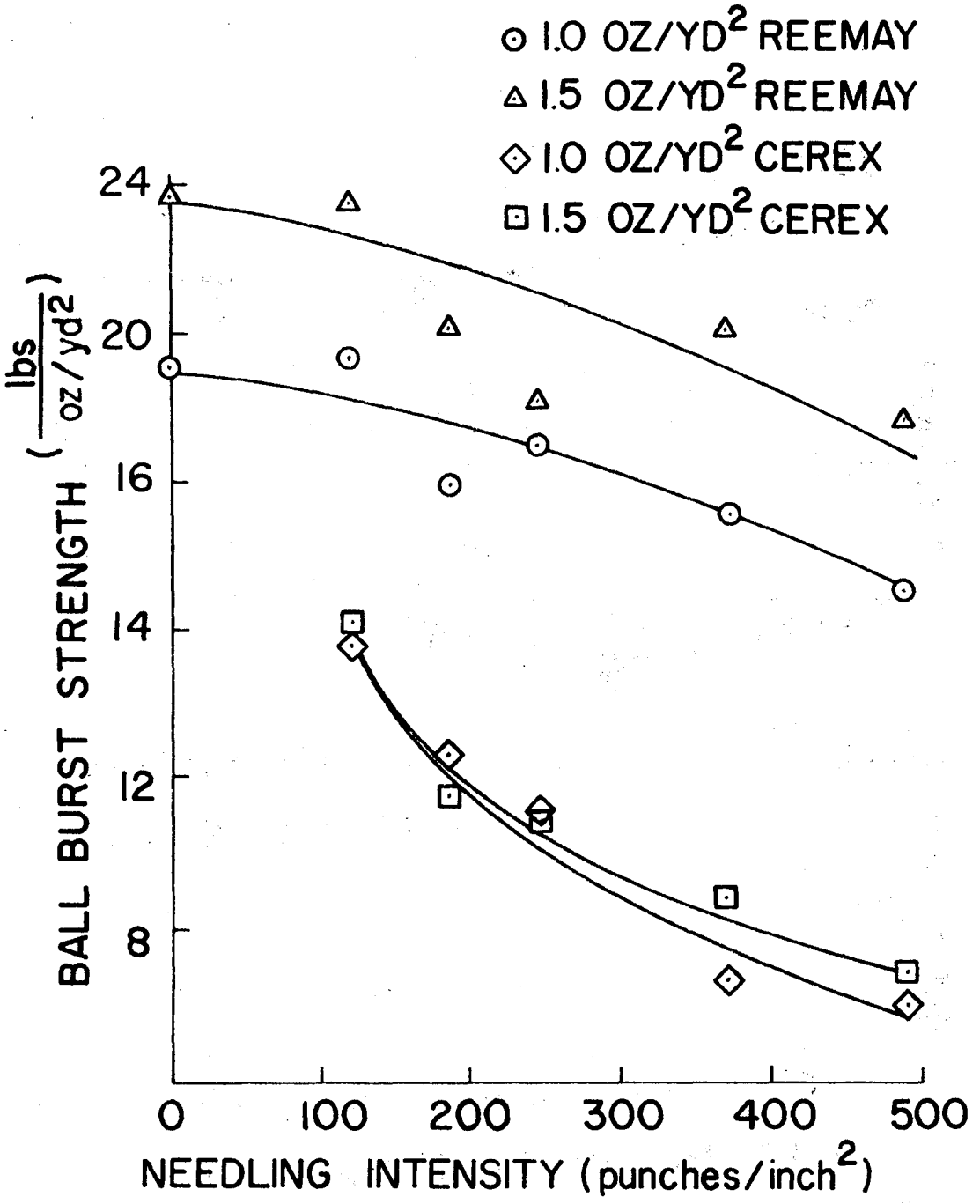

Figure 44. Ball burst vs. needling intensity (Cerex and Reemay spunbonded fabric only)

high levels of filament damage with the increase in needling intensity. The bursting strength curves also show an appreciable reduction for the Cerex with needling as indicated by Figure 44.

Needle punched fabrics were produced using two layers of web 4.8 oz./yd^2 one on each side of the scrim. The fabrics were tested for all physical properties and filtration performance. Figure 45 shows the changes in thickness with needling intensity. The lowest fabric thickness was obtained with the 1.5 oz./yd^2 Cerex scrim. Cerex in general gives lower thickness than Reemay which is an indication of higher packing density due to good locking of the fibers into the Cerex. Figure 46 shows little change in fabric weight per unit area with needling intensity and minor differences between Reemay and Cerex scrim fabrics. In both cases, it was observed that the level of fiber spreading was greatly reduced as compared to the no scrim situation. Cerex scrim fabric, as mentioned earlier, gave higher fabric density as shown in Figure 47. In spite of this high density, Cerex scrim fabric had higher air permeability than the Reemay fabrics as shown in Figure 48. The effect of needling intensity was not appreciable in both cases which indicated that the role played by the scrim is more effective than the needling intensity. The air permeability-thickness product curves are shown in Figure 49. Although needling the Cerex fabric by itself gives lower bursting strength than the corresponding Reemay fabric, it can be seen from Figure 50 that the opposite is true when needling is done with fibrous webs. The presence of the fibers protected the filaments of the scrim from damage.

Samples of all these fabrics were batch tested for filtration performance using flyash. Table 7 gives the data for the flyash concentration and the results of the final pressure drop (after 10 minutes) and the collection efficiency. It can be seen that, in general, the Cerex scrim fabrics gave slightly higher pressure drop than the corresponding Reemay scrim fabrics. This can be related to the high packing density obtained with the Cerex scrim as discussed earlier. The efficiency results indicate that there was no significant difference between Cerex and Reemay scrim fabrics. However, the heavier the scrim fabric the higher the efficiency.

7.6 Bag Fabrics

In all previous experiments, the fabrics were made of web layers without prepunching each layer. The layers were assembled and punched only from one side and with minimum number of passages through the needling process. This was done to study the effects of needling

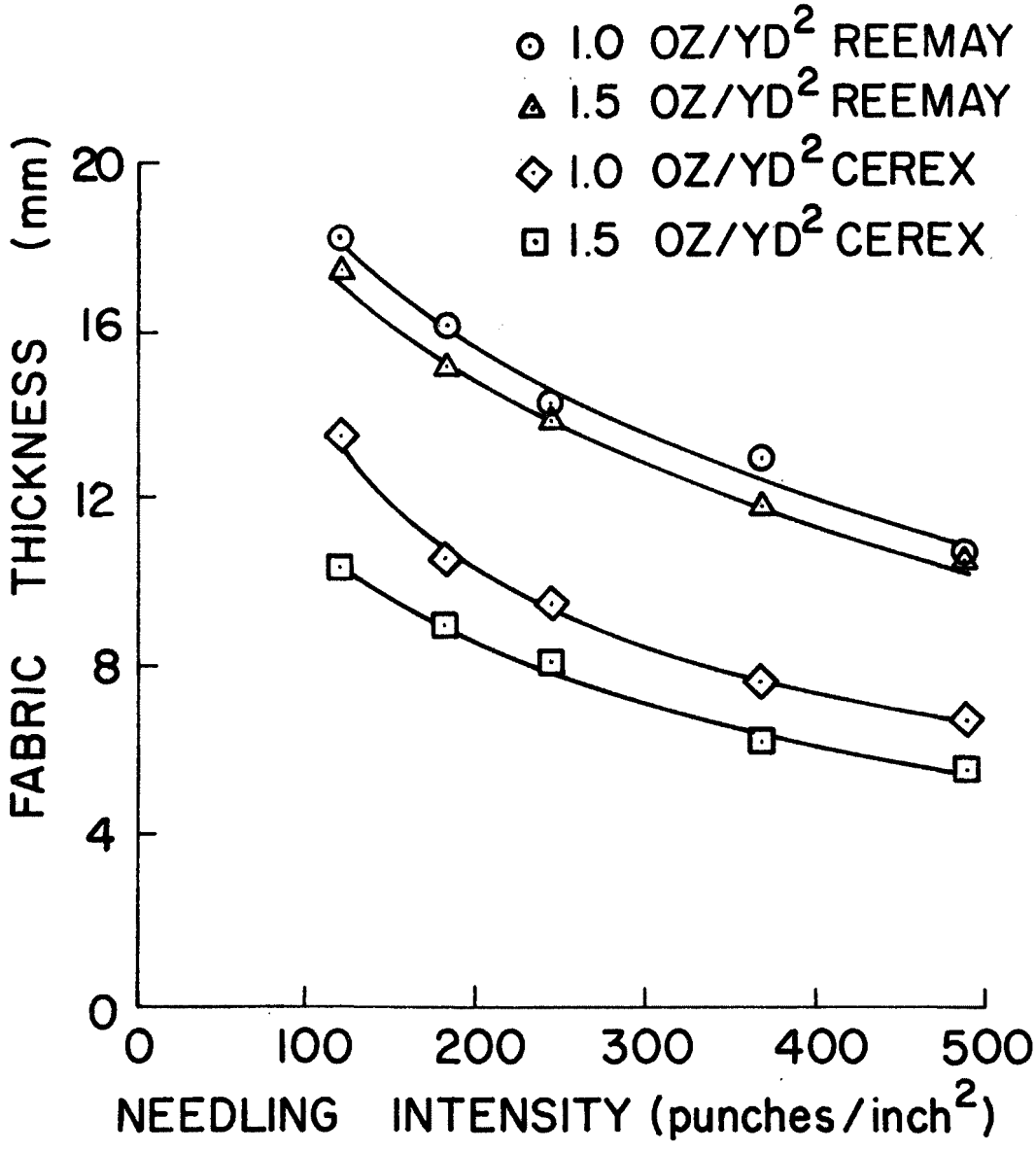

Figure 45. Fabric thickness vs. needling intensity (spunbonded scrim)

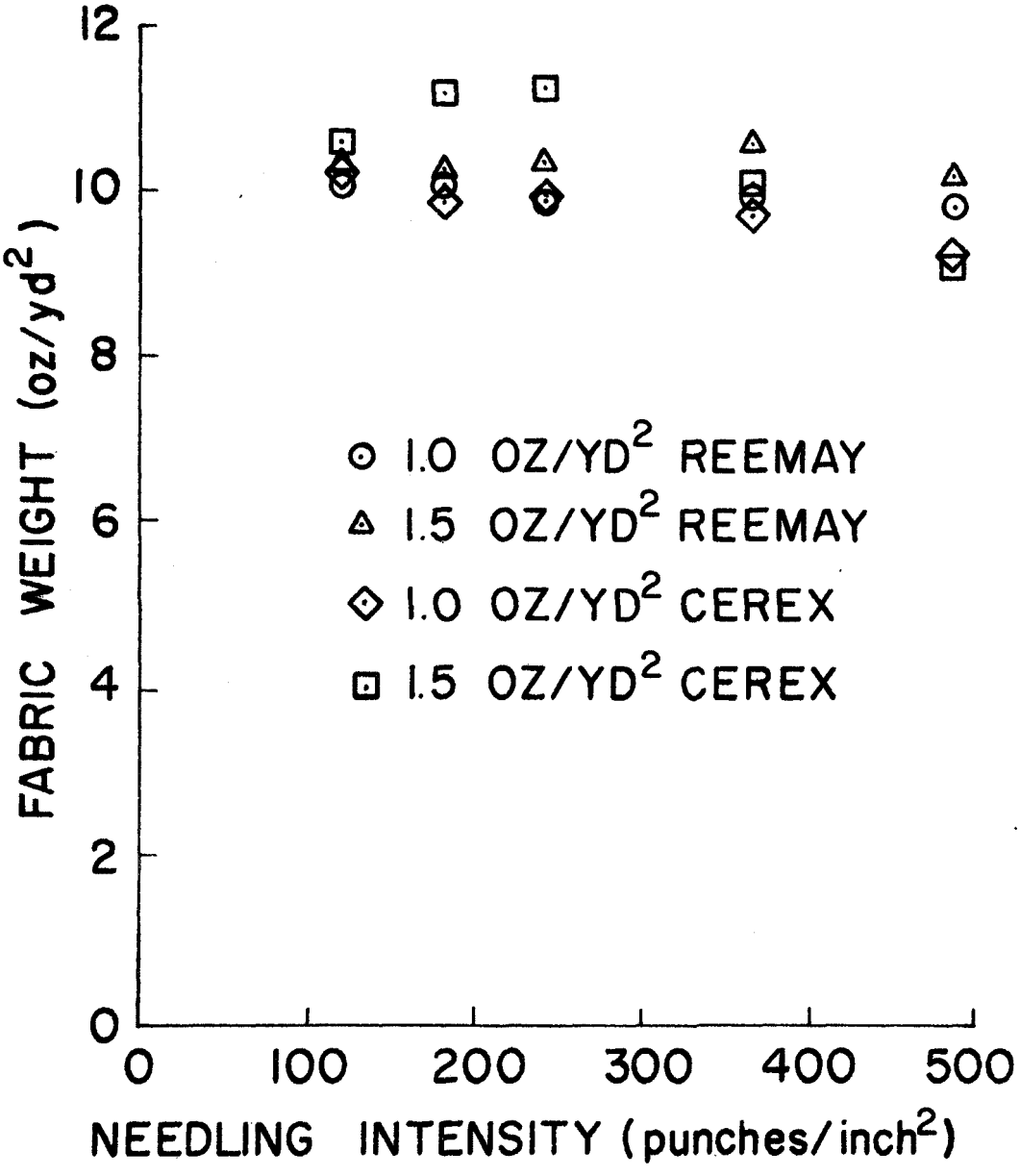

Figure 46. Fabric weight vs. needling intensity (spunbonded scrim)

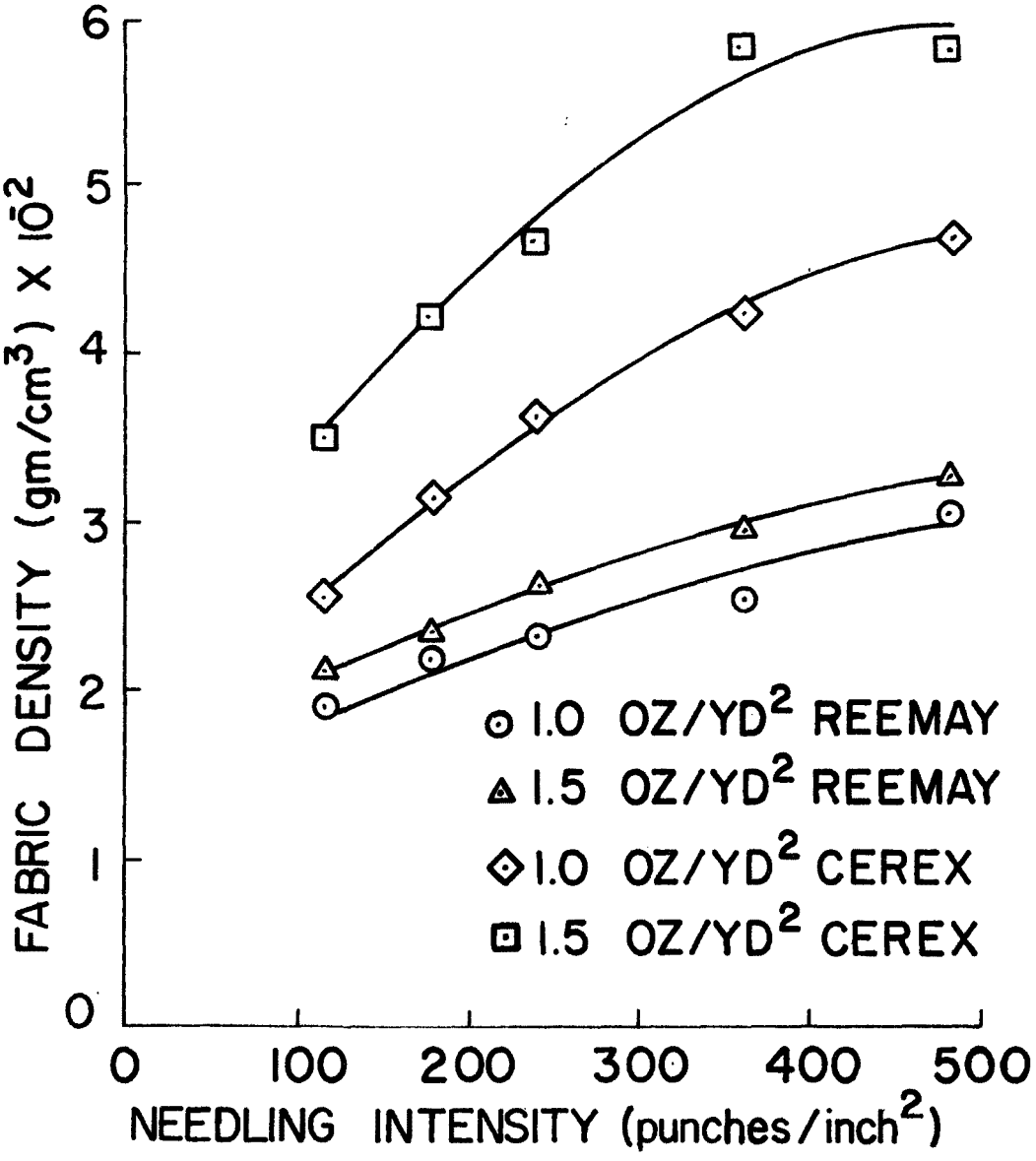

Figure 47. Fabric density vs. needling intensity (spunbonded scrim)

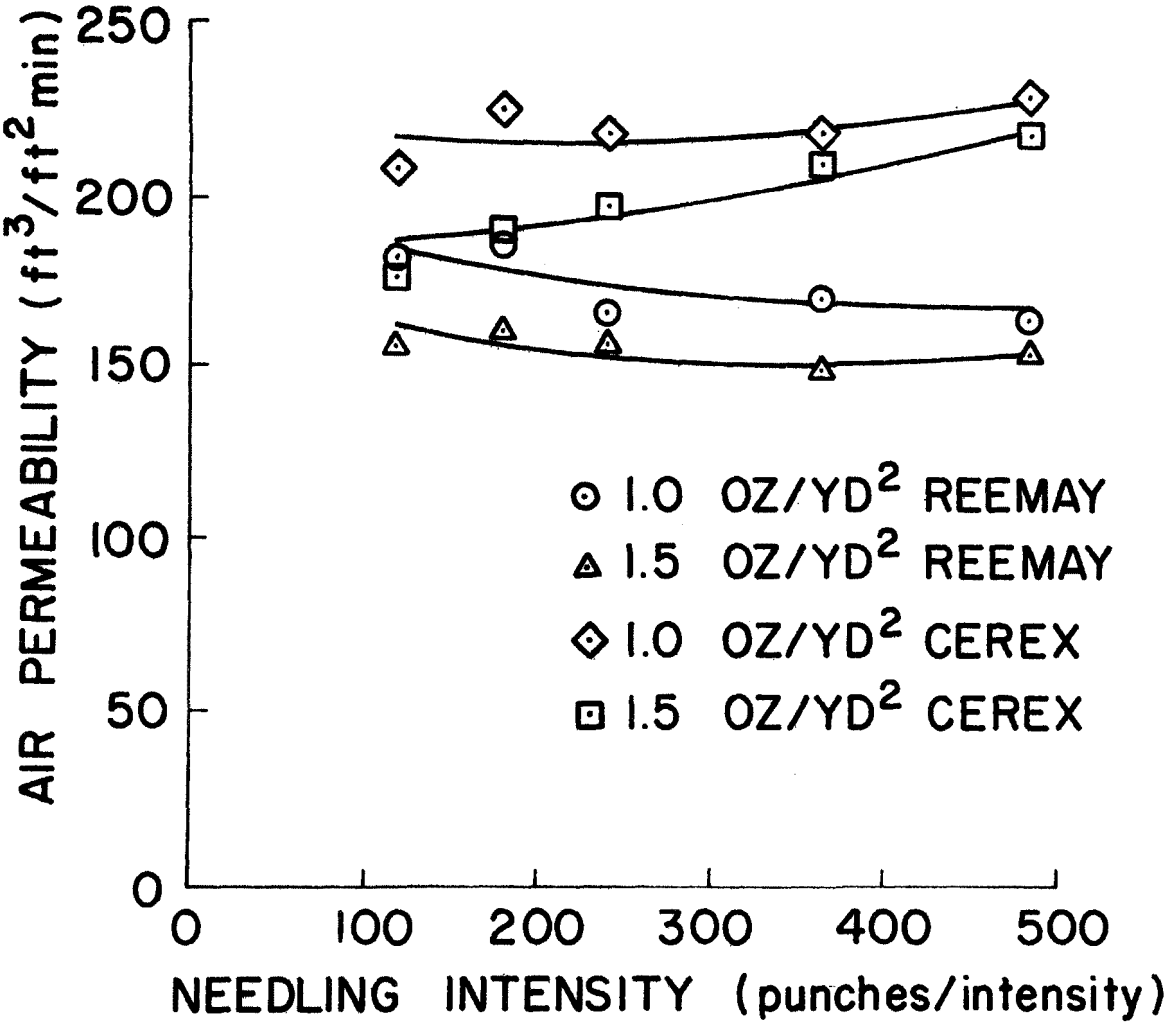

Figure 48. Air permeability vs. needling intensity (spunbonded scrim)

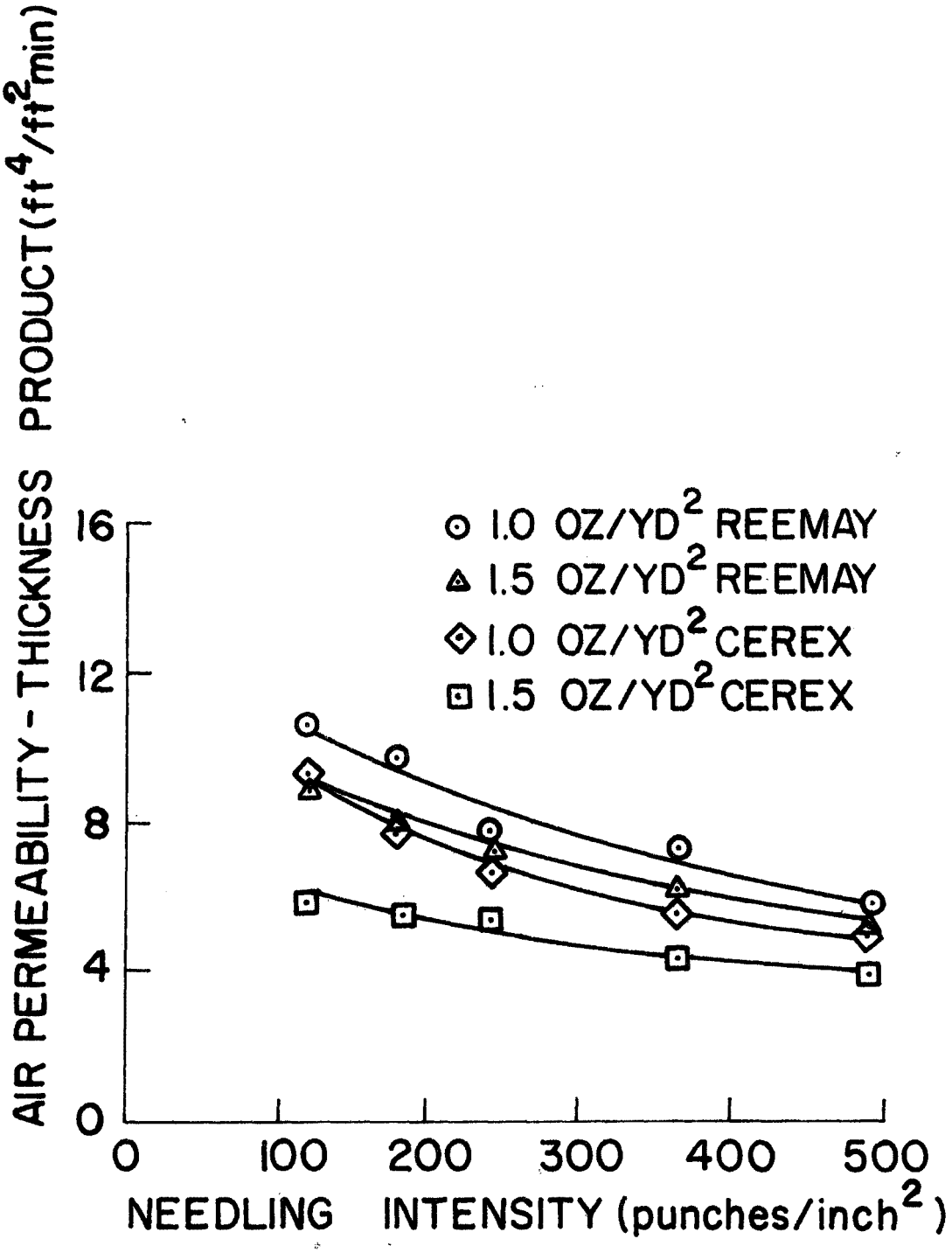

Figure 49. Air permeability - thickness product vs. needling intensity (spunbonded scrim)

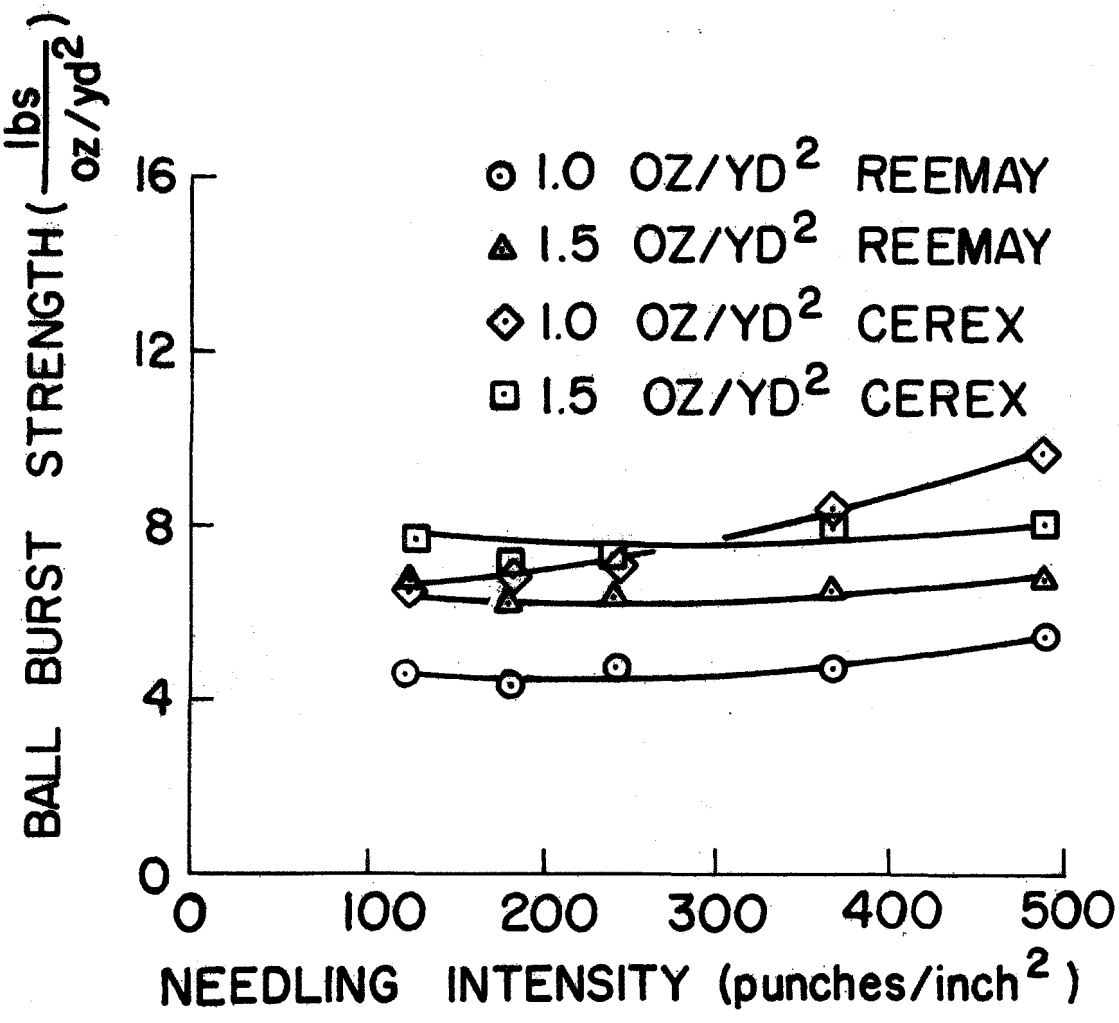

Figure 50. Ball burst strength vs. needling intensity (spunbonded scrim)

Table 7. BATCH FILTRATION PERFORMANCE OF SPUNBONDED SCRIMMED FABRICS

Scrim Fabric	Needling Intensity Punches/in.^{2}	C_i gr./ft.^{3}	ΔP_c Inches H_2O	ΔP_f Inches H_2O	Efficiency %
Reemay 1.0 oz./yd.^{2}	122	1.44	0.105	0.55	97.68
	245	1.61	0.122	0.64	98.32
	368	1.64	0.115	0.77	97.77
	490	1.66	0.120	0.62	98.28
Cerex 1.0 oz./yd.^{2}	122	1.86	0.110	0.96	97.46
	245	1.56	0.102	0.73	97.55
	368	1.46	0.122	0.94	97.39
	490	1.64	0.143	1.5	97.63
Reemay 1.5 oz./yd.^{2}	122	2.05	0.120	0.83	98.32
	245	1.65	0.130	0.73	98.22
	368	2.20	0.120	1.17	98.35
	490	1.41	0.110	0.85	98.10
Cerex 1.5 oz./yd.^{2}	122	1.71	0.115	1.05	98.51
	245	1.60	0.145	0.95	98.52
	368	2.13	0.133	1.22	98.63
	490	1.80	0.094	0.83	98.40

Air velocity = 45 ft/min.
Needle penetration = 0.333 inch
Random-laid, 25 gauge, Dacron $1\frac{1}{2}$" x 3.0 denier
p_1 = 0.250", p_2 = 0.333", p_3 = 0.416", p_4 = 0.500"

intensity and the other fabric parameters to avoid complicating the fabric structure. It is well known that prepunching the individual layers before assembly increases the packing density of each layer and hence the packing density of the final fabric. For this reason it was decided to prepunch the layers in preparation for the bag fabrics which produces fabrics with multi-layer structures. In baghouse applications with needle punched fabrics, cleaning is normally done by using pulse jet in the opposite direction to the flow. If needling is done from one side only, the face side of the fabric should be identified and has to be used as the collecting surface. The backside of the fabric will have fibers that are not securely held in the fabric structure and may cause problems in use. Needling from both sides was found to yield better consolidated fabrics than needling from one side only with the same total number of punches per square inch. Fabrics produced by needling from both sides will not require identification of a particular side which makes fabric manufacturing less troublesome. It is also speculated that such fabrics will make the cleaning process easier. To increase the strength of the fabric and the interlocking between the layers and the scrim, punching was done over four or six passes through the needle punching machine at 122 punches per square inch each pass. In the manufacture of these bag fabrics, the webs were passed through the machine several times. In manufacturing line this could be achieved by using multiple heads needling consecurtively or simultaneously from both sides in one pass to increase productivity and reduce handling and cost.

Bag fabrics were manufactured in the laboratories of Hercules Incorporated, Research Triangle Park, North Carolina. Four layers of random-laid webs, 4.0 oz./yd.^{2} each made from 3.0 denier x $1\frac{1}{2}$-inch Dacron® staple, were used in every fabric. The layers were prepunched with 25 gauge needles at 122 punches/inch^2. Four fabrics were made without scrim and four with Cerex 1.5 oz./yd.^{2} scrim with two layers on each side. The assembled layers were punched with 25 or 32 gauge needles at a speed of 500 punches/minute.

Table 8 gives the properties of the eight fabrics. It can be seen that the fabrics without scrim suffered badly from fiber spreading as indicated by the reduction in fabric weight which was also observed during manufacturing. Needling over six passes with the 25 gauge needle reduced the fabric strength as compared to that of the fabrics with four passes. This effect was not pronounced in the case of the 32 gauge fabrics. The bursting strength results also show that the 25 gauge needle caused more damage than the 32 gauge needle.

Table 8. PROPERTIES OF BAG FABRICS

Fabric	Thickness (inches)	Weight ($oz./yd.^2$)	Air Permeability ($ft.^3/ft.^2$ min.)	Ball Bursting Load (lbs)
Scrim* (25 gauge) 4 x 122	0.213	12.8	206.3	153.4
Scrim* (25 gauge) 6 x 122	0.141	11.3	217.9	105.0
Scrim* (32 gauge) 4 x 122	0.220	13.4	89.0	220.0
Scrim* (32 gauge) 6 x 122	0.199	13.3	84.2	225.6
No Scrim (25 gauge) 4 x 122	0.182	7.8	208.6	118.6
No Scrim (25 gauge) 6 x 122	0.119	5.8	208.4	86.8
No Scrim (32 gauge) 4 x 122	0.204	9.8	150.4	191.6
No Scrim (32 gauge) 6 x 122	0.167	8.8	144.1	187.4

Scrim used was Cerex 1.5 $oz./yd.^2$
4 x 122 means 4 passes 122 punches/$inch^2$ each (2 from each side)
6 x 122 means 6 passes 122 punches/$inch^2$ each (3 from each side)

Table 9 gives the results of the filtration performance of the bag fabrics in batch testing according to the procedure described under 6.7. The scrim fabrics gave higher pressure drop and efficiency than the no scrim fabrics. Needling six times resulted in higher pressure drop than needling four times although there was no significant effect on efficiency. In spite of the large differences in the air permeability of the fabrics made with the 25 gauge and 32 gauge needles, little differences were detected in pressure drop and efficiency.

Bags of $4\frac{1}{2}$-inch diameter and 48 inches length were manufactured from the eight fabrics and were tested in a pulse-jet baghouse at the Industrial Environmental Research Laboratory, Environmental Research Center, EPA, Research Triangle Park, North Carolina. Table 10 gives details of the testing conditions and results for pressure drop and efficiency for six fabrics. Bags from the two 25 gauge fabrics without scrim were not tested since they were apparently damaged due to fiber spreading. For the four fabrics (1 to 4) the results indicated high efficiency and low pressure drop for inlet dust loading range from 0.5 to 12 grains/ft^3 and air-to-cloth ratio up to 9/1. In comparison with a commercial needle felt fabric (tested under the same conditions at EPA) the four fabrics with scrim were superior for the above conditions. The no scrim fabrics tested showed high efficiency only at low air-to-cloth ratio (6/1). At higher air-to-cloth ratios, the efficiency was low which can be related to the low dimensional stability of these fabrics. When fabrics 1 and 4 were tested at high air-to-cloth ratios (40/1 and 33.6/1 respectively) low efficiency and low pressure drop were reported even at low inlet dust loading. This could be due to either the high pulse pressure expanding the fabric or due to the tight fit on the wire cage reported which might have resulted in fabric stretch which could lead to fabric damage. Figure 51 shows the appearance of one of the bags tested (fabric 5) at high air-to-cloth ratio as compared to the commercial felt bag. The bad appearance is due to the removal of fibers from the fabric surface by handling which can be overcome by finishing treatments. Treatments such as calendering, resin application or shrinking could increase fabric stability and durability. However, these treatments would lead to an increase in the pressure drop. The effect of calendering was investigated and the results will be discussed later. Work is needed in the areas of shrinking and resin treatments to determine their effect on filtration performance of needle punched fabrics.

Table 9. BATCH FILTRATION PERFORMANCE OF BAG FABRICS

Fabric	C_i gr./ft.^{3}	ΔP_c Inches H_2O	ΔP_f Inches H_2O	Efficiency %
Scrim (25 gauge) 4 x 122	1.91	0.14	1.70	99.30
Scrim (25 gauge) 6 x 122	1.81	0.23	3.07	99.35
Scrim (32 gauge) 4 x 122	1.69	0.21	1.61	99.23
Scrim (32 gauge) 6 x 122	2.11	0.24	2.70	99.20
No Scrim (25 gauge) 4 x 122	1.62	0.07	1.02	98.01
No Scrim (25 gauge) 6 x 122	2.06	0.07	1.12	97.93
No Scrim (32 gauge) 4 x 122	1.86	0.12	1.52	98.85
No Scrim (32 gauge) 6 x 122	2.09	0.09	1.67	98.86
Commercial Needle Felt (15.27 oz/yd^2)	1.03	0.40	5.20	99.70

Air velocity = 45 ft/min.
Random-laid, Dacron $1\frac{1}{2}$" x 3.0 denier
Needle penetration = 0.333 inch
Scrim used was Cerex 1.5 oz/yd.^{2}

Table 10. BAGHOUSE TESTING RESULTS

	Fabric	C_i Inlet Loading Grains/ft^3	C_o Grains/ 1000 ft^3	Pulse Pressure Psig	Pulse Interval Sec.	Air/cloth Ratio ft./min.	ΔP_f Inches H_2O	Efficiency %	Run Time Hours
1	25 gauge Scrim 4 x 122	0.5	.2668	50	140	6/1	0.625	99.961	24
		3.0	.3134	60	140	6/1	0.99	99.989	20
		6.0	.0820	60	140	6/1	1.51	99.999	21
		12.0	4.4587	80	100	6/1	4.22	99.961	21
		3.0	11.2842	85	60	9/1	4.23	99.656	12
		0.5	90.9600	90	140	40/1	3.80	82.267	16
2	32 gauge Scrim 4 x 122	0.5	.1833	50	140	6/1	0.73	99.967	25
		3.0	.3954	60	140	6/1	1.23	99.987	21
		6.0	.3665	60	140	6/1	1.72	99.994	12
		12.0	.8125	60	140	6/1	2.62	99.993	15
		3.0	1.8960	75	140	9/1	3.62	99.937	11
3	25 gauge Scrim 6 x 122	0.5	.3761	50	140	6/1	0.62	99.938	23
		3.0	.1109	60	140	6/1	0.91	99.996	22
		6.0	.1279	60	140	6/1	1.11	99.998	12
		12.0	.5931	60	140	6/1	1.67	99.995	13
		3.0	2.6612	65	140	9/1	3.18	99.912	12

Table 10 (continued). BAGHOUSE TESTING RESULTS

	Fabric	C_i Inlet Loading Grains/ft^3	C_o Grains/ 1000 ft^3	Pulse Pressure Psig	Pulse Interval Sec.	Air/cloth Ratio ft./min.	ΔP_f Inches H_2O	Efficiency %	Run Time Hours
	32 gauge								
	Scrim	0.5	.1575	60	140	6/1	0.68	99.972	25
	6 x 122	3.0	.0563	60	140	6/1	1.21	99.998	21
		6.0	.0842	60	140	6/1	1.69	99.999	13
4		12.0	.1051	60	140	6/1	2.60	99.991	13
		3.0	23.7140	85	45	9/1	6.42	99.210	12
		0.5	83.1800	90	110	33.6/1	4.85	85.619	12
	32 gauge								
	No Scrim	0.5	.4774	50	140	6/1	0.60	99.926	29
	6 x 122	3.0	.3129	60	140	6/1	0.90	99.989	21
5		6.0	.4019	60	140	6/1	1.10	99.993	12
		12.0	.4543	60	140	6/1	1.73	99.996	11
		3.0	343.9600	85	140	9/1	4.30	88.663	15
	32 gauge								
	No Scrim -	0.5	.4082	50	140	6/1	0.57	99.932	25
	4 x 122	3.0	.3874	60	140	6/1	0.90	99.987	21
6		6.0	.5353	60	140	6/1	1.11	99.991	12
		12.0	.6172	60	140	6/1	1.55	99.995	10
		3.0	57.6599	80	140	9/1	3.47	98.0781	10

Table 10 (continued). BAGHOUSE TESTING RESULTS

Fabric	C_i Inlet Loading Grains/ft^3	C_o Grains/ 1000 ft^3	Pulse Pressure Psig	Pulse Interval Sec.	Air/cloth Ratio ft./min.	ΔP_f Inches H_2O	Efficiency %	Run Time Hours
Commercial								
Dacron	0.5	0.1511	55	140	6/1	0.60	99.9698	12
Felt	3.0	1.7471	55	140	6/1	1.73	99.9412	75
16 oz/sq.yd.	6.0	9.8174	55	140	6/1	2.92	99.8339	24
	12.0	46.3768	80	108	6/1	7.55	99.6080	14
	3.0							
	0.5	2.8594	90	85	32.6/1	5.84	99.4500	17

RH = 50% Temp = 70° F Δp at end of filter cycle C_o = Outlet concentration

Tests for the NCSU and commercial felt fabrics with 3.0 grains/ft.^{3} inlet concentration and air/cloth ratio resulted in blinding and the tests were terminated.

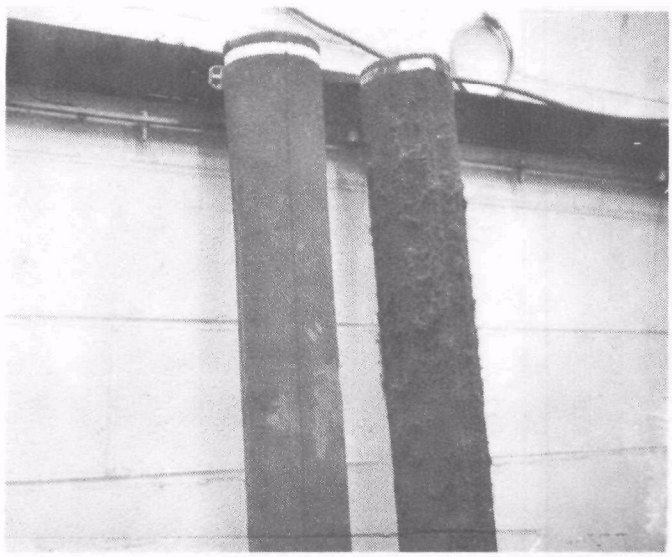

A B

Figure 51. Bag Appearance
A - Commercial Bag
B - Bag Made From Fabric 5

7.7 Experimental Verification of The Theory

Fabric samples were tested for various properties which were needed for verification of the pressure drop theory. The data of these fabrics given in Table 11 was used to calculate theoretical values of the pressure drop. Pressure drop measurements were carried out without dust and the results are given in Figure 52. It is seen that the theoretical predication is in good agreement with the experimental values. The dependence of this approach on counting the number of pores per unit area and the number of fibers reoriented in the pores, makes this process time consuming. It is felt that more work is needed to relate the number of fibers in the pore to the other fabric parameters which is a very large undertaking.

To establish the role of the collection mechanisms, tests were carried out using latex spheres having diameters of 0.5, 1.099 and 2.02 microns and face velocities ranging from 1.1 to 15.75 cm./sec. in ten intervals. For each velocity, the particle count before and after the test filter was repeated three times and the average was used to determine the penetration. The data presented in Figures 53 to 55 give the particle penetration as a function of the face velocity. From these curves the velocity at which maximum penetration occurs was used in equations (48) and (49) to determine the Dorman parameters for the fabrics designated A to E in Table 12. From this table it is noticed that the values of k_D for all the filters tested were much smaller than those of k_R and k_I parameters. This is mainly due to the very low particle loading (no cake formation) and the use of monodisperse latex particles which indicates little contribution from the diffusion mechanism. This may render the fabrics tested unsuitable for use in the submicron region. It is anticipated that modifications of the fabric structure by post treatments, as mentioned earlier, would improve the performance of these fabrics in the submicron range.

7.8 Mechanics of Cake Formation

Each of the three collection mechanisms functions efficiently over limited ranges of particle size, gas velocity, packing density and other gas/fabric properties. The inertial mechanism is highly efficient when large particles and gas velocities are used. The interception mechanism is independent of gas velocity and is more influenced by the increase in size of the particles, while the diffusion mechanism dominates when submicron particles and low gas velocity conditions prevail.

Table 11. FABRIC PROPERTIES USED FOR VERIFICATION OF THEORY

Needle Size	Needling Intensity Punches/inch^2	Actual No. of Pores Per Inch^2 N^*	Mean Pore Diameter D^* mm	No. of Fiber Per Pore n	Fabric Thickness ΔL mm	Packing Density %
20 gauge	122	120	0.501	133	26.2	1.0
	245	170	0.590	134	18.2	1.3
	368	215	0.730	103	17.5	1.0
	490	235	0.796	151	14.5	1.5
25 gauge	122	115	0.457	62	16.2	1.6
	245	160	0.478	83	12.0	2.1
	368	210	0.511	82	9.5	2.5
	490	250	0.580	139	8.2	2.7
32 gauge	122	110	0.427	162	22.5	1.2
	245	135	0.435	130	17.5	1.5
	368	185	0.460	81	15.3	1.7
	490	230	0.470	102	12.6	1.9

Needle Dimension

20 gauge, d = 0.924 mm
25 gauge, d = 1.178 mm
32 gauge, d = 1.409 mm

(Dacron 3 denier x $1\frac{1}{2}$-inch, Cross-Lapped)

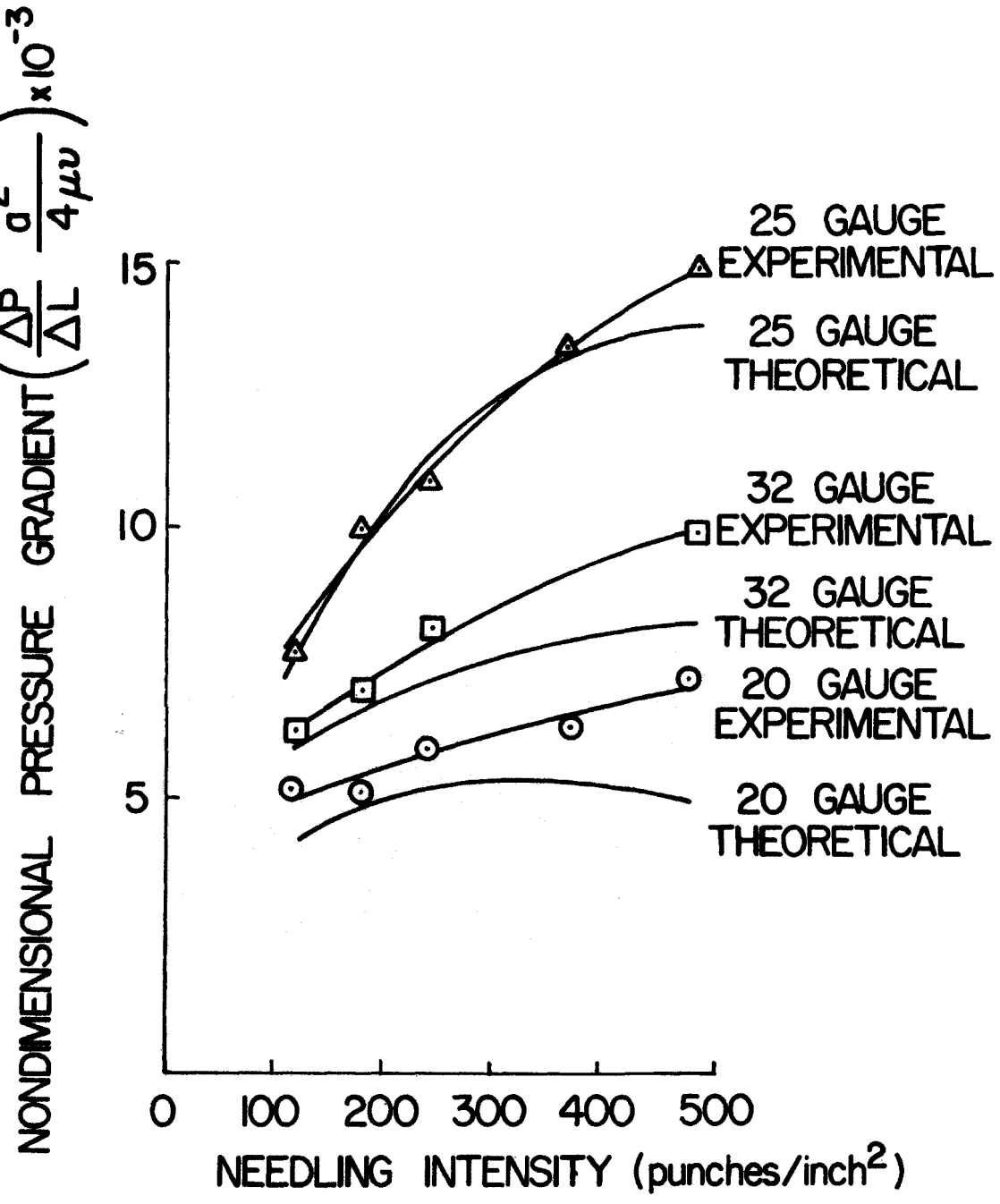

Figure 52. Nondimensional pressure gradient vs. needling intensity (Dacron 3 den. x 1.5 in., crossed - lapped)

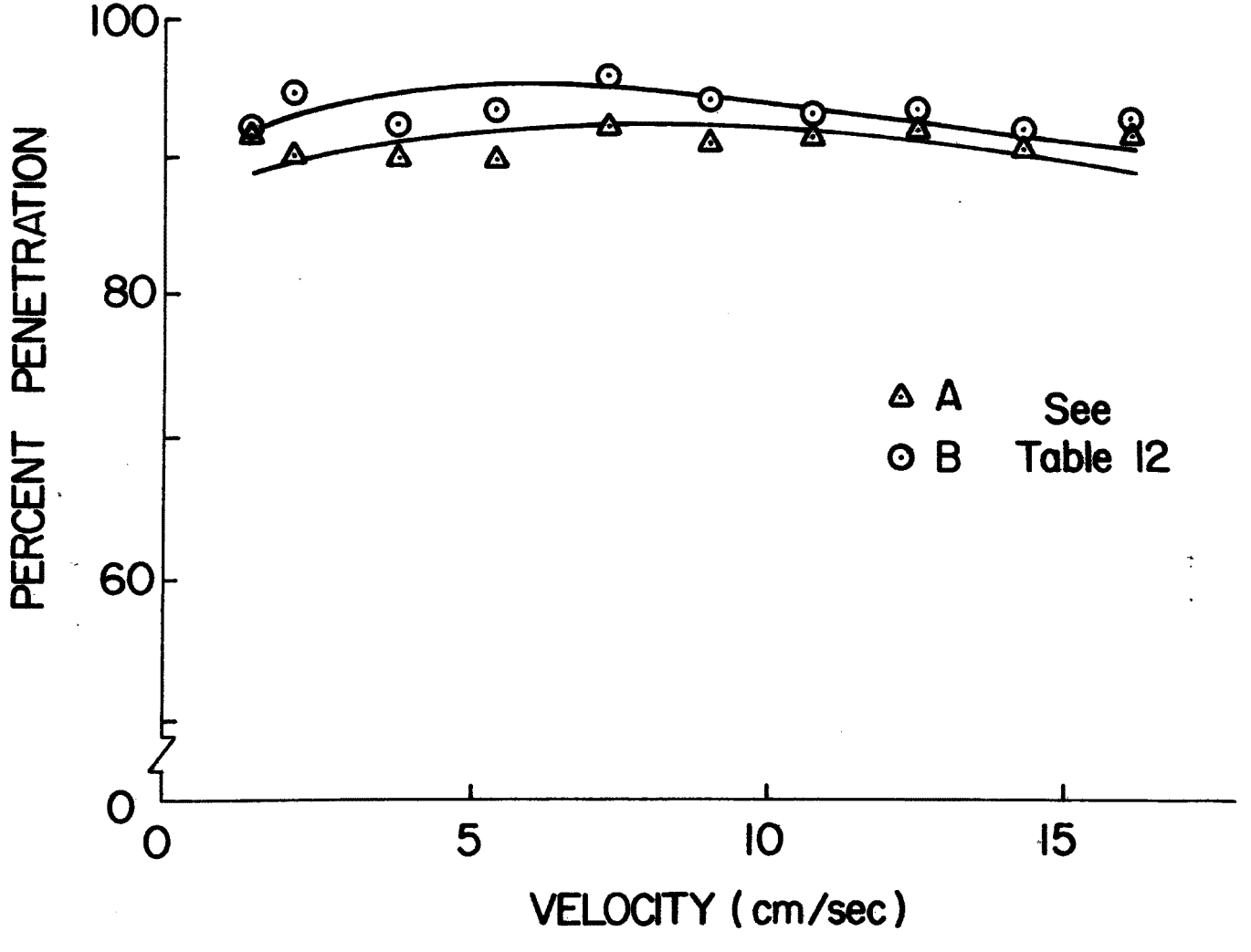

Figure 53. Percent penetration vs. velocity for 0.5 μm

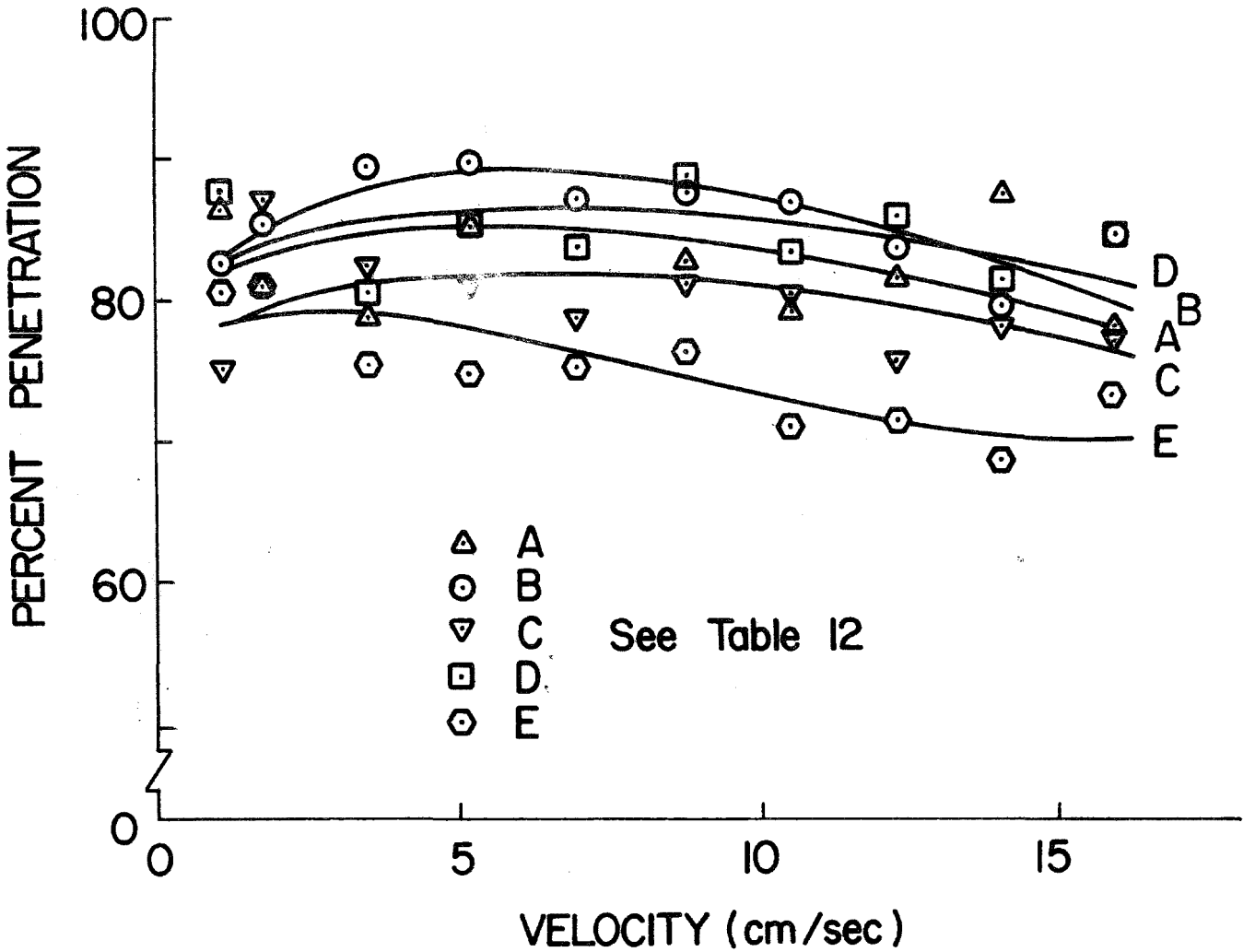

Figure 54. Percent penetration vs. velocity for 1.099 μm

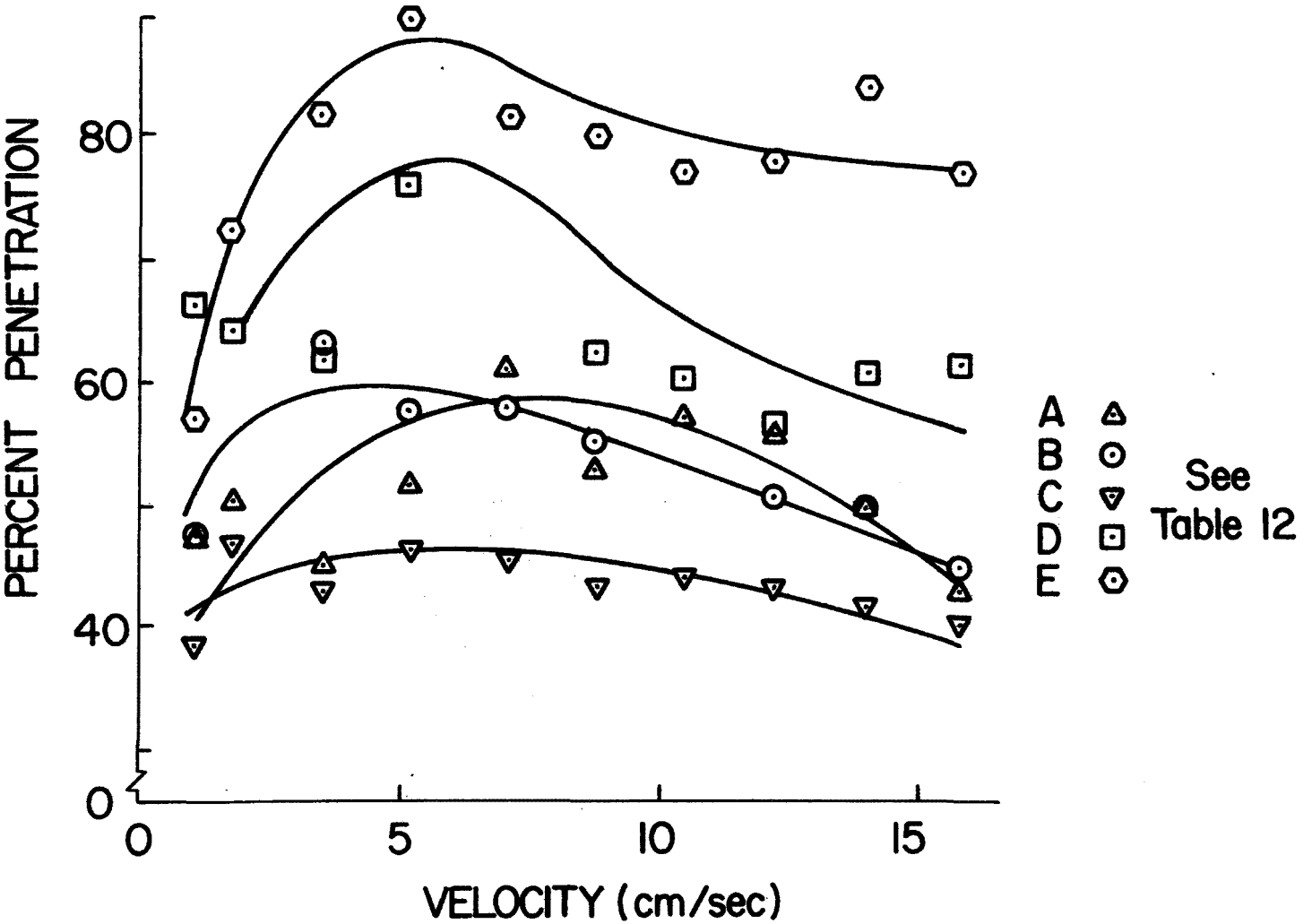

Figure 55. Percent penetration vs. velocity for 2.02 μm

Table 12. DORMAN PARAMETERS

	Fabric	Particle Size μm	k_I (Interception) cm^{-1}	k_R (Impaction) $cm^{-3} \cdot sec^2 \times 10^{-5}$	k_D (Diffusion) $cm^{-1/3} \cdot sec^{-2/3}$
A	4 x 122	0.50	0.070	2.30	0.0095
	32 gauge	1.099	0.133	16.30	0.0411
	Cerex 1.5 oz./yd.^{2} Scrim	2.02	0.404	65.60	0.0990
	(185 punches/min.)				
B	6 x 122	0.50	0.050	9.04	0.0710
	32 gauge	1.099	0.102	13.70	0.0720
	Cerex 1.5 oz./yd.^{2} Scrim	2.02	0.402	64.30	0.2190
	(185 punches/min.)				
C	4 x 122	0.50	*	*	*
	32 gauge	1.099	0.373	74.09	0.0141
	Cerex 1.5 oz./yd.^{2} Scrim	2.02	1.373	151.36	0.3682
	(500 punches/min.)				
D	4 x 122	0.50	*	*	*
	25 gauge	1.099	0.128	16.15	0.0014
	Cerex 1.5 oz./yd.^{2} Scrim	2.02	0.223	43.39	0.1694
	(500 punches/min.)				
E	4 x 122	0.50	*	*	*
	25 gauge	1.099	0.239	44.14	0.0083
	No Scrim	2.02	0.853	110.87	0.0298
	(500 punches/min.)				

*Flat penetration curves were obtained leading to no V_m value to calculate the parameters.

The cake formed on needle punched uncalendered filters differs distinctively from that formed on any other filter media. Normally the developed cake over the surface of a filter is homogeneous and has a uniform thickness, whereas in needle punched filters the dust forms distinct three-dimensional mounds around the pores as shown in Figure 56. This is mainly due to the variation in the packing density over the surface of the filter caused by the needling process. The tendency of the flow to follow the least resistance path causes the large particles to depart from the streamlines by inertia and deposit around the pores, and causes the small particles to ride the streamlines and deposit in the pores as was explained earlier. The increase in packing density around the pores allow the inertial and interception mechanisms to be effectively employed. The increase in the surface area of collection, due to the orientation of the fibers in the pores parallel to the flow direction, gives a better chance for the collection of small particles in the pores. The characteristics of the cake formed will also reduce the time rate of pressure rise across the filter as mostly the small size particles are deposited in the pore area. Figure 57 shows the reduction in the number of pores due to their being progressively plugged when the test time was increased from five minutes to 20 minutes.

A commercial needle felt bag fabric having 15.3 oz./yd.^{2} weight (which is believed to be calendered) was batch tested and the cake formed was homogeneous similar to that obtained with woven fabrics. It is worthy of mention that with inlet concentration (C_i) of 1.03 gr./ft.^{3} the efficiency was 99.7% and the pressure drop (ΔP_f) 5.2 inches of water. When a needle punched fabric was calendered similar results were obtained. This indicates that calendering needle punched fabrics destroys the structure and give high levels of pressure drop.

7.9 Effect of Dust Concentration On Efficiency In Batch Testing

Figure 58 shows the effect of concentration on efficiency for a needle punched fabric. The figure indicates that the efficiency increases with concentration up to 1.6 gr./ft.^{3} after which the efficiency does not increase substantially. However, it must be remembered that although this trend remains the same for different conditions, yet the level of concentrations after which the efficiency levels off may vary with test conditions.

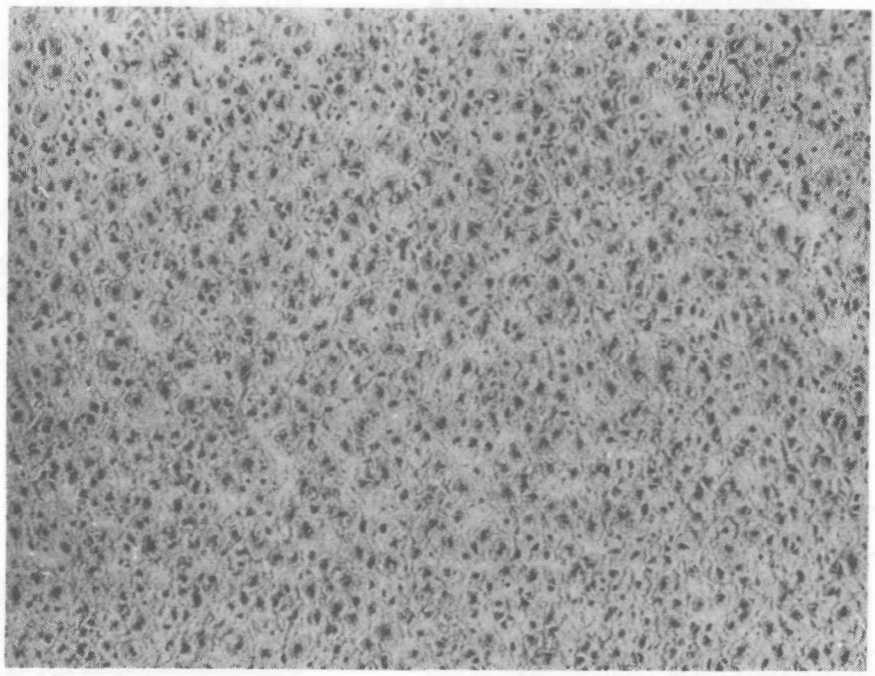

Figure 56. Dust Cake on a Needle Punched Filter

Figure 57. Effect of Filtration Time on Cake Formation

Air Velocity = 45 ft/min.
Flyash Concentration: 1.54 gr./ft.^{3}

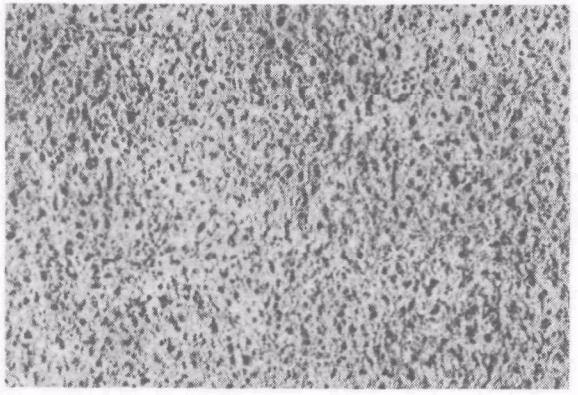

5 minutes

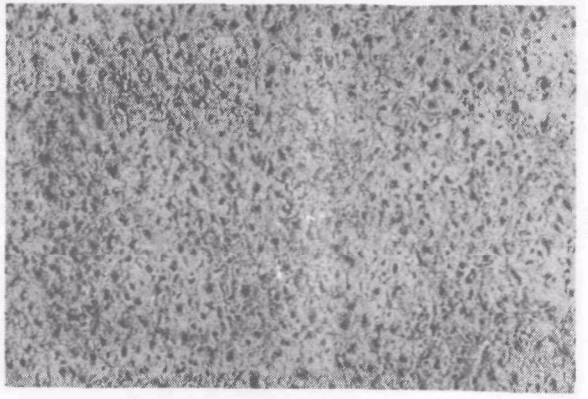

10 minutes

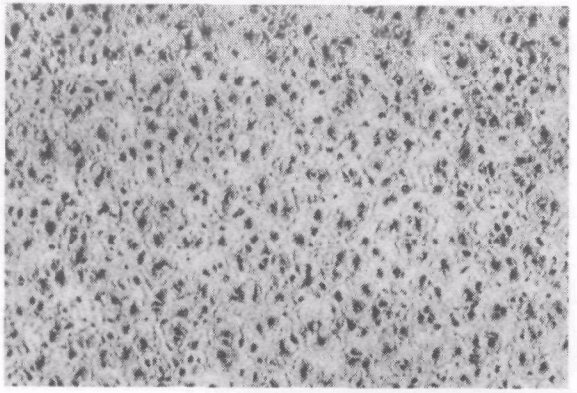

15 minutes

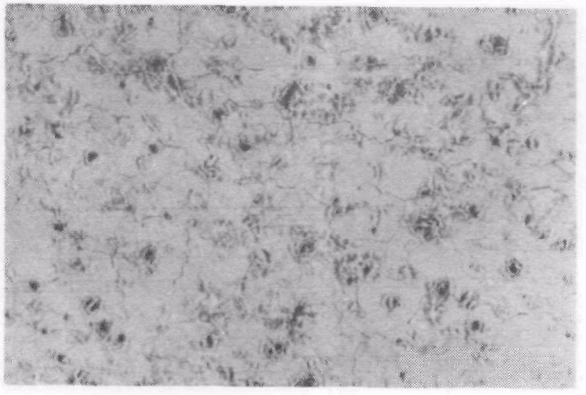

20 minutes

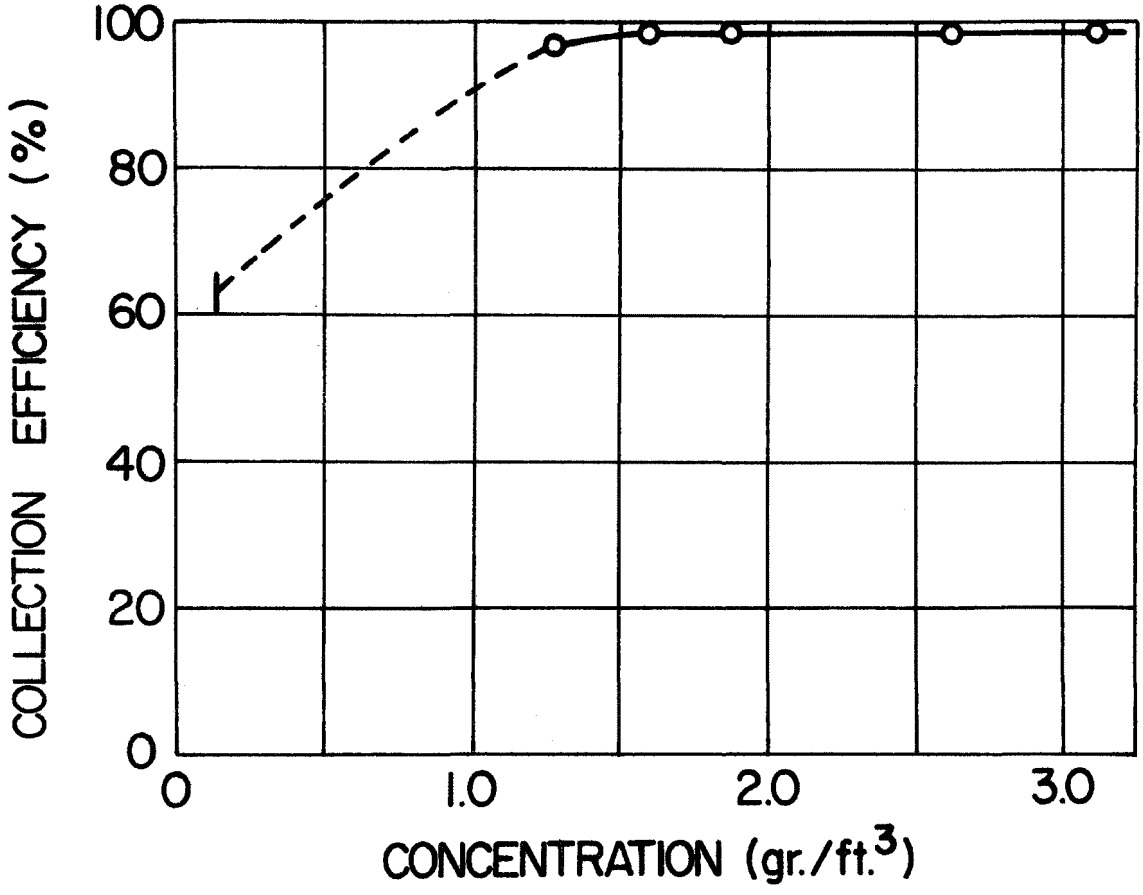

Figure 58. Effect of flyash concentration on efficiency (368 punches/inch^2, 25 gauge, 3.0 denier x 1½ in. Dacron) 10 minutes test duration, Batch Testing, Air Velocity = 45 ft./min.

7.10 Effect of Filtration Time On Efficiency and Pressure Drop

Filtration time is an important factor in the determination of the optimum collection efficiency. Long filtration time is prohibitive because of the high pressure drop developed across the filter. While short filtration time will yield low efficiency values. The effect of filtration time on collection efficiency is shown in Figure 59. It is seen that for the needle punched filters tested the variation of efficiency with time is not significant after 10 minutes, which was used in all the batch tests.

The effect of filtration time on the pressure drop is given in Figure 60. It is noticed that the time rate of pressure drop increases due to the increase in flow resistance with the deposition of flyash on the surface of the filter. The same figure shows the comparison between the pressure drop-time curves for woven and needle punched filter fabrics. The comparison illustrates the effectiveness of needle punched filters in reducing the time rate of pressure rise in support of the hypothesis explained earlier.

7.11 Effect of Humidity

The filtration results previously reported were for air at relative humidity of about 50%. A limited experiment was carried out to determine the effect of humidity on filtration performance. The results are given in Table 13 and it is seen that the pressure drop ΔP_f increases with the increase in relative humidity. There is also a slight increase in efficiency but this may not be significant to draw any conclusion. At relative humidity about 90%, the control on the flyash concentration was very difficult.

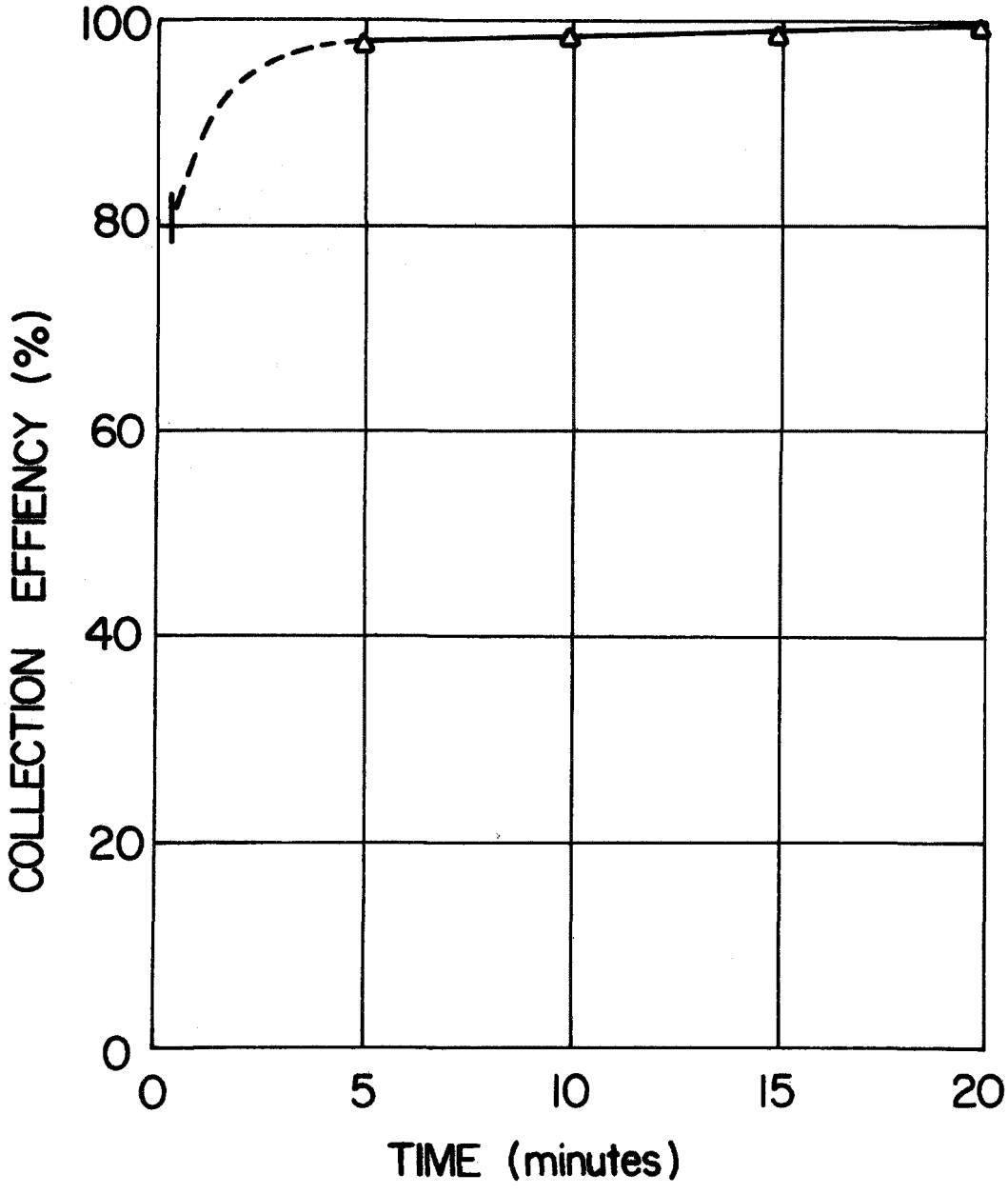

Figure 59. Effect of filtration time on collection efficiency (245 punches / inch^2 , 25 gauge needle , 3.0 denier x 1.5 in. Dacron) , Batch Testing, Air Velocity = 45 ft/min.

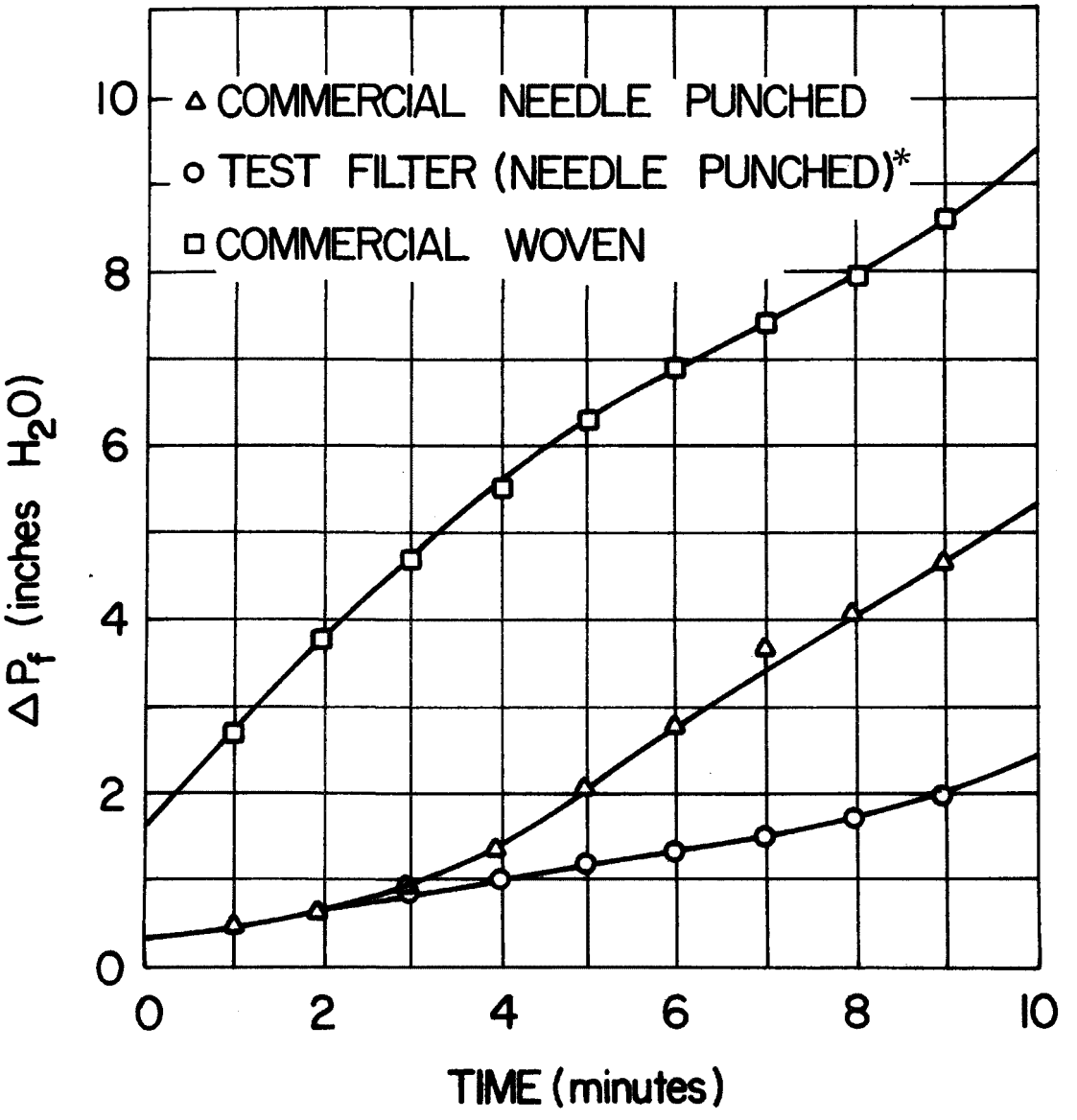

Figure 60. Effect of filtration time on pressure drop (Batch Testing)

*(245 punches/inch^2, 25 gauge , 3.0 denier x 1.5 Dacron)
Air Velocity = 45 ft./min.

Table 13. EFFECT OF HUMIDITY

RH %	C_i gr./ft.^{3}	ΔP_c Inches H_2O	ΔP_f Inches H_2O	Efficiency %
30	4.11	0.075	1.90	99.05
50	4.17	0.075	2.35	99.42
70	5.95	0.070	3.60	99.44

Fabric with Reemay 1.5 oz./yd.^{2} scrim
245 punches/inch^2, 25 gauge, 10.6 oz./yd.^{2}

SECTION VIII

REFERENCES

1. Billings, C. E. and Wilder, J., "Handbook of Fabric Filter Technology". Volume 1, 1-37, 38, Contract No. CPA-22-69-38, EPA, 1970.

2. Draemel, D. C., "Relation Between Fabric Structure and Filtration Performance in Dust Filtration", Environmental Protection Technology Series, Report No. EPA-R1-73-288, July 1973.

3. Turner, J. H., "Performance of Nonwoven Nylon Filter Bags", Paper No. 73-300, APCA Annual Meeting, June 1973.

4. Miller, B., Lamb, G. E. R., and Costanza, P., "Influence of Fiber Characteristics on Particulate Filtration", Environmental Protection Technology Series, Report No. EPA-650/1-75-002, January 1975.

5. Chen, C. Y., "Filtration of Aerosols by Fibrous Media", Chemical Review, 55, 3, 595, 1951.

6. Stern, S. C., Zeller, H. W., and Schekman, A. I., "The Aerosol Efficiency and Pressure Drop of a Fibrous Filter at Reduced Pressures", J. Colloid Sci., 15, 6, 546, 1960.

7. Linkson, P. B., Caffin, D. A., and Brough, J., "Pressure Drop Across Fibrous Filters", Chemical and Process Engineering, p. 68, December 1970.

8. Kozney, J., Wasserkraft U. Wasserwirtech, 22, 67, 68, 1927. (In German).

9. Scheidegger, A. E., "The Physics of Flow Through Porous Media", University of Toronot Press, P. 137, Third Edition, 1974.

10. Blake, F. E., "The Resistance of Packing to Fluid Flow", Trans. Am. I. Chem. E., 14, 415, 1922.

11. Camran, P. C., "Fluid Flow Through Granular Beds", Trans. Inst. Chem. Engrs., 15, 150, 1937.

12. Sullivan, R. R., and Hertel, K. L., "The Flow of Air Through Porous Media", Journal of Applied Physics, 11, 761, 1940.

13. Brinkman, H. C., "On the Permeability of Media Consisting of Closely Packed Porous Particles", Applied Science Research, A-1, 27, 1949.

14. Iberall, A. S., "Permeability of Glass Wool and Other Highly Porous Media", Journal Research National Bureau of Standards, 45, 398, 1950.

15. Emersleben, O., Z. Physik., Bd. 26, 601, 1925 (In German).

16. Wong, J. B., Ph.D. Thesis in Chemical Engineering, University of Illinois, 1954.

17. Wheat, J. A., "The Air Flow Resistance of Glass Fibre Filter Paper", Can. J. Chem. Eng., 41, 67, 1963.

18. Kwualbara, S., "The Forces Wxperienced by Randomly Distributed Parallel Circular Cylindere or Spheres in Viscous Flow at Small Reynolds Numbers", J. Phys. Soc. Japan, 14(4), 527, 1959.

19. Happel, J., "Viscous Flow Relative to Arrays of Cylinders", Am. Inst. Chem. Eng. J., 5, 174, 1959.

20. Brinkman, H. C., "A Calculation of the Viscous Force Exerted By a Flowing Fluid on a Dense Swarm of Particles", Appl. Sci. Res., A1, 27, 1947a.

21. Debye, P., and Bueche, A. M., "Intrinsic Viscosity, Diffusion and Sedimentation Rate of Polymers in Solution", J. Chem. Phys., 16, 573, 1948.

22. Spielman, L. and Goren, S. L., "Model For Predicting Pressure Drop and Filtration Efficiency in Fibrous Media", Environmental Science and Technology, 2(4), 279, 1968.

23. Davies, C. N., "The Separation of Airborne Dust and Particles", Proc. Inst. Mech. Engrs. (London) B1, 185, 1952.

24. Clarenburg, L. A., and Pickaar, H. W., "Aerosol Filters - I - Theory of the Pressure Drop Across Multi Component Glass Fibre Filters", Chem. Eng. Sci., 23, 773, 1968.

25. Beavers, G. S. and Sparrow, E. M., "Non-Darcy Flow Through Fibrous Porous Media", J. Appl. Mech., Paper No. 69-APM-CC, 1969.

26. Werner, R. M. and Clarenberg, L. A., "Aerosol Filters", Ind. Eng. Chem. Proc. Des. Dev. 4(3), 288, 1965.

27. Dorman, R. G., "Filtration", in Aerosol Science" (edited by C. N. Davies) Academic Press, London and New York, p. 192, 1966.

28. Jonas, L. A., "Aerosol Filtration by Fibrous Filter Mats", Environmental Science and Technology, 6, 9, 821, 1972.

29. Hampl, V. and Rimberg, D., "Aerosol Penetration of Felt Filters", Presented at Annual Conference of Association for Aerosol Research, October 16, 1974 in Bad Soden, West Germany.

30. Lockheed-Georgia Company, Marietta, Georgia, "Velocity of Particulate in Laminar and Turlulent Gas Flow by Holographic Techniques", Contract EHSD 71-34, October 1971.

31. Hearle, J. W. S., Sultan, M. A. I., and Choudhari, T. N., "A Study of Needle Fabrics: Part II Effects of the Needling Process", J. Text. Inst., 59, 2, 103, 1968.

32. Adley, F. E. and Anderson, D. E., "The Effect of Holes on the Performance Characteristics of High-Efficiency Filters", Presented at the Eighth AEC Air Cleaning Seminar, Oak Ridge National Laboratory, Oak Ridge, Tennessee, October 25, 1963.

SECTION IX

LIST OF PUBLICATIONS

1. Mohamed, Mansour H., Afify, El Sayed M. and Vogler, John W. "Needle Punched Fabrics In Filtration", Book of papers of the Second Technical Symposium of the International Nonwovens and Disposables Association (INDA), pages 17-47, March 1974.

2. Saleh, L. L., "Pressure Drop Through Nonwoven Needle Punched Fibrous Filters", M.S. Thesis in Mechanical Engineering, North Carolina State University, Raleigh, North Carolina, May 1974.

3. Vogler, J. W., II, Walsh, W. K. and Mohamed, M. H., "Electron Beam Curing of Binders For Nonwoven Filter Fabrics", Tappi, Vol. 58, No. 9:125-128, September 1975.

4. Afify, E. M. and Mohamed, M. H., "Collection Efficiency and Pressure Drop of Needle Punched Filters", Transactions of the ASME, Journal of Engineering for Industry, Vol. 98, No. 2:675-608, May 1976.

SECTION X

NOMENCLATURE

A	=	cross-section area of the filter
a	=	fiber radius
A_e	=	mean fiber radius
A^*, B^*	=	constant
b	=	free surface radius
C	=	Cunningham correction factor
$Cd_{\alpha i}$	=	drag coefficient for fiber diameter d_i in filter with volume fraction α_i
Cd_{α}	=	drag coefficient of a fiber of average size $(df)_{av}$ in a filter with fiber volume fraction α
C_i	=	inlet concentration
d	=	fiber diameter
D^*	=	average pore diameter
d_E	=	effective fiber diameter
F	=	drag force
F_i	=	drag force per unit length of fiber with diameter d_i
$(df)_{av}$	=	average fiber diameter
$(df)_s$	=	surface average fiber diameter
$f(\ )$	=	function of
F_1^*	=	drag force per unit volume of filter having fibers normal to the superficial velocity
F_2^*	=	drag force per unit volume of fiber having fibers parallel to the superficial velocity

F_1 = drag force per unit volume of filter due to fibers normal to the superficial velocity

F_2 = drag force per unit volume of filter due to fibers parallel to the superficial velocity

F_{D_1} = drag force per unit length of fibers with axes normal to the superficial velocity

F_{D_2} = drag force per unit length of fibers with axes parallel to the superficial velocity

$g_1(\ ), g_2(\ ), f_1(\ ), f_2(\ )$ = function of

k = Darcy's coefficient

$k^*, k_g, k_f, k_e, k_d, k_c, k_b, k_a$ = constant

k_R = inertial impaction parameter

k_D = diffusion parameter

k_I = interception parameter

$\bar{k}$ = function of Cunningham slip correction factor

K_o, K_1 = modified Bessel functions of zero and first order respectively

k_1 = Darcy's drag coefficient for fibers normal to the direction of flow

k_2 = Darcy's drag coefficient for fibers parallel to the direction of flow

K'_n = Knudson number

$\bar{l}$ = mean fiber length

L_E = effective thickness

$\frac{L_E}{L}$ = tortuosity factor

n = number of solid cylinders per unit area

n^* = average number of fibers per pore

N^* = average actual number of pores per inch^2

N_p = number of pores on surface area 1^{-2}

p = needle penetration

$P\%$ = percentage particle penetration

r = radial coordinate

R_c = Reynolds number

S = surface area per unit volume of porous media

S_o = surface area per unit volume of solid material

t = thickness of the filter

U = superficial velocity

$\bar{u}$ = vectorial velocity

$\bar{u}_1$ = velocity normal to the fiber

$\bar{u}_2$ = velocity parallel to the fiber

u_{1r} = radial component of the normal velocity

$u_{1\theta}$ = angular component of the normal velocity

V = face velocity of contaminated air

V_m = velocity at maximum particle penetration

X_1, X_2 = non-dimensional factors

α = volume fraction or packing density of porous medium, i.e., volume of solids per unit volume of the porous medium

α_1 = volume of fibers normal to the thickness direction of the filter per unit volume of filter

α_2 = volume of fibers parallel to the thickness direction of the filter per unit volume of filter

α_1^* = solid fraction of filter with fibers all normal to the superficial velocity

α_2^* = solid fraction of filter with fibers all parallel to the superficial velocity

ΔP = pressure drop

ΔP_c = pressure drop for clean filter

ΔP_f = pressure drop at the end of filtration test

ΔL = filter thickness

ϵ = porosity

γ, η = constant

θ = angular coordinate

λ = gas molecules mean free path

μ = viscosity

ρ = density of gaseous medium

∇P_1, ∇P_2 = pressure gradient for fibers normal and parallel to the superficial velocity

$\varphi( )$ = function of

ψ = stream function

SECTION XI

APPENDIX A

FABRIC PROPERTIES

Table A-1. FABRIC THICKNESS
(Dacron 3 den. x 1.5 in.)

Needling Intensity Punches/in.^{2}	Fabric Thickness (mm)					
	Random-Laid*			Cross-Lapped**		
	20 gauge	25 gauge	32 gauge	20 gauge	25 gauge	32 gauge
122	22.5	16.6	24.1	28.0	17.8	22.1
184	22.3	11.6	18.9	21.8	14.3	20.8
245	17.3	10.7	17.9	21.5	11.6	20.0
368	20.0	8.5	17.5	15.6	9.3	15.6
490	13.0	7.5	14.2	15.7	8.2	13.9
735	12.5	5.9	9.8	10.4	6.9	12.4

* Five layers of web 2.52 oz/yd^2 each.

** Four layers of web 3.0 oz/yd^2 each.

Table A-2. FABRIC WEIGHT
(Dacron 3 den. x 1.5 in.)

Needling Intensity Punches/in.^{2}	Fabric Weight (oz./yd^2)					
	Random-Laid			Cross-Lapped		
	20 gauge	25 gauge	32 gauge	20 gauge	25 gauge	32 gauge
122	9.7	9.8	11.5	10.3	10.8	10.7
184	10.5	8.6	10.7	9.6	10.5	10.6
245	8.9	8.9	11.0	9.7	9.6	10.8
368	10.0	8.3	11.7	8.6	8.6	9.9
490	7.4	8.9	10.5	8.2	8.5	9.1
735	8.3	7.7	7.7	6.9	7.7	9.2

Table A-3. FABRIC PACKING DENSITY
(Dacron 3 den. x 1.5 in.)

Needling Intensity Punches/in.^{2}	Packing Density %					
	Random-Laid			Cross-Lapped		
	20 gauge	25 gauge	32 gauge	20 gauge	25 gauge	32 gauge
122	1.1	1.4	1.2	.9	1.5	1.2
184	1.1	1.8	1.4	1.1	1.8	1.2
245	1.3	2.0	1.5	1.1	2.0	1.3
368	1.2	2.4	1.6	1.3	2.3	1.6
490	1.4	2.9	1.8	1.3	2.5	1.6
735	1.6	3.2	1.9	1.6	2.7	1.8

Table A-4. FABRIC TENACITY
(25 gauge) (Dacron 3 den. x 1.5 in.)

Needling Intensity Punches/in.^{2}	Tenacity (gf/tex)					
	Random-Laid			Cross-Lapped		
	$\parallel$	$\perp$	45°	$\parallel$	$\perp$	45°
122	.07	.08	.08	.03	.11	.04
184	.10	.08	.10	.04	.12	.06
245	.12	.11	.13	.05	.15	.09
368	.20	.19	.23	.12	.20	.15
490	.31	.30	.31	.17	.22	.23
735	.75	.52	.62	.44	.41	.56

Table A-5. FABRIC ELONGATION
(25 gauge) (Dacron 3 den. x 1.5 in.)

Needling Intensity Punches/in.^{2}	Elongation %					
	Random-Laid			Cross-Lapped		
	$\parallel$	$\perp$	45°	$\parallel$	$\perp$	45°
122	83.2	86.2	77.0	131.8	65.2	109.5
184	81.9	86.4	87.1	145.1	66.0	118.2
245	88.9	85.3	94.1	159.9	66.9	128.2
368	97.6	95.2	101.4	189.7	71.7	143.2
490	90.6	116.7	104.6	159.5	79.8	128.3
735	101.5	103.4	96.5	155.3	84.7	143.3

$\parallel$ Along machine direction.

$\perp$ Perpendicular to machine direction.

APPENDIX B

EFFECT OF FLOW RATE ON PRESSURE DROP

The results of the effect of flow rate for the clean filters tested are presented in Figures B-1 and B-2. In Figure B-1 it is noticed that the pressure gradient $\Delta P/\Delta L$ for needle punched filters varies linearly with the flow rate up to 180 ft./min. In this range the flow is considered viscous and follows Darcy's law. For rates of flow above this range, which correspond to Reynold's Number (based on fiber diameter) larger than unity, the linear relationship ceases to exit. Adley and Anderson [32] found that the pressure drop of filters having holes to be nonlinear with air velocity. His explanation was based on the fact that the flow through the holes follows the poiseiulle flow (i.e. $\Delta p \alpha V^2$) whereas the pressure drop through the remainder of the filter is proportional to the velocity. The fact that needle punched filters show a linear relationship between the pressure drop and air velocity is an indication that needle punched filters can be treated macroscopically as homogeneous filters. Thus the pores of a needle punched filter cannot be considered as holes.

In Figure B-2 comparison is made between two clean filters having approximately the same weight per unit area; a cotton woven fabric and a needle punched fabric. It is seen that the needle punched filter offers considerably less resistance to the flow than the woven one.

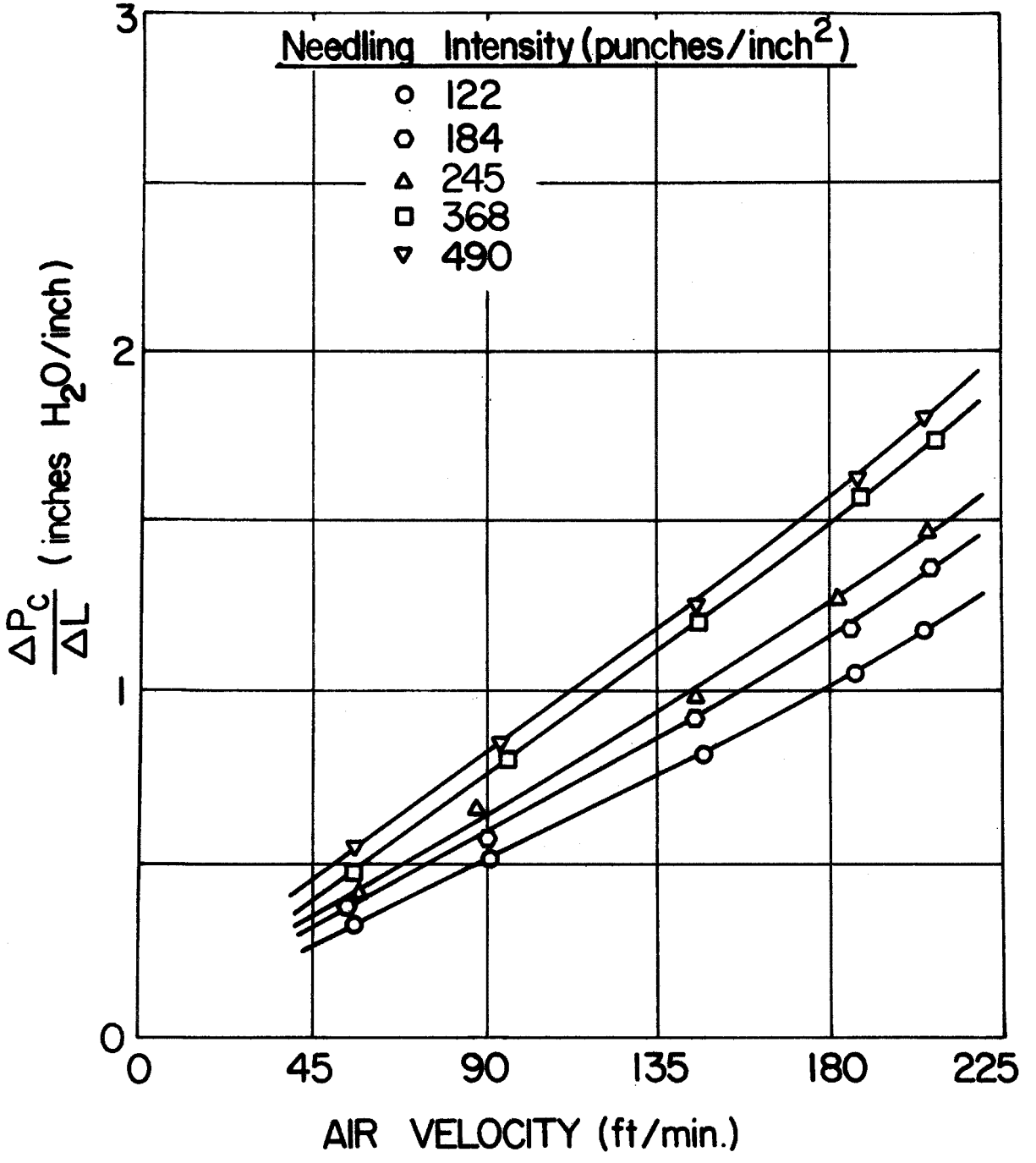

Figure B-1. Effect of air velocity on pressure gradient

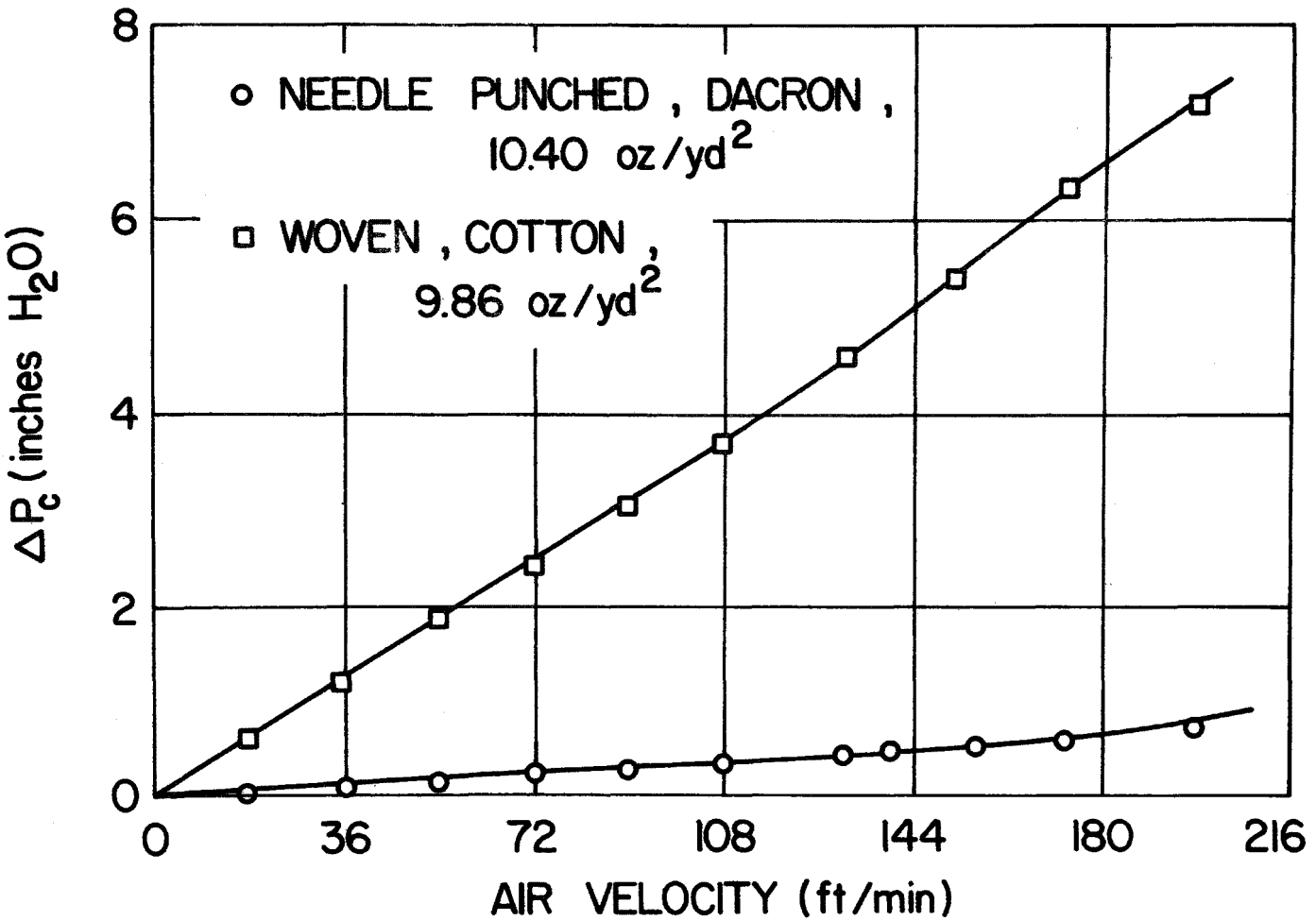

Figure B-2. Effect of air velocity on pressure drop

APPENDIX C

The pressure drop theory was based on the measurement of certain fabric parameters, as given in Table 11. The procedure for measuring some of these parameters is given in the following:

C.1 Actual Number of Pores Per Unit Area

Because of the difficulty to count the pores in a needle punched fabric, the following method was used. A chemically bonded nonwoven fabric was passed through the needle punching machine with a web of red Dacron fiber glued to it. Using a pick-glass, the positions where the red fibers showed on the back of the nonwoven fabric, in an area of one square inch, were counted. Five counts were made for each needling intensity and the average was plotted against the calculated needling intensity. The measured number of pores was found to be less than the calculated number. At high needling intensity the rate of increase of pores was reduced indicating the high probability that the pores may have been punched more than once. The effect of needle size on the number of pores does not seem to be significant between the 32 and 25 gauge needles. The large needle (20 gauge) gave less pores than the other two.

C.2 Pore Diameter

Fabric cross sections prepared by the method explained later were used. The diameter of the pore was measured on the Projectina Screen. Ten measurements were taken for every fabric and the average values of pore diameter are given in Table 11. It can be seen that the larger the needle the larger is the pore diameter. It can also be seen that the higher the needling intensity, the larger is the pore diameter with every needle. This is due to the increased packing density which reduces the disruption of the fibers in the pore as the needling intensity is increased.

C.3 Number of Fibers In The Pores

Fabrics made with red tracer layer on top were examined in this investigation using exactly the same conditions of the pore diameter experiment. Representative punches were cut away from the fabric using small scissors and tweezers. The white fibers in the plane of the fabric were removed. The red fibers were then separated and evenly distributed in mineral oil on a slide and examined on the Projectina. Each end was counted and tagged with ink so it was counted once. Assuming that the number of fibers equals half the number of fiber ends, the number of fibers was calculated 10 times for each fabric. The average numbers are also given in Table 11. This experiment is a very tedious one and the variation in the number of fibers between pores is so great which makes it difficult to obtain statistically significant result. However, the experiment gives rough average for the number of fibers. The average number of fibers per pore for all fabrics was 112. The results indicate that the number of fibers was higher with the large and small needles than with the medium needle. There was no particular pattern as far as the effect of needling intensity.

C.4 Method of Preparing Cross-Sections

Fabric samples were mounted in a Dow epoxy resin mixture of both hard resin (D.E.R. 332) and soft resin (D.E.R. 732). Many resin proportion ranges and curing times were experimented with before the best properties were attained to allow microtoming of thin cross-sections. The best mixture of resins was three parts soft D.E.R. 732 to one part hard D.E.R. 332 with 15% by weight curing agent (D-126, diethylene triamine). A gel time of three hours at room temperature and curing time of 30 minutes at 55°C oven temperature was used.

Formulation: 65% D.E.R. 732
22% D.E.R. 332
13% D-126

This particular mixture provided the proper consistency for microtoming thin sections as thin as 200 microns. This thickness is ample to provide information about the fabric structure. The thin sections were mounted in mineral oil for microscopic examination and photomicrography.

Better contrast was attained by using a top tracer layer of red fibers (same fiber type). For better contrast in photomicrography, monocromatic light was used for illumination. The photomicrographs were produced with a projection microscope (Projectina) which used transmitted light source and is equipped with a Polaroid Land Camera — (Graphic).

TECHNICAL REPORT DATA
(Please read Instructions on the reverse before completing)

1. REPORT NO.	2.	3. RECIPIENT'S ACCESSION NO.
EPA-600/2-76-204		

4. TITLE AND SUBTITLE	5. REPORT DATE
Efficient Use of Fibrous Structures in Filtration	July 1976
	6. PERFORMING ORGANIZATION CODE

7. AUTHOR(S)	8. PERFORMING ORGANIZATION REPORT NO.
M. Mohamed and E. Afify	

9. PERFORMING ORGANIZATION NAME AND ADDRESS	10. PROGRAM ELEMENT NO.
North Carolina State University Schools of Engineering and Textiles Raleigh, NC 27607	EHE624
	11. CONTRACT/GRANT NO.
	Grant R801441

12. SPONSORING AGENCY NAME AND ADDRESS	13. TYPE OF REPORT AND PERIOD COVERED
EPA, Office of Research and Development Industrial Environmental Research Laboratory Research Triangle Park, NC 27711	Final; 6/72-6/76
	14. SPONSORING AGENCY CODE
	EPA-ORD

15. SUPPLEMENTARY NOTES Project officer for this report is J.H. Turner, Mail Drop 61, Ext 2925.

16. ABSTRACT The report gives results of a project to develop fibrous structures for air filtration which are economical and efficient, and have low pressure drop. The structure of needle punched fabrics showed excellent characteristics as filter media. Fundamental studies were carried out to investigate the effect of different needled fabric parameters on their filtration performance and mechanical properties. High efficiency levels were obtained at relatively low pressure drop, compared to woven fabrics. Fabric parameters studied were: needling intensity, fiber orientation and length, needle size and penetration, scrim material, fabric weight, and number of passages through the needling process. Spunbonded scrims were used to improve the strength and dimensional stability of needle punched fabrics without sacrificing air permeability. The pressure drop for clean filters was predicted theoretically. Based on literature review of existing theories, the Brinkman model was used. Analytical study of the roles played by the various mechanisms of collection (using Dorman's theory) showed that the diffusion mechanism is not fully utilized in the developed needle punched fabrics. Based on the fundamental studies, fabrics were developed in which Cerex 1.5 oz/sq yd was used as scrim and punching was done on stages and from both sides. These fabrics have been evaluated in batch filter testing as well as baghouse application and were found superior in many respects to commercial fabrics.

17. KEY WORDS AND DOCUMENT ANALYSIS

a. DESCRIPTORS	b. IDENTIFIERS/OPEN ENDED TERMS	c. COSATI Field/Group
Air Pollution	Air Pollution Control	13B
Air Filters	Stationary Sources	13K
Fabrics	Fibrous Structures	11E
Dust	Particulate	11G
	Fabric Filters	
	Needled Fabrics	
	Baghouses	

18. DISTRIBUTION STATEMENT	19. SECURITY CLASS *(This Report)*	21. NO. OF PAGES
Unlimited	Unclassified	145
	20. SECURITY CLASS *(This page)*	22. PRICE
	Unclassified	

EPA Form 2220-1 (9-73)